HEINRICH-HERTZ-INSTITUT FÜR SCHWINGUNGSFORSCHUNG
BERLIN-CHARLOTTENBURG

Technischer Bericht Nr. 136

Versuche zur interkontinentalen Lokalisierung von Quellen der Atmosphericsaktivität durch Bestimmung von Einfallsrichtungen und Gruppenlaufzeitdifferenzen

von

Ing. G. Heydt

Berlin

1971

Technischer Bericht Nr. 136

Versuche zur interkontinentalen Lokalisierung von Quellen der Atmosphericsaktivität durch Bestimmung von Einfallsrichtungen und Gruppenlaufzeitdifferenzen

Zusammenfassung:

Im Herbst 1970 sind in den USA, in Japan, in Deutschland und in Argentinien vier Anlagen zur Registrierung der Atmosphericsaktivität aufgebaut worden, die mit vom Heinrich-Hertz-Institut entwickelten Atmospherics-Analysatoren ausgerüstet sind.
Es wird berichtet über erste Auswertungen photographischer Registrierungen von Einfallswinkeln und Gruppenlaufzeitdifferenzen von Atmospherics zur Zeit der Jahreswende 1970/71.
Die Ergebnisse werden mit von H a r t h (1971) errechneten Ausbreitungsparametern verglichen, wobei sich eine Reflektionsfaktor-Bezugshöhe für die Ionosphäre von 86 km ergibt.
Als Quellen erhöhter Atmosphericsaktivität wurden das Küstengebiet südlich des Golfes von Panama, das Amazonasgebiet und das nördliche Südamerika, ein Gebiet vor der niederkalifornischen Küste, das Gebiet der Hawaii-Inseln, der indonesische Raum sowie einige Bereiche des Atlantischen Ozeans und die Umgebung des Mittelmeeres ermittelt.

Heinrich-Hertz-Institut für Schwingungsforschung

Der Bearbeiter
G. Heydt
(Ing. G.Heydt)

Der Abteilungsleiter
(Prof. Dr.-Ing. F.W.Gundlach)

Der stellv. Institutsdirektor
(Prof. Dr.-Ing. L.Cremer)

Berlin-Charlottenburg, den 3.8.1971

Technical Report No. 136

Experiments in Global Localizing Sources of Atmospherics Activity by Measurements of the Directions of Arrival and Group Delay Differences

by G.Heydt

Abstract:

In the fall of 1970 four stations have been established to observe the atmospherics activity in the USA,in Japan,in Germany and in Argentina.These stations are equiped with atmospherics analyzers developed by the Heinrich-Hertz-Institut. This report gives first results of evaluation of photographic records of directions of arrival and of group delay differences of atmospherics recorded at the turn of the year 1970/71. The results are compared to the results of calculations for a night time propagation model carried out by H a r t h (1971). This comparison leads to an ionospheric reflection reference height of 86 km.

Sources of considerable atmospherics activity were indicated at the coastal area south of the gulf of Panama,in the area of the Amazonas,in the northern Southamerica,in an area in front of the Californian peninsula,in the area of the islands of Hawaii,in the area of Indonesia,in some areas of the Atlantic and in the area of the Mediterranean Sea.

1. Introduction

In the fall of 1970 four stations have been established to observe statistical parameters of the atmospherics activity in the USA, in Japan, in Germany and in Argentina. These stations are equiped with a new type of atmospherics analyzer developed by the Heinrich-Hertz-Institut.
Joint measurements of the direction of arrival ψ, the spectral amplitude (SA), the spectral amplitude ratio (SAR) and the group delay difference (GDD) of atmospherics by photographic records are carried out in a very similar manner as described in detail by Frisius and Heydt 1968. (This reference is called A in this report.)
Besides these photographic records additional strip-chart records of atmospherics rates as a function of the direction of arrival are carried out at the stations.
This report presents first results of the evaluation and interpretation of photographic records taken in the GDD mode of operation of the atmospherics analyzers.

2. Description of stations

The following institutes are participating in this experiment:

Office of Naval Research/Naval Research Laboratory, USA, Washington DC, station located in Waldorf near Washington DC, 38,64° North, 77,01° West.

The Research Institute of Atmospherics of the Nagoya University, Japan, Toyokawa, 34,83° North, 137,36° East.

Observatorio de Fisica Cosmica, San Miguel, Argentina, 34.59° South, 58.80° West.

Heinrich-Hertz-Institut für Schwingungsforschung, Berlin-Charlottenburg (West-Berlin), station located in Berlin-Waidmannslust, 52,62° North, 13,13° East.

Fig.1 shows the position of the four stations on a world map. Each station is equiped with an atmospherics analyzer with antenna system, oscilloscope, camera and strip chart recorders. Additionally the stations in San Miguel and in Berlin have an analog digital converter and a magnetic recorder to store the

data which are simultaneously recorded by the strip-chart recorders.
Fig.2 shows the antenna system set up in Waldorf,USA consisting of balanced crossed loops with an area of 1 m^2 and 72 turns per loop and a whip antenna with a length of 4.8 m.
Fig.3 shows the whole equipment working in Berlin-Waidmannslust since Dec. 1970.

3. Description of photographic records

In the new type of the atmospherics analyzer three selective channels are used for analyzing the atmospherics:
5.00 , 7.00 and 9.00 kHz.
Thus,the measurements of the spectral parameters are executed at the following frequencies:
Measurement of the spectral amplitude at 7 kHz (SA_7).
Measurement of spectral amplitude ratio between spectral amplitudes at 9 kHz and 5 kHz (SAR_{9-5}).
Measurement of group delay difference between 8 kHz and 6 kHz (GDD_{8-6}).
The operating frequency of the direction finding unit is 9 kHz. The spectral amplitude of an atmospheric has to be greater than 0.8 $\mu V/Hz \cdot m$ at 5 kHz to release the measuring circuits.If the spectral amplitude of an atmospheric exceeds 110 $\mu V/Hz \cdot m$,the instrument is overdriven and the measuring circuits will be blocked.
For taking photographic records the y-input of a XY-oscilloscope is fed to the output voltage of the direction finding unit of the atmospherics analyzer.The x-input of the oscilloscope can be connected as needed with one of the output voltages of the analyzer indicating SA_7,SAR_{9-5} or GDD_{8-6}.
If an atmospheric releases the measuring process,a sensitizing pulse causes a light spot on the screen of the oscilloscope. The vertical position of this spot indicates the direction of arrival of the atmospheric,while the horizontal position gives the SA_7,SAR_{9-5} or GDD_{8-6} respectively.
A measurement of the distribution of the atmospherics with respect to both direction of arrival and GDD_{8-6} or SAR_{9-5} or SA_7 can be performed by photographing the oscilloscope sreen with an exposition time of several minutes.The photo collects light spots produced by some hundreds orthousands of atmospherics.

Fig. 4 a-c give examples of photos of that kind.
Compared with the photographic records as described in reference A the records taken by means of the new analyzer show some improvements:

a) The indication of SA_7 and SAR_{9-5} is given in decibel (dB) on a linear scale.
b) The dynamic range of the new analyzer is 43 dB, compared with a range of about 30 dB of the former analyzer.
c) The indication of negative values of the GDD is unique.
d) The zero and full scale points of the deflection area of the oscilloscope screen are marked by corner points on the photos. These points are important for data processing.

Just as the former analyzer the new one allows automatic operation of a suitable camera. So, a set of three photos as demonstrated in fig. 4 a-c is started at 0, 3, 6, 9, 12, 15, 18 and 21^{00} GMT at all stations with an exposition time of 10 or 5 minutes depending on the atmospherics rates.
At 1^{00} GMT an additional set of photos is started for checking the performance of the equipment. In this operation mode the East-West loop is short-circuited. For this reason the light spots produced by atmospherics are concentrated in the south and north direction.
In addition to this checking of the direction finder unit two different calibration pulses are fed into the whip antenna input. The one calibration pulse has a SAR_{9-5} of 0 dB, a GDD_{8-6} of 0 µs and a SA_7 of 15 dB.
The other calibration pulse has a SAR_{9-5} of -6 dB, a GDD_{8-6} of 140 µsec and a SA_7 of 20 dB.
The light spots caused by these calibration pulses are concentrated on two vertical lines, indicating zero points and sensitivity of the measuring devices for the spectral parameters. Fig. 5 a-c show a set of these calibration photos.

4. Data processing

For the GDD and SAR mode of operation it is experienced that the light spots caused by atmospherics are clustered at certain ranges of the direction of arrival and the GDD or SAR respectively. Generally these clusters are attached to atmospherics sources i.e. limited regions of storm activity.

So,a photographic record taken in the GDD or SAR mode of ope-- ration may be described by characterizing its clusters.
A cluster may be characterized by the following values:

a) Co-ordinates of the centre of the cluster
   ($\overline{\psi}$ = average direction of arrival, $\overline{GDD}$ = average GDD or $\overline{SAR}$ = average SAR),
b) scattering range of ψ,
c) scattering range of GDD or SAR,
d) density of light spots.

So,the first step in data processing the photographic records is to characterize the clusters by means of a pencil follower type PF!MK!1B manufactured by D-MAC Ltd.
For this purpose the film containing the records is projected on the reading table of the pencil follower.
This reading table contains a XY servo system.A coil situated in the reading pen radiates a AC-signal which is picked up by detection coils on the gantry below the reading surface.These signals are fed to the servo amplifiers which drive the motors in such a direction that the follower head below the surface always centres itself on the reading pencil.
The X- and Y-co-ordinates of the position of the follower head i.e. the position of the reading pen are digitized by encoders and by pressing a footswitch the readout of the co-ordinates is stored on punched cards.
At the begin of characterizing a photo the reading pen must be set manually at the three visible corner points of the photo to state the position of the projected photo in the XY-plane.
After storing the co-ordinates of the corner points by pressing the footswitch the co-ordinates of the cluster centres may be stored in the same way.
A fixed address for dating the photos and key numbers for characterizing the scatttering ranges and density of a cluster are punched by keystrokes on a special keyboard.
At this time the data of about 1600 photos were converted into data on punched cards at which a card contains the data of up to 4 clusters.
Subsequently the data were computed by a computer CAE 90-40 using a Fortran II program.The data output of the computer is

obtainable in punched tape or magnetic tape and in tabulated form from the line printer.
Table 1 shows an example of these data, containing the data processed from photographic records of two days.
The heading line gives for each day the station key number K_s, the year and the day number of observation and eight sequences of the abbreviations PSI, PAR and K. PSI means the angle of arrival in degrees, PAR the spectral parameter $\overline{GDD}$ or $\overline{SAR}$ and K a key number characterizing the scattering ranges and the density of spots.
The data obtained from a single set of photographic records are arranged in two immediately succeeding lines.
The first number in the upper line gives the starting time of the set in GMT. This upper line presents the data obtained from a record taken in the GDD mode of operation in up to eight sequences of data for PSI, PAR = $\overline{GDD}$ in µsec and K, characterizing up to eight clusters.
In the lower line the data for a SAR mode photo are given in just the same manner except that PAR means now $\overline{SAR}$ in dB_times_ten.
The data of the clusters in both lines are ordered to increasing angle of arrival.
The keying of the station key number K_s is the following:

K_s = 1 means observing station San Miguel
K_s = 2 means observing station Berlin-Waidmannslust
K_s = 3 means observing station Waldorf
K_s = 4 means observing station Toyokawa

The key number K which characterizes the single clusters consists of three figures:

$K = K_1K_2K_3$

K_1 characterizes the scattering range of PSI as follows:

Scattering range of PSI = $4.5^\circ \cdot K_1$

K_2 characterizes the scattering range of PAR as follows:

Scattering range of GDD = 62 µsec $\cdot K_2$

Scattering range of SAR = 3 dB $\cdot K_2$

The key number K_3 gives the density of spots:

K_3 = 0 means "a few spots"
K_3 = 1 means "cluster with weak density of spots"
K_3 = 2 means "cluster with normal density of spots"
K_3 = 3 means "cluster with strong density of spots"
K_3 = 4 means "cluster with very strong density of spots"
K_3 = 5 means "cluster with extremelstrong density of spots"
K_3 = 9 means "corona effect"

A key number K = 999 means "no cluster measured".

It must be pointed out that the way of estimating the key number K by viewing the photos is a rather subjective one. However, tests executed by different persons estimating the key number showed frequently a good conformity of the the estimated key number for the same cluster. Deviations of the key numbers were restricted to one unit of K_1, K_2 or K_3 .

5. Results

The first available films from the four stations were handled in a way as described in chapter 4 and were converted in data ready for evaluation.
The observation periods of the films were :

Station 1 (San Miguel) : 16.11.1970 - 30.11.1970
Station 2 (Berlin-Wm) : 30.12.1970 - 8.2. 1971
Station 3 (Waldorf) : 19.12.1970 - 1.2. 1971
Station 4 (Toyokawa) : 9.12.1970 - 23.12.1970

These observation periods are not completely overlapping. The main reason for this fact were drop outs of the photographic records.
Of course this amount of prepared data offers many potentialities for evaluation work. A first step in this work is to collect the positions of all cluster centres for each station and for each observation time on a GDD - PSI - plot.
This method, first executed by Frisius and Heydt 1969 for GDD measurements of the year 1967 recorded in Berlin, allows a good survey on the atmospherics activity in relation to the diurnal occurrence of atmospherics sources.

On these plots a cluster centre is shown in GDD - PSI co-ordinates.The spot density is indicated by squares with a size proportional to the key number K_3 of the cluster concerned. Fig. 6 - 37 show the GDD - PSI -plots derived from the prepared data.

6. Interpretation

6.1. Converting the GDD - PSI - plots into Map - plots

Evidently the cluster centres show a tendency of clustering themselves at certain regions on the GDD - PSI -plots. Assuming that these cluster of cluster centres (CCC) are attached to regions of considerable storm activity on the globe it is a matter of interest to locate these centres.
Former joint measurements with atmospherics analyzers on the research vessel "Meteor" and in Berlin in 1969 pointed at receiving ranges of the order of 10.000 km on night time conditions (Frisius and Heydt, 1971).So,it should be useful to seek on the GDD - PSI - plots of different stations for CCC which may be caused by the same centre of storm activity.
For this purpose the plots of Berlin and Waldorf are most suitable because of the length of overlapping of their observation periods.
Looking at these plots we find two marked CCC on the plots for 0^{oo} GMT:
The 0^{oo} GMT Berlin plot (Fig. 6) shows among other clusters a CCC with averaged values of 315 µsec for GDD and 273^{o} for PSI. On the corresponding Waldorf plot (Fig. 14) a CCC with averaged values of 125 µsec for GDD and 182^{o} for PSI may be supposed being caused by the same centre of storm activity as the Berlin CCC mentioned before.
Fig. 38 shows the cross bearing from Berlin and Waldorf,using upper and lower limits for the bearing of the two CCC.
The sinusoidal line on the map gives the boundary between day and night on the surface of the globe.
The common area of the two bearing sectors has its centre at the coastal area of Columbia south of the gulf of Panama.
The distance of this centre to the receiving station in Berlin is about 9.800 km,to the station in Waldorf 3900 km respectively.

There are three hints for the two CCC being caused by the same centre of storm activity:

a) The ratio of the distances to the receiving stations is nearly the same as the ratio of the received GDD. This is just what one has to expect in the case of one mode propagation.

b) A correlation analyzis has been carried out with respect to the key number K_3 of single clusters belonging to the two CCC during the overlapping period. For this purpose for each day of the overlapping period the presence of a cluster in the area of the CCC was stated by a key number $K_c = K_3 + 1$. If there was a day with no cluster in the area of the CCC this day was characterized by $K_c = 0$. The sequences of K_c derived from records of Berlin and Waldorf were correlated. The result was a correlations coefficient of +0.59. Considering the way of estimating the key number K_3 this result points to a common origin of the two CCC.

c) A distance of 9.800 km from the centre of the storm activity to Berlin and an averaged GDD of 315 µsec gives a GDD coefficient of 32 µsec/Mm.
Fig.39 shows computations of GDD as a function of distance for a night time model of the ionosphere given by Harth (1971). It is easily readable from this diagram that a GDD coefficient of 32 µsec/Mm is corresponding to a reflection height of about 86 km in the case of West-East propagation. This is a very reasonable value of the reflection height.

For other directions of arrival we have to consider the dependence of GDD on the direction of propagation caused by the terrestrial magnetic field. Looking at Fig.39 we find at a distance of 3.000 km and at different directions of propagation different values of GDD:

$$GDD_{3.000\ km,H=85\ km,N\text{-}S\ path\ /\ S\text{-}N\ path} = 90\ \mu sec$$

$$GDD_{3.000\ km,H=85\ km,W\text{-}E\ path} = 100\ \mu sec$$

$$GDD_{3.000\ km,H=85\ km,E\text{-}W\ path} = 60\ \mu sec$$

So, to consider this dependence, we use the following approximation:

$$GDD_{(\varphi)} = GDD_{\text{N-S path}} \cdot \left(1 - \sin(\varphi) \cdot \frac{360 - \varphi}{900} \right)$$

Of course this equation is merely valid on one mode propagation conditions.
Using this equation it is possible to produce "map plots" by means of a calculator type 9100 A (Hewlett Packard) with additional plotter.
For this purpose the data of a cluster (PSI, GDD, K_3) are entered to the special programmed calculater by keystrokes. After that the plotter pen moves to a position on the map computed corresponding to the night time propagation model and draws a square the size of which is indicating the density of light spots of the cluster.
Collecting the data on the map in the same manner as on the GDD-PSI plots we get plots which are showing the positions of centres of storm activity on the world map as derived from the night time propagation model.
The two sinusoidal lines on the maps give the position of the boundary between day and night on the surface of the globe computed and drawed by the calculator system by means of another special program. One line gives the position of this boundary for the begin and the other line for the end of the observation period.

6.2. Discussion of map plots of Berlin records

a) Map plot 21^{00}GMT (Fig.43)
This plot shows two main CCC: the strongest one in the area of the Amazonas river, the other one in the northern South America. The local time at these areas is about one hour before sunset, but the main part of the two propagation pathes to Berlin is on night time conditions.
A few cluster centres are indicated on the Atlantic and in the vicinity of the Mediterrarean Sea showing no marked tendency of clustering.

b) Map plot 0^{00}GMT (Fig.40)
This plot shows the marked CCC being discussed in 6.1. in the area of the gulf of Panama where the local time is about one hour past sunset.

The CCC in the Amazonas area is almost completely vanished whereas the activity on the Atlantic and in the vicinity of the Mediterrarean Sea is about the same as on the 21^{00} GMT plot.

c) Map plot 3^{00}GMT (Fig.41)
On this plot we see a lot of cluster centres with no marked tendency of clustering themselves.The amount of cluster centres on the Atlantic is somewhat surprising but it is backed for the Northern Atlantic by the records taken in Waldorf. A weak CCC is located in the area of the Red Sea near the Nubean desert.That seems to be not so very probable.On the other hand the neighbouring cluster centres at the coastal area of the Mediterranean Sea are placed very well with respect to climatic experiences.
A few cluster centres with strong densities are located at the eastern coastal area of the USA.If these cluster centres are placed right on the map they must have been recorded by the Waldorf station as nearby sources.It should be one of the next tasks to examine these cases.

d) Map plot 6^{00}GMT (Fig. 42)
This plot is very similar to the 3^{00}GMT plot.It's interesting to see that the storm activity is clearly increased compared with the 3^{00}GMT plot.A new weak CCC is located in the gulf of Guinea at local sunrise.

6.3. Discussion of map plots of Waldorf records

a) Map plot 21^{00}GMT (Fig.48)
On this plot most of the propagation pathes are on day time conditions.So,the location of the cluster centres on the map may be expected to be inaccurate.The interesting fact on this plot is the complete absence of cluster centres in the area of the Amazonas,considering the strong CCC at 21^{00}GMT at this region on the Berlin plot.This is obviously due to different propagation conditions at the day and night.

b) Map plot 0^{00}GMT (Fig.44)
This plot shows the marked CCC at the gulf of Panama,a CCC south of the Californian peninsula,a lot of cluster centres on the Atlantic and a few centres in the gulf of Mexico.

c) Map plot 3^{00}GMT (Fig.45)
On this plot we see the CCC at the gulf of Panama noticeable

decreased whereas the CCC south of the Californian peninsula has about the same activity as on the 0^{00}GMT plot. The activity on the Atlantic is lasting at which the number of cluster centres on the Northern Atlantic is considerable high compared with the number of cluster centres in the same area on the corresponding Berlin plot.The reason for this fact should be investigated carefully.
A new CCC is located in the area of the Hawaiian islands where the local time is just about sunset.

d) Map plot 6^{00}GMT (Fig.46)
This plot looks rather similar to the 3^{00}GMT plot.
The CCC at the gulf of Panama and in front of the Californian peninsula are noticeable decreased.

e) Map plot 9^{00}GMT (Fig.47)
This plot looks quite similar to the 6^{00}GMT plot.

6.4. Discussion of map plots of Toyokawa records

The map plots derived from the Toyokawa records show only a few cluster centres due to the shortness of the observation period.

a) Map plot 9^{00}GMT (Fig.49)
Most of the cluster centres on this plot are located in the area of Indonesia where the local time is about one hour before sunset.A few cluster centres are located in the northern Pacific.

b) Map plot 12^{00}GMT (Fig.50)
This plot shows additional to the cluster centres mentioned at the 9^{00}GMT plot some cluster centres south of India and a few in Africa.

c) Map plot 15^{00}GMT (Fig.51)
On this plot the activity in the area of Indonesia nearly completely vanished.A few cluster centres are located in the Indian Ocean and a few in Africa.The locating of storm activity in the northern Africa is rather doubtful.It should be investigated the possibility of bearing errors of the station in Toyokawa because a direction of about ten degrees more to the North would locate the cluster centres at the southern coastal area of the Mediterrarean Sea which would make them fitting to the Berlin records.It needs more records to make a decision on this thing.

6.5. Discussion of a map plot derived from San Miguel records

Because of the shortnessof the observation period only the map plot of 0^{00}GMT is shown (Fig.52).This plot is backing the Berlin map plot of 0^{00}GMT by indicating cluster centres in the middle and in the North of the continent of Southamerica in an excellent manner.

6.6. Summarizing the results of the map plots (Fig.53)

Looking at the map plots we have found two different types of storm activity.

One type,showing a marked tendency of clustering of the cluster centres,seems to have the maximum of activity at the hours short before and past sunset.This maximum of cluster activity has not to be the maximum of storm activity because of the high attenuation on day time propagation conditions.Examples of this type are the CCC located in Southamerica.

The other type,for example the activity on the Atlantic,has a flat maximum of cluster activity at the hours before sunrise. There is a weak tendency of clustering of the cluster centres at this areas.

Generally it may be stated that the indication of areas with enhanced storm activity on the map plots is mostly in good conformity with climatic experiences.

It may be also stated that there are several cases of map plots of different stations which are backing each other.

7. GDD - PSI maps

To facilitate the work of interpretation of GDD records,maps containing lines of constant PSI and GDD have been computed and plotted using the night time propagation model with a reflectionheight of 86 km (Fig.54 - 57).

There may be some effects which may reduce the accuracy of these maps,for example the magnetic declination and the inconstancy of the reflection height and of the direction of propagation on the propagation path.However,these effects will produce deviations of second order.

It must be pointed out that these maps are not applicable for short distances because of the effects of multi-mode-propagation (see Fig. 39).

8. Conclusions

This attempt on locating sources of atmospherics by means of measurements of the directions of arrival and of group delay differences seems to be promising.It should be continued using records of other seasons with good overlapping of the observation periods of the different stations and extended to SAR observations too.Succeeding in this work it would be possible to develope a technique of quantitative controlling the areas of enhanced storm activity by a few observation stations.

9. Acknowledgements

The establishment of the observation stations in Waldorf,Toyokawa and Berlin has been enabled by the Deutsche Forschungsgemeinschaft.The installation of the station in San Miguel has been supported by the Bundesministerium für Bildung und Wisssenschaft.

The author is grateful to Mr.H.Dolezalek (Office of Naval Research),Mr.R.V.Anderson (Naval Research Laboratory),Dr.T.Takeuti (Institute of Atmospherics Research),Dr.W.Harth (Max-Planck-Institut für Radioastronomie,Bonn) and Mr.C.Hofmann (Observatorio de fisica cosmica) for operating the observation stations and for data exchanging.

He wishes to express his thank to Dr. J.Frisius (HHI) for helpful discussions and to Mr. G.Abraham (HHI) and Mr.K.Schölzke (HHI) for plotting and graphic work.

10. References

Frisius,J., Heydt,G. 1968 Berichte über Beobachtungen an Längstwellen-Atmospherics mit dem Atmospherics-Analysator des Heinrich-Hertz-Instituts

Techn. Bericht Nr. 95 des Heinrich-Hertz-Instituts für Schwingungsforschung,Berlin-Charlottenburg

Frisius.J., Heydt,G. 1969 Beobachtungen der Atmospherics-Aktivität mit dem Atmospherics-Analysator des Heinrich-Hertz-Instituts

Kleinheubacher Berichte 13,53-62

Frisius,J., Heydt,G. 1971 "ergleichende Beobachtungen der Einfallswinkel-Verteilung von Atmospherics auf dem F.S. "Meteor" und in Berlin.

Kleinheubacher Berichte 14 (in print)

Harth,W. 1971 Der Einfluß höherer Mode auf VLF-Atmosphericsparameter

Beitrag zum Kolloquium "Luftelektrizität" 17. - 19. March,Oberpfaffenhofen (in print)

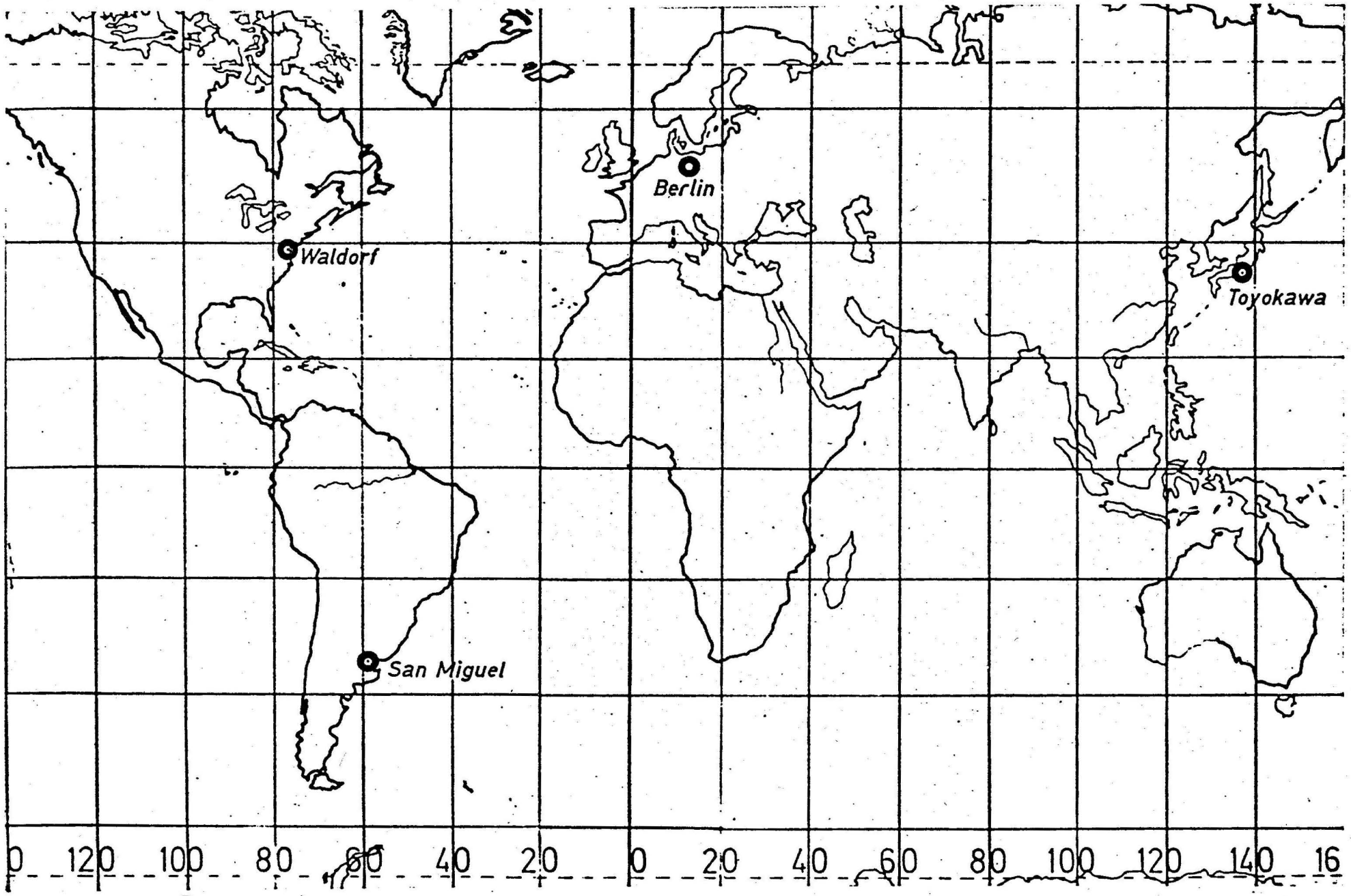

Fig. 1: Position of the observation stations

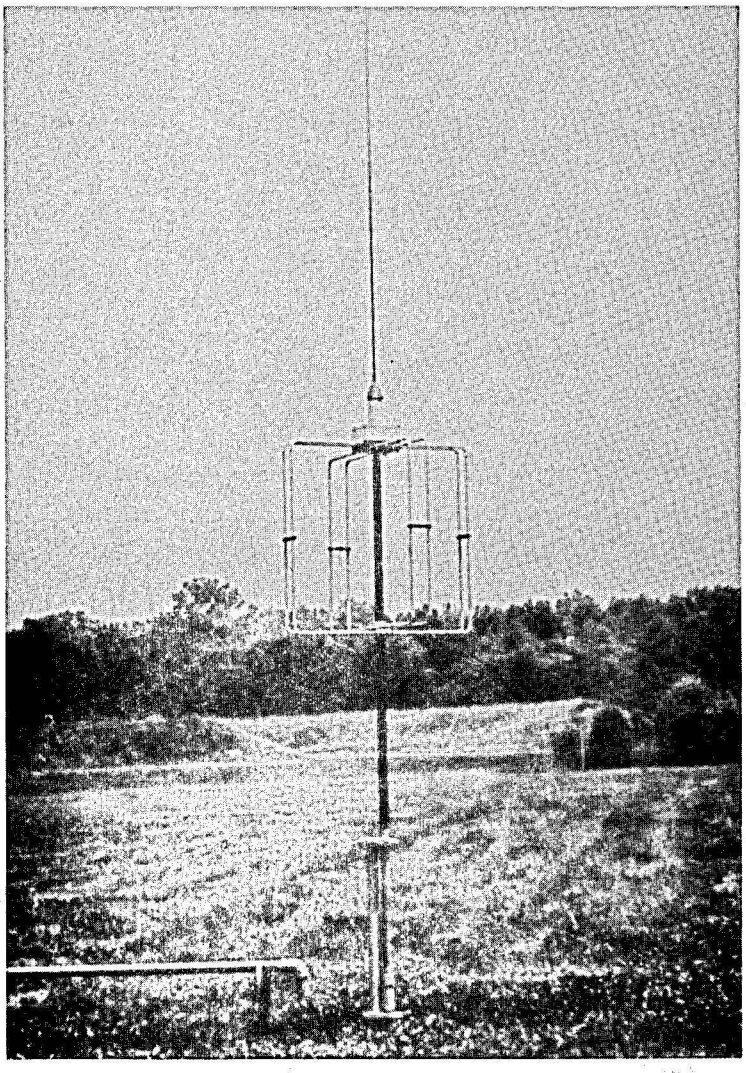

Fig. 2 : Antenna system, set up in Waldorf , USA

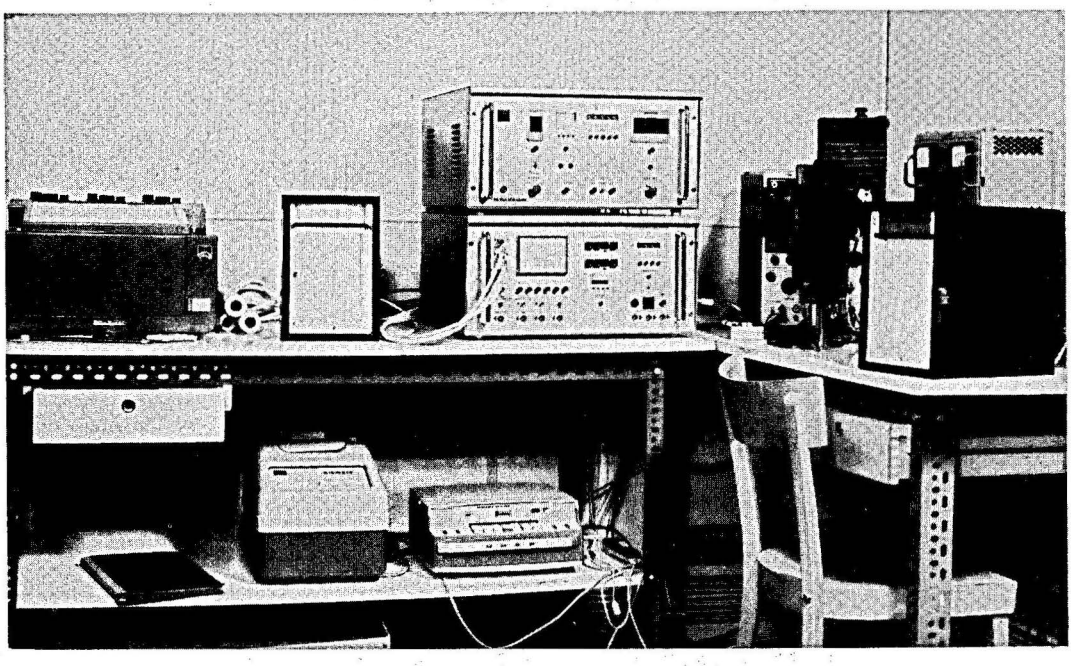

Fig. 3 : Equipment in Berlin - Waidmannslust

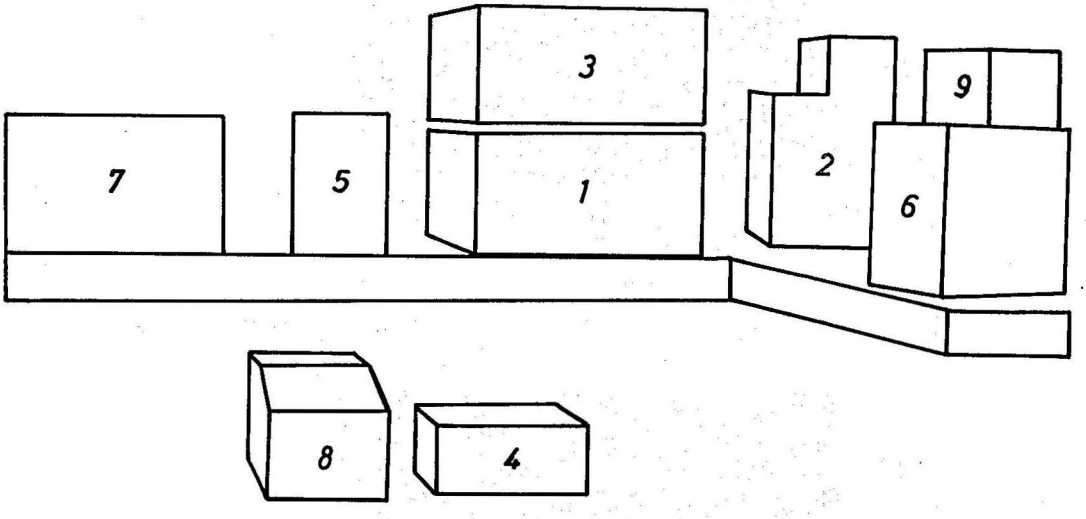

1 : VLF - Atmospherics - Analyzer

2 : Oscilloscope and camera

3 : Analog - digital-converter and timing system

4 : Tape recorder

5 - 7 : Strip chart recorders

8 : Printer

9 : Power supply unit

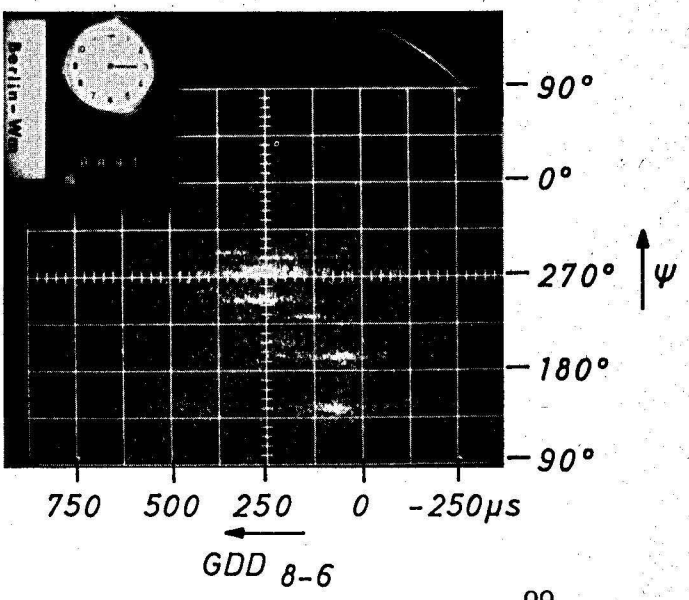

Fig. 4a : Photographic record GDD mode, 1.4.71, 3^{00} GMT, Berlin-Wm

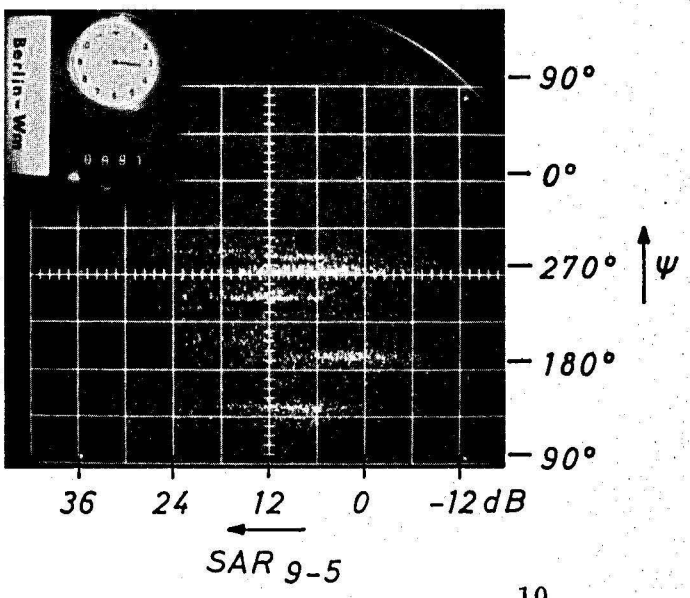

Fig. 4b : Photographic record SAR mode, 1.4.71, 3^{10} GMT, Berlin -WM

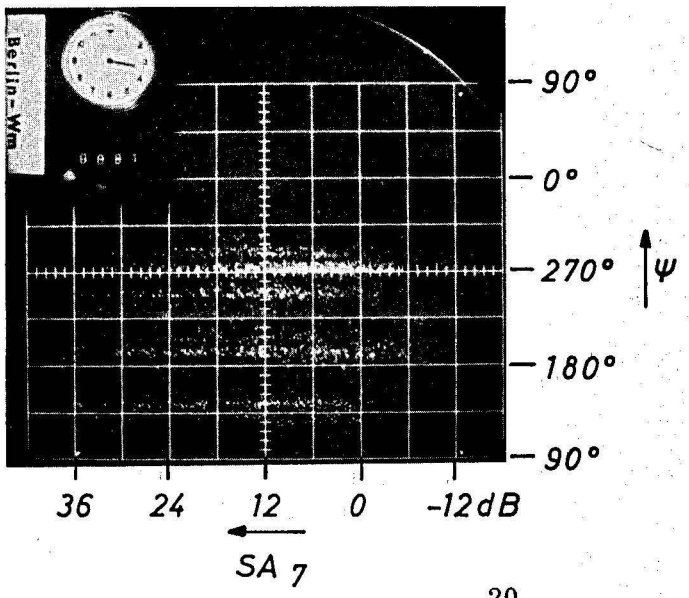

Fig. 4c: Photographic record SA mode, 1.4.71, 3^{20} GMT, Berlin-Wm

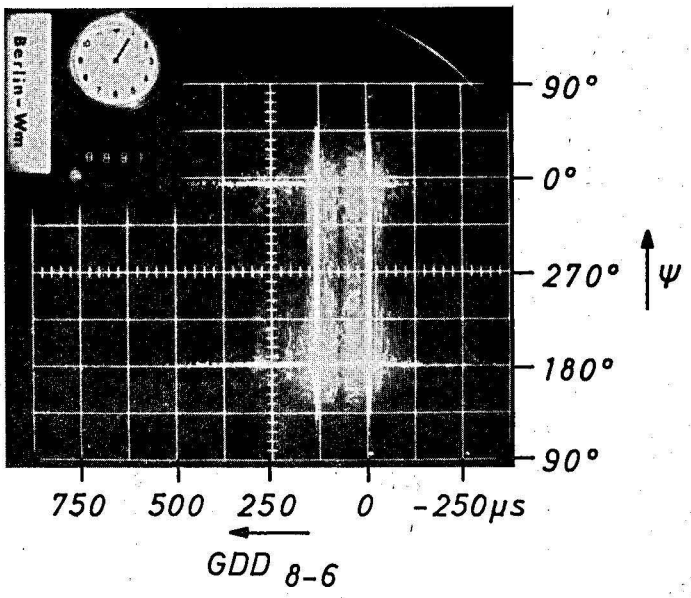

Fig. 5a: Calibration, GDD mode

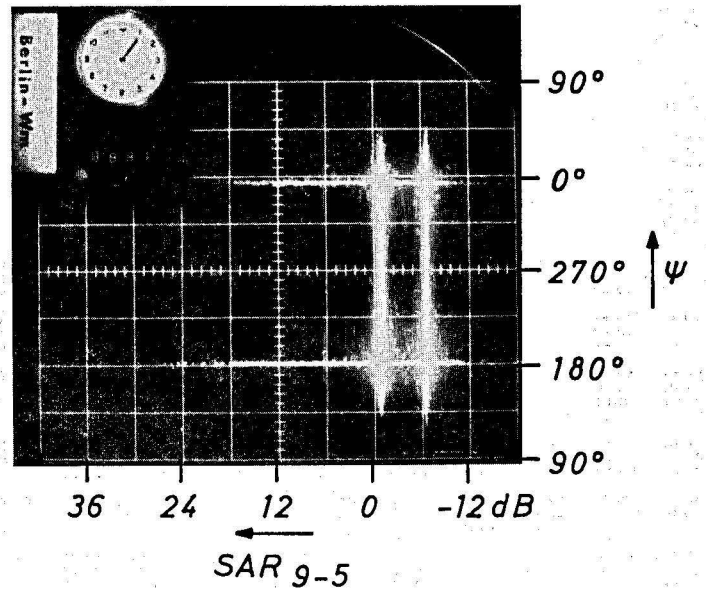

Fig. 5b: Calibration, SAR mode

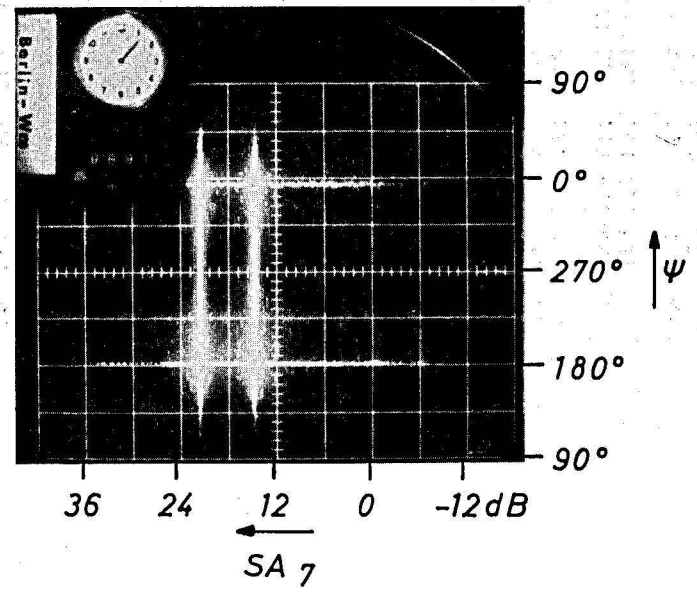

Fig. 5c : Calibration, SA mode

2 1971	35	PSI	PAR	K	PSI	PAR	K	PSI	PAR	K	PSI	PAR	K	PSI	PAR	K	PSI	PAR	K	PSI	PAR	K	PSI	PAR	K
	0	145	103	422	177	57	321	222	221	222	250	115	422	250	347	222	274	275	321						
		142	120	331	170	38	430	224	144	141	248	47	332	250	176	331	276	88	331						
	3	138	96	211	153	99	310	167	73	221	249	107	333	250	338	332	273	266	321						
		138	96	232	154	38	331	169	44	231	249	45	343	250	165	332	274	77	331						
	6	137	80	211	154	88	310	174	65	320	247	353	332	250	103	334	281	239	233						
		141	125	231	156	72	321	248	27	344	248	163	332	282	66	233									
	9	147	109	411	251	143	323																		
		147	135	421	249	95	243																		
	12	140	121	110	154	121	110	249	234	311															
		140	186	230	156	175	120	249	268	331															
	15	142	89	322	159	78	220	242	165	122	256	135	321												
		140	42	331	159	36	230	241	80	142	256	60	331												
	18	136	113	622	180	49	631	239	109	222	249	98	221												
		141	57	332	183	12	321	240	28	232	248	24	232												
	21	147	115	721	183	96	320	238	99	222	248	80	232	250	329	333	262	359	322	274	185	231			
		147	91	631	237	31	232	249	5	232	250	118	343	273	96	342									
2 1971	36	PSI	PAR	K	PSI	PAR	K	PSI	PAR	K	PSI	PAR	K	PSI	PAR	K	PSI	PAR	K	PSI	PAR	K	PSI	PAR	K
	0	142	88	421	248	115	231	277	282	333	310	286	211												
		148	93	441	248	24	341	279	37	333	309	95	231												
	3	143	103	311	169	76	321	186	65	321	243	115	320	279	289	133	306	282	121						
		140	74	231	168	37	341	186	23	241	244	103	360	307	150	121									
	6	147	88	420	176	65	421	241	254	141	253	345	120	260	370	120	277	302	222	302	306	221			
		149	76	330	176	23	430	241	107	151	254	192	140	262	182	140	279	119	143	303	135	220			
	9	161	98	421	274	252	230	304	313	120															
		160	96	431	276	124	331	301	144	140															
	12	148	112	320	167	101	121	237	127	120															
		148	122	330	169	88	231	239	86	331															
	15	123	104	211	152	101	211	168	85	211	237	131	211												
		123	113	131	150	64	230	165	68	232	238	68	231												
	18	123	98	322	147	68	421	169	68	522	231	106	522	242	363	320	273	219	220						
		121	29	332	146	25	431	165	4	431	231	2	332	248	181	140	274	103	320						
	21	143	106	421	170	79	321	225	371	130	229	128	311	248	346	323	267	320	323	271	160	322	301	255	211
		147	48	331	168	6	321	225	169	140	249	156	233	266	115	432	269	10	332	300	133	131			

Table 1: Result of data processing of photographic records of two days

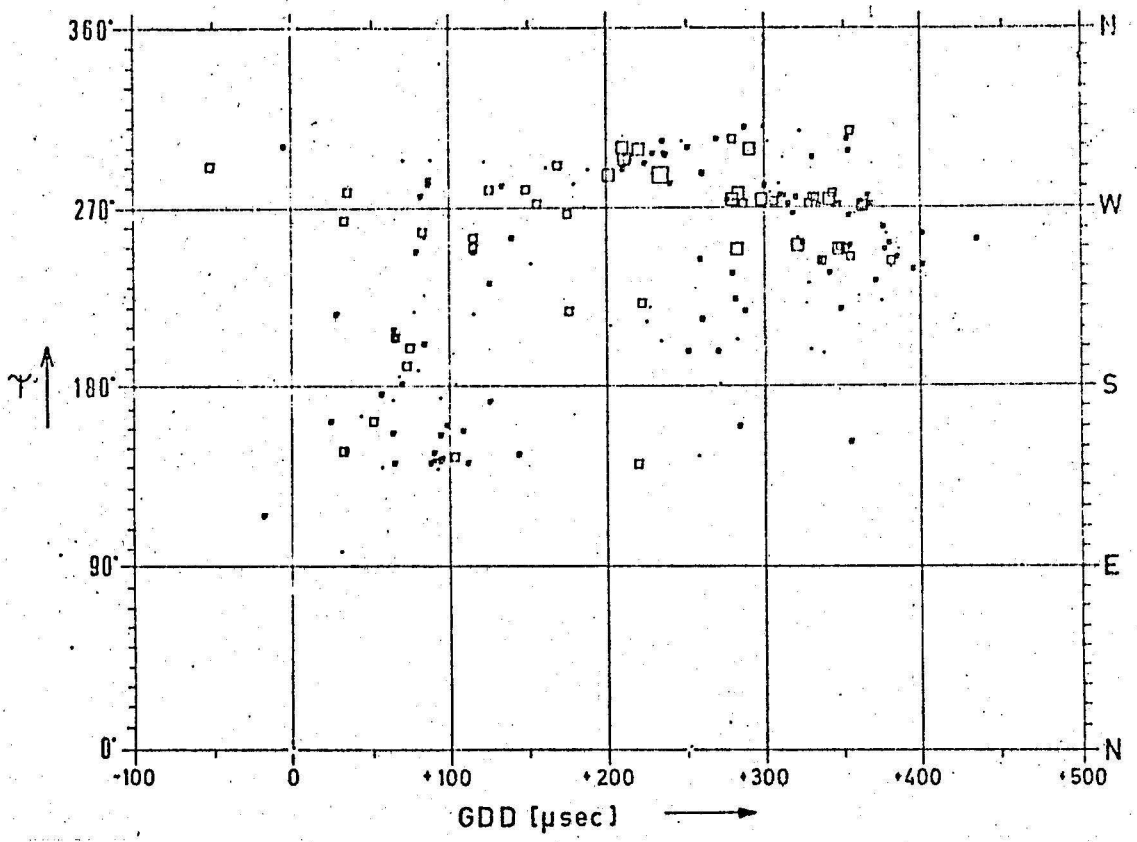

Fig. 6 : GDD - ♈ - plot, Berlin , 30.12.70 - 8.2.71 , 0^{00} GMT

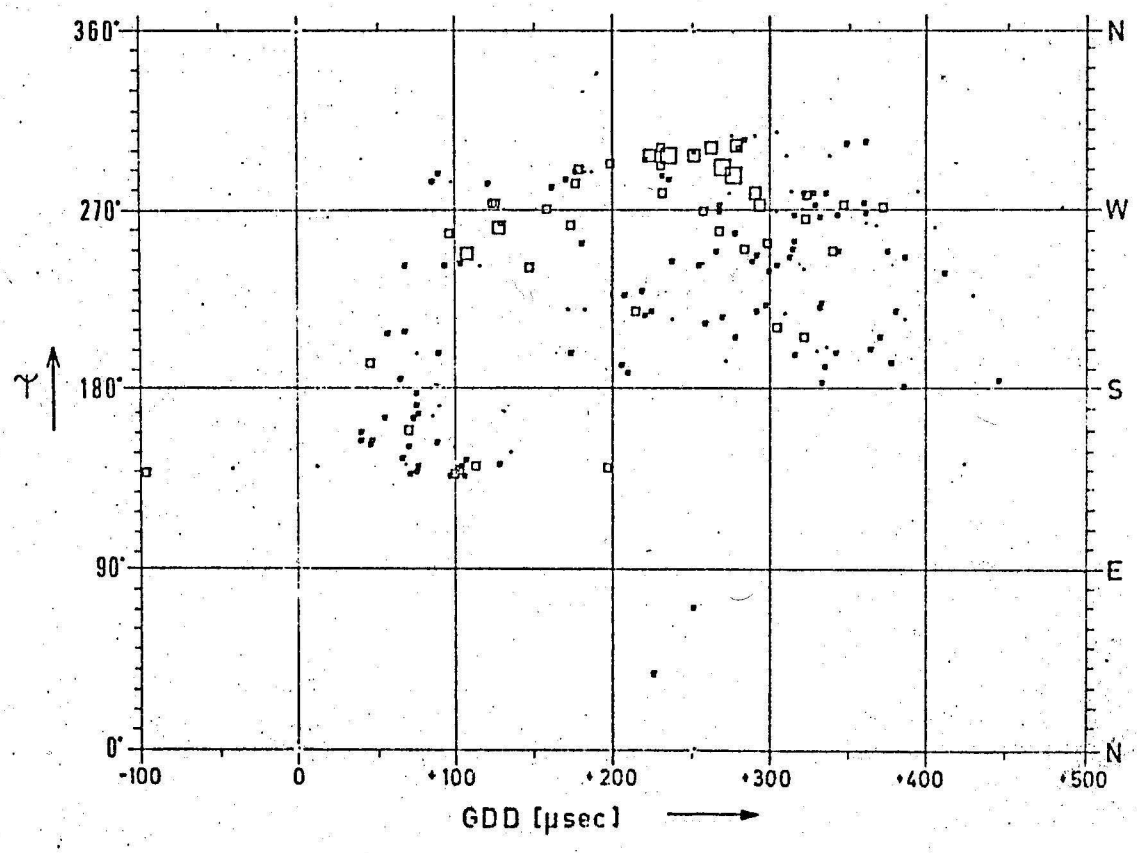

Fig. 7 : GDD - ♈ - plot, Berlin, 30.12.70 - 8.2.71, 3^{00} GMT

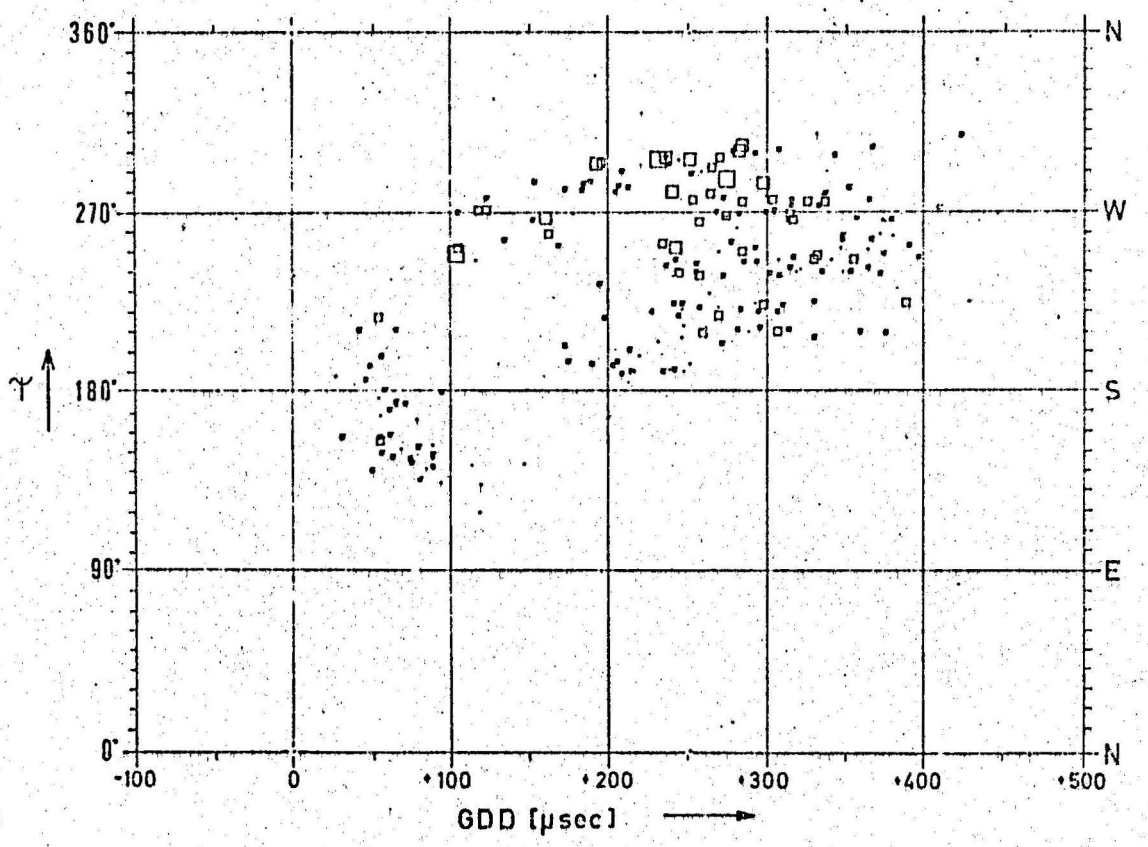

Fig. 8 : GDD - Ψ - plot , Berlin , 30.12.70 - 8.2.71, 6^{00} GMT

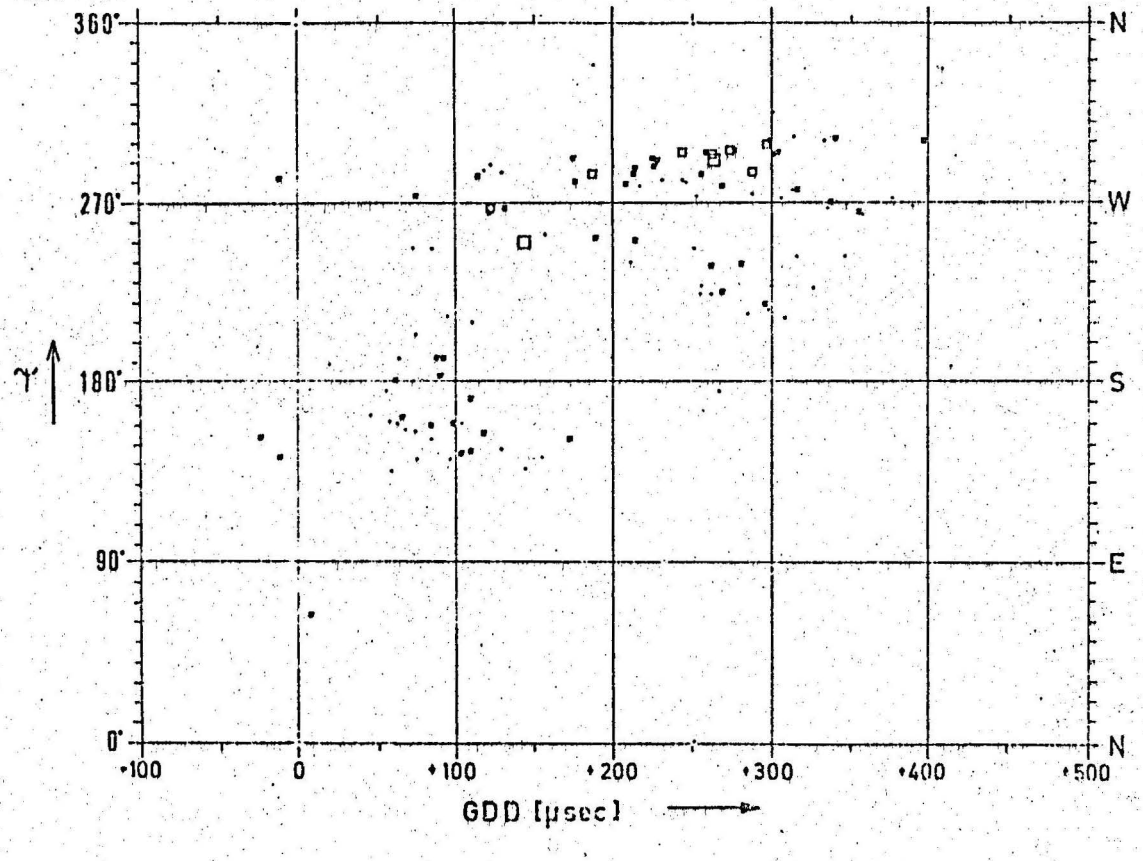

Fig. 9 : GDD - Ψ - plot, Berlin, 30.12.70 - 8.2.71, 9^{00} GMT

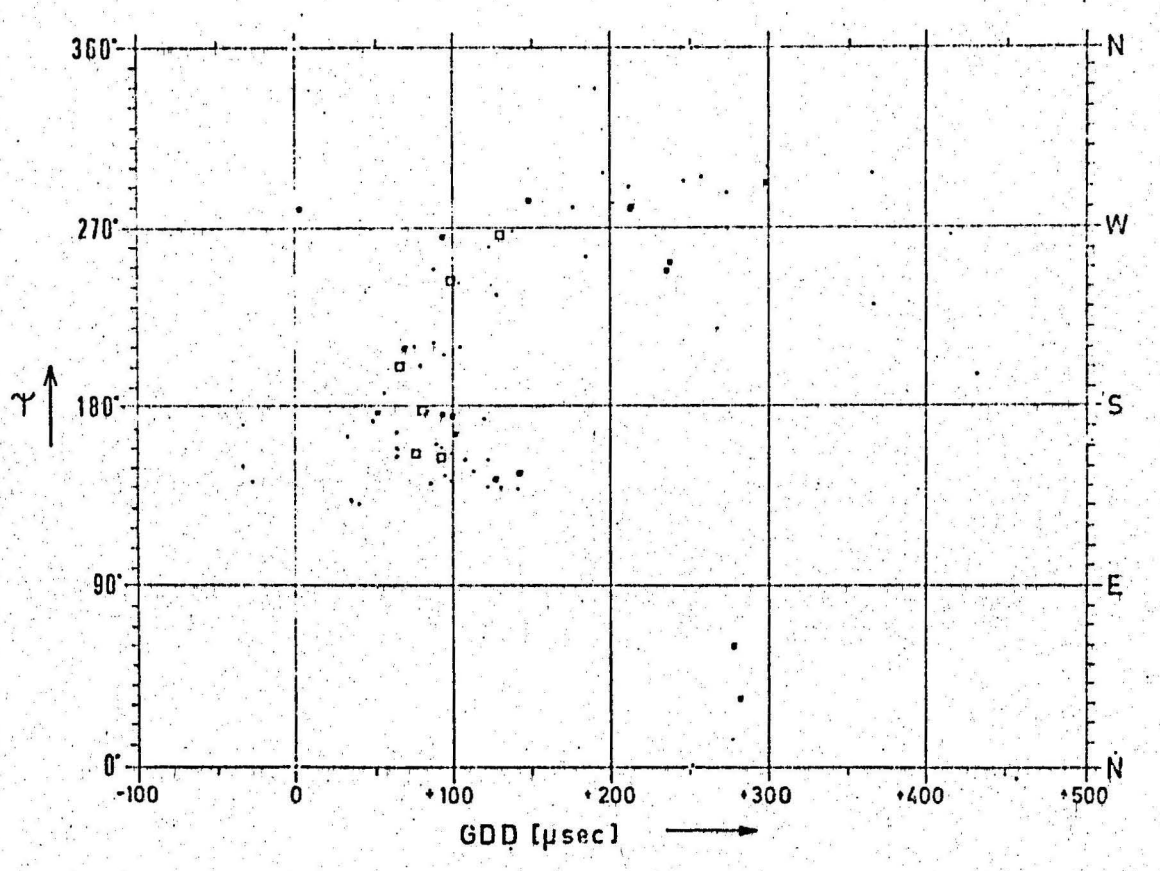

Fig. 10: GDD - Ψ - plot, Berlin , 30.12.70 - 8.2.71, 12^{00} GMT

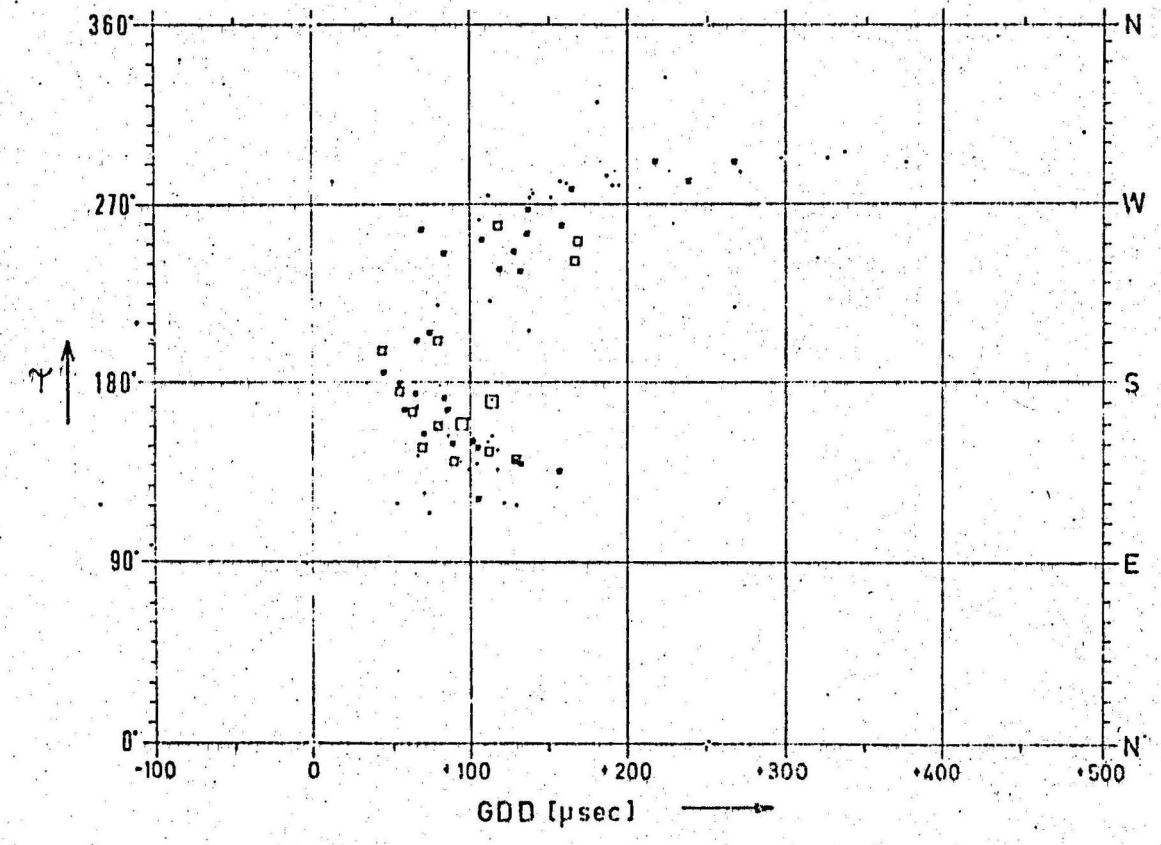

Fig. 11 : GDD - Ψ - plot, Berlin , 30.12.70 - 8.2.71, 15^{00} GMT

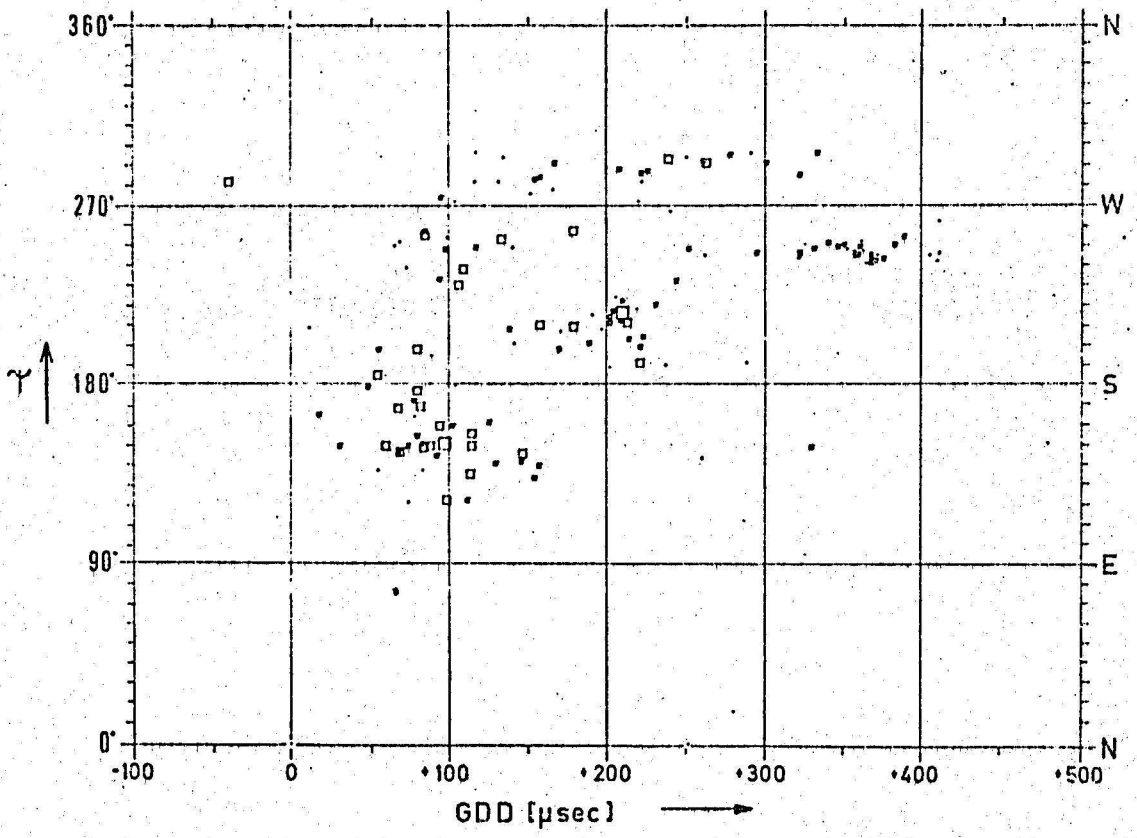

Fig. 12 : GDD - Ψ - plot, Berlin, 30.12.70 - 8.2.71, 18^{00} GMT

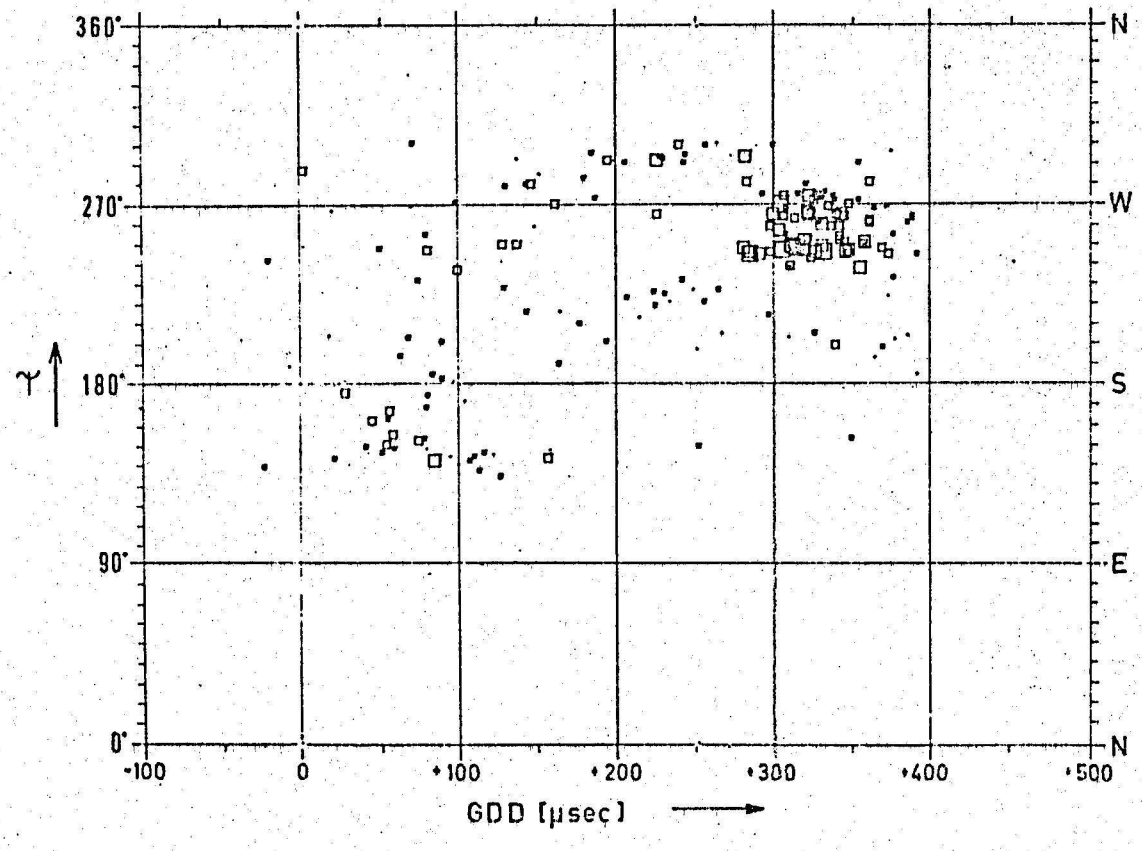

Fig. 13 : GDD - Ψ - plot, Berlin, 30.12.70 - 8.2.71, 21^{00} GMT

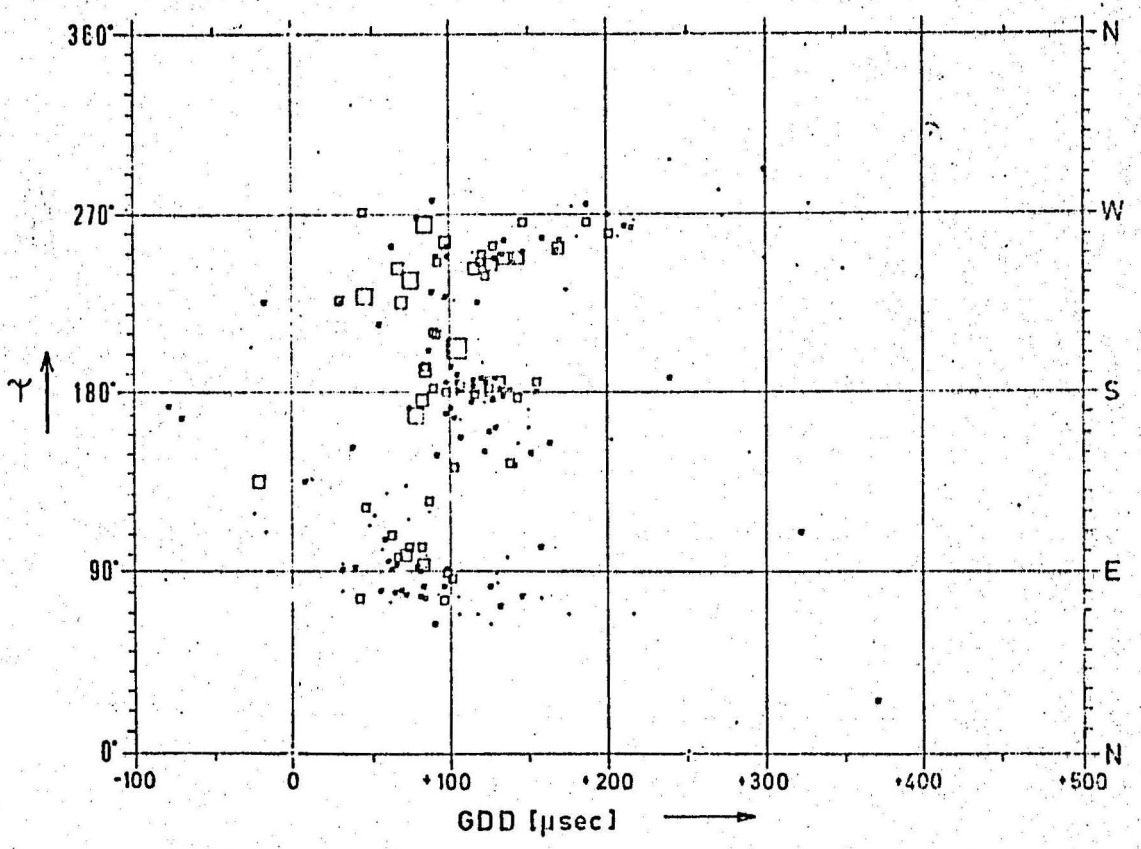

Fig. 14 : GDD - Ψ - plot, Waldorf, 19.12.70 - 1.2.71, 0^{00} GMT

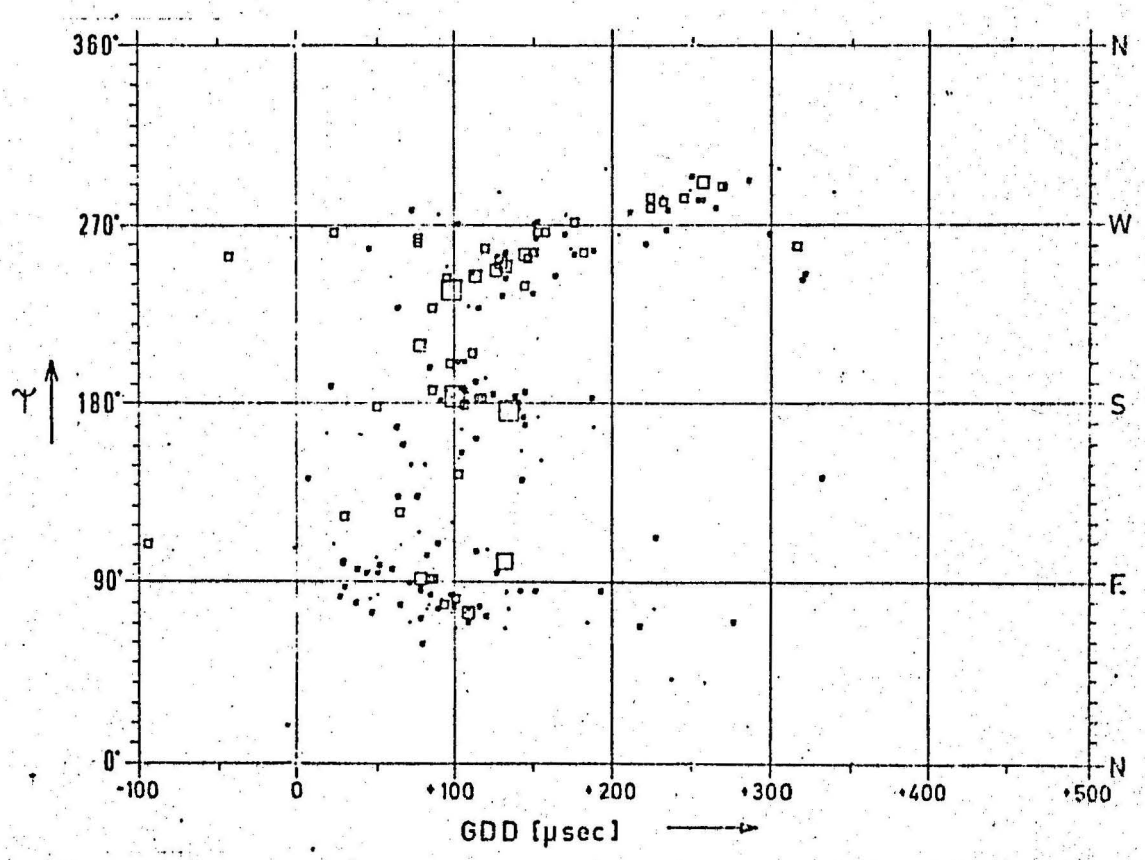

Fig. 15 : GDD - Ψ - plot, Waldorf, 19.12.70 - 1.2.71, 3^{00} GMT

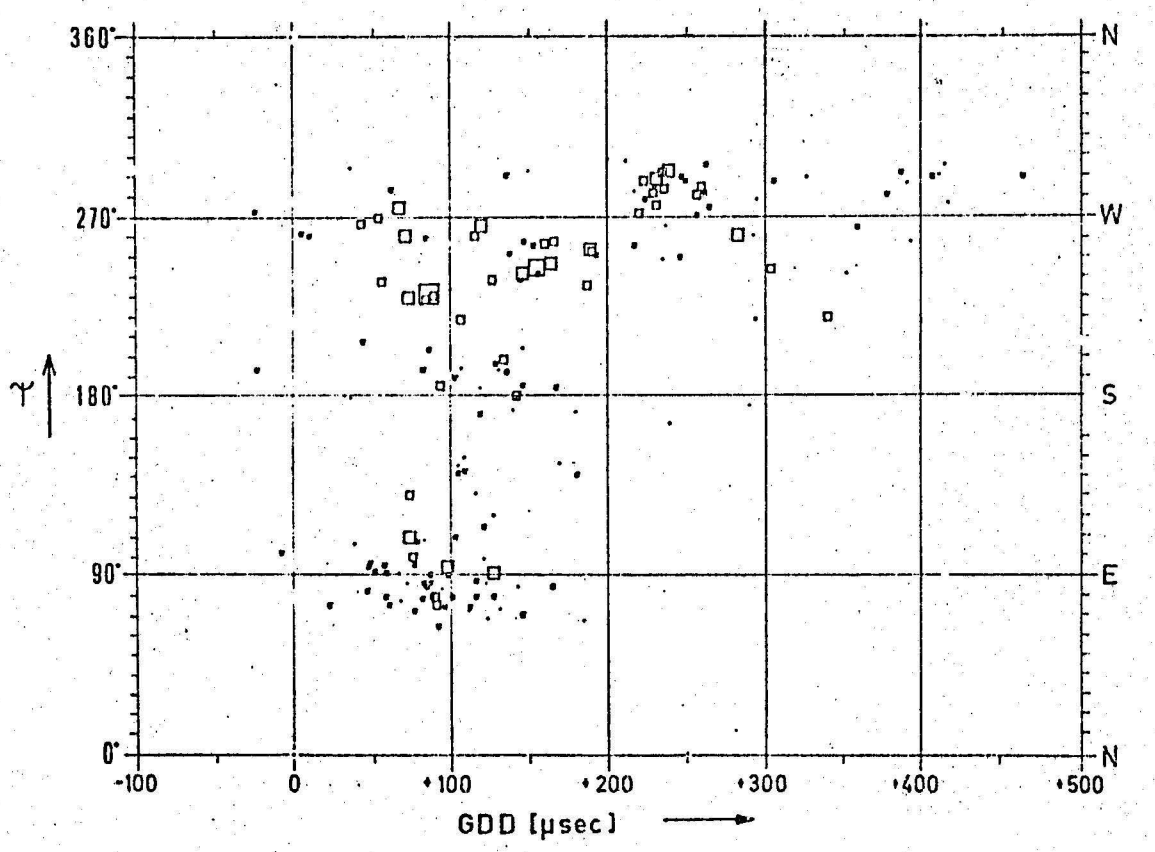

Fig. 16 : GDD - Ψ - plot, Waldorf , 19.12.70 - 1.2.71 , 6^{00} GMT

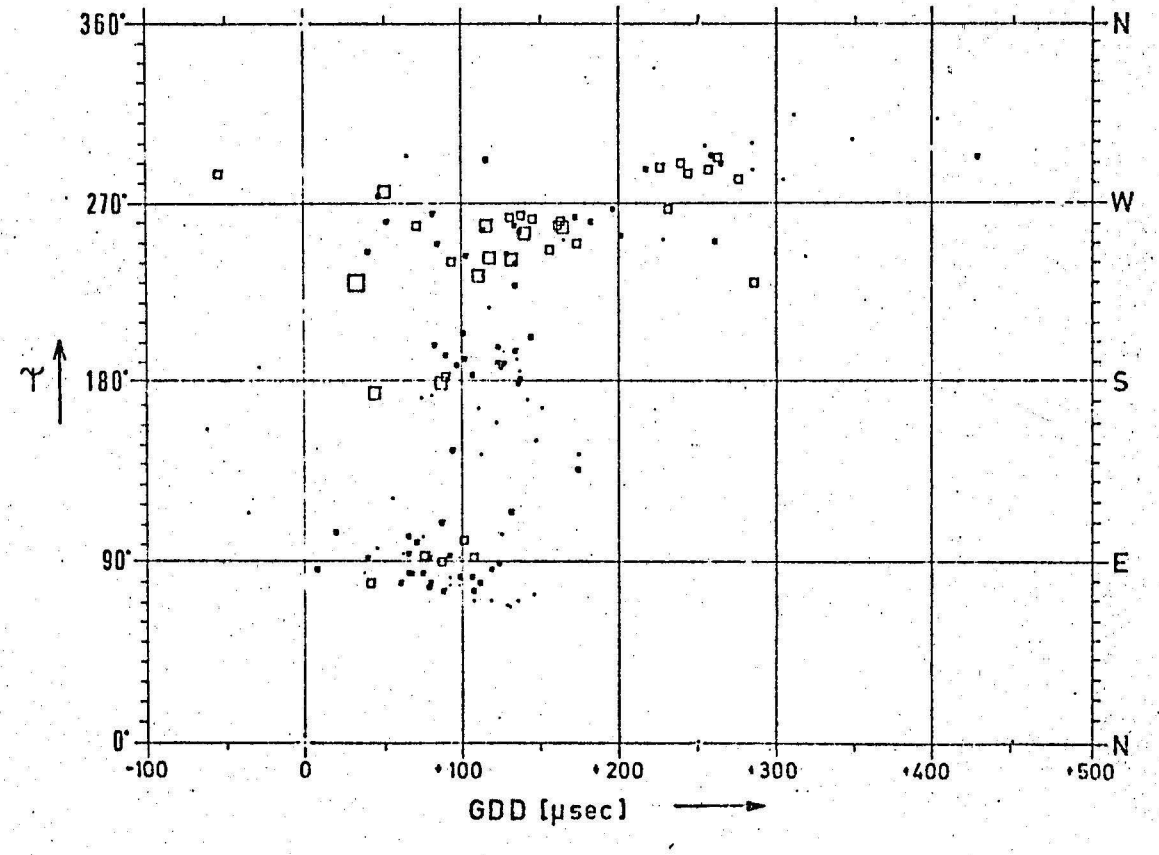

Fig. 17 : GDD - Ψ - plot, Waldorf, 19.12.70 - 1.2.71,9^{00} GMT

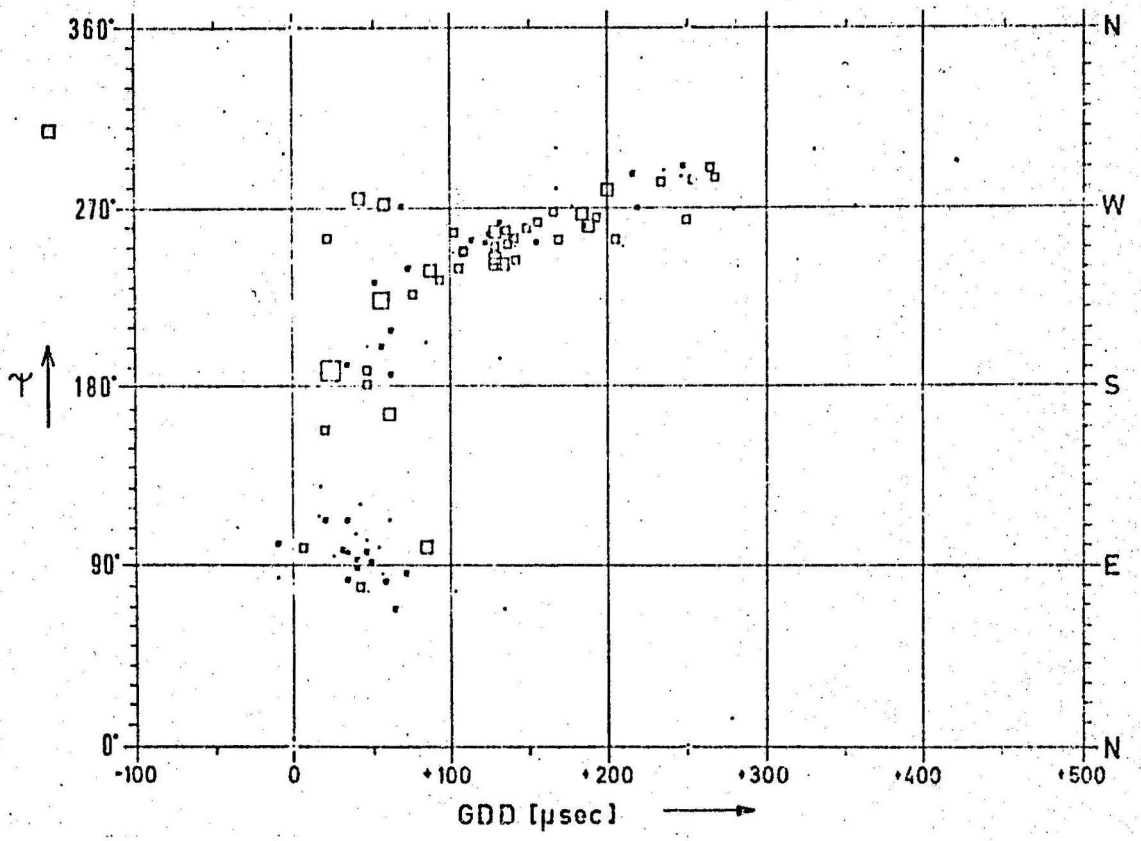

Fig. 18 : GDD - Ψ - plot , Waldorf , 19.12.70 - 1.2.71 , 12^{00} GMT

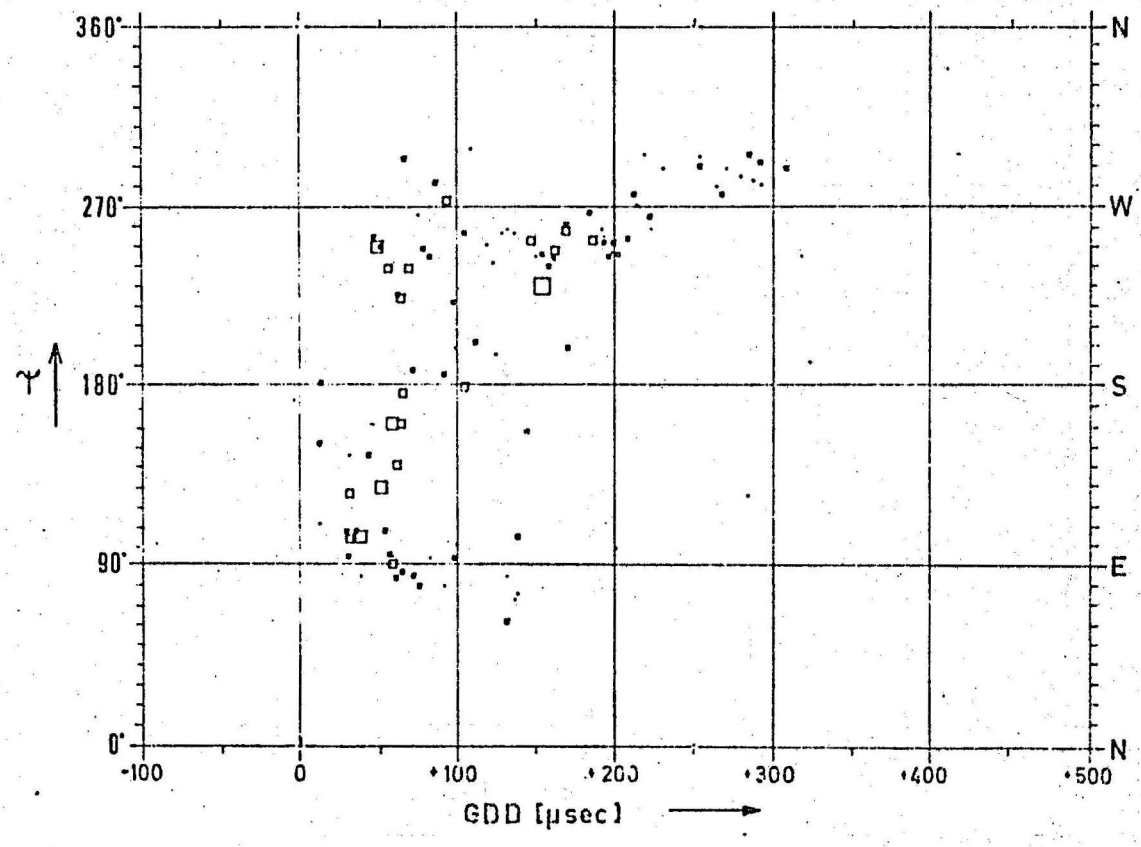

Fig. 19: GDD - Ψ - plot, Waldorf, 19.12.70 - 1.2.71, 15^{00} GMT

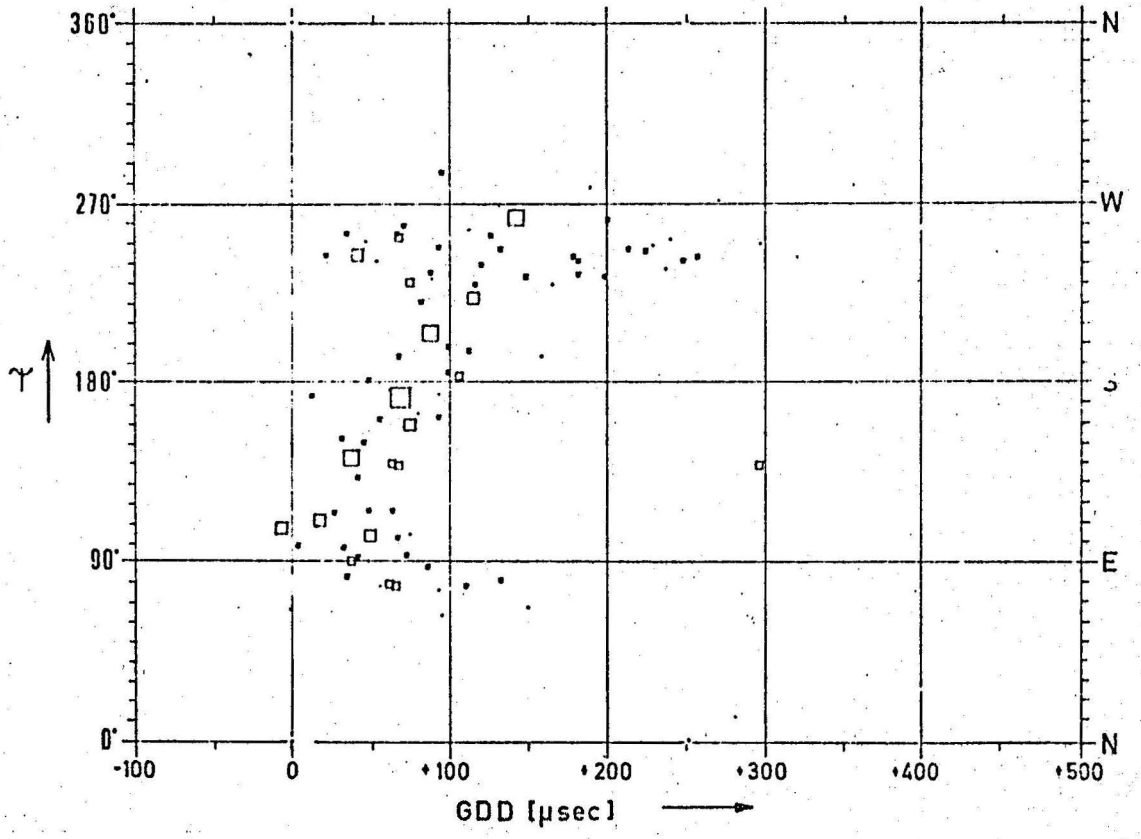

Fig. 20 : GDD - Ψ - plot, Waldorf, 19.12.70 - 1.2.71, 18^{00} GMT

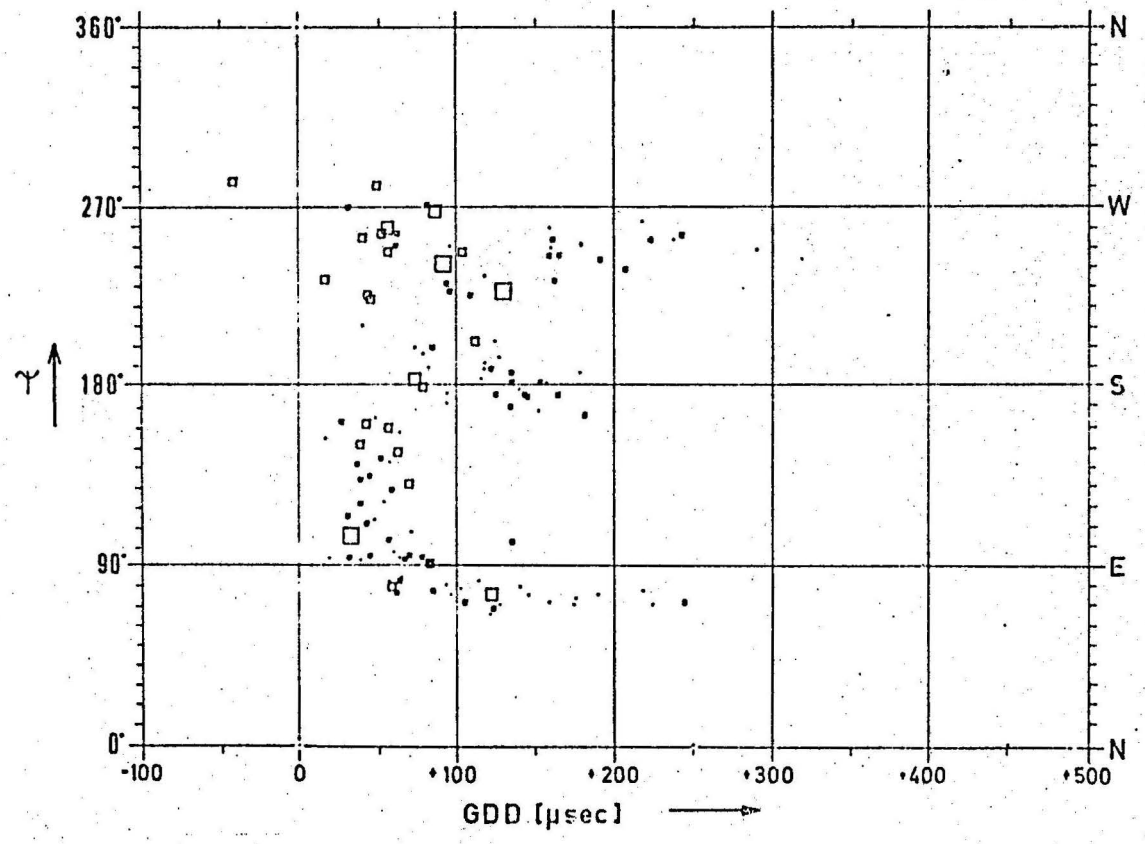

Fig. 21: GDD - Ψ - plot, Waldorf, 19.12.70 - 1.2.71, 21^{00} GMT

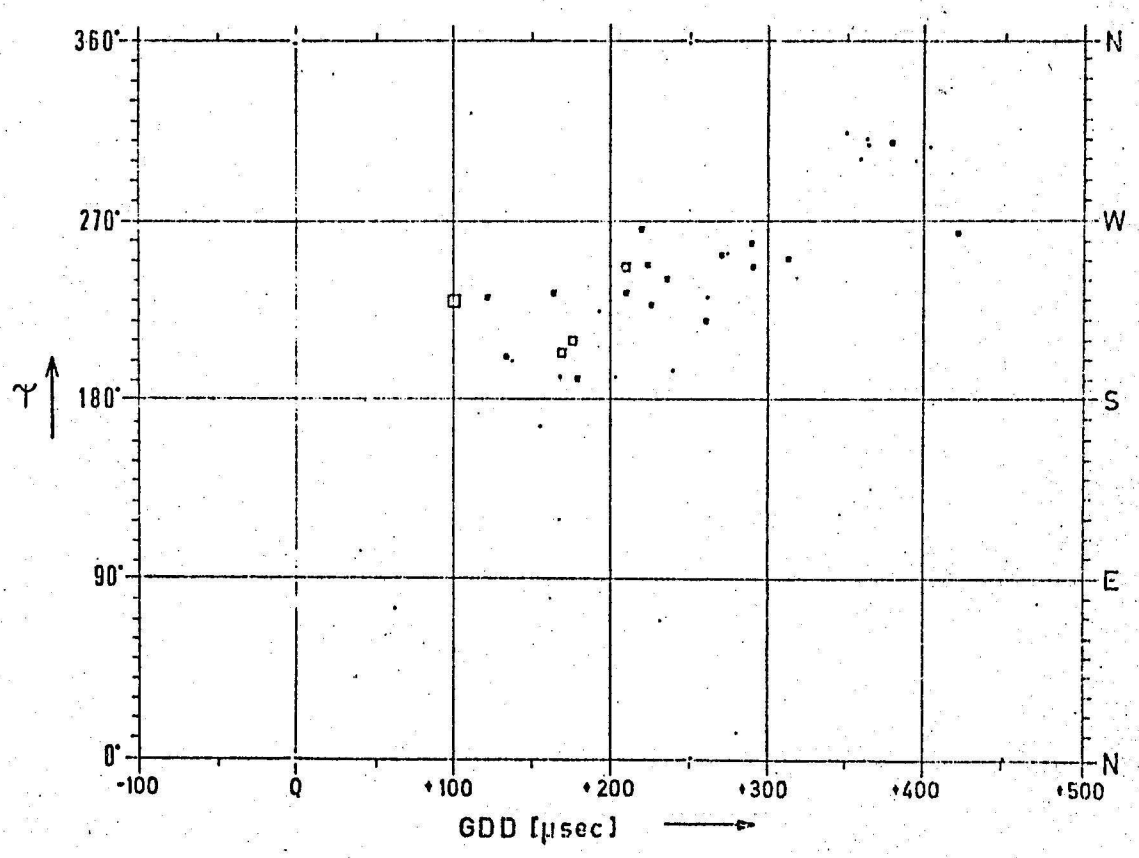

Fig. 22 : GDD - Ψ - plot, Tyokawa , 9.12.70 - 23.12.70 , 0^{OO} GMT

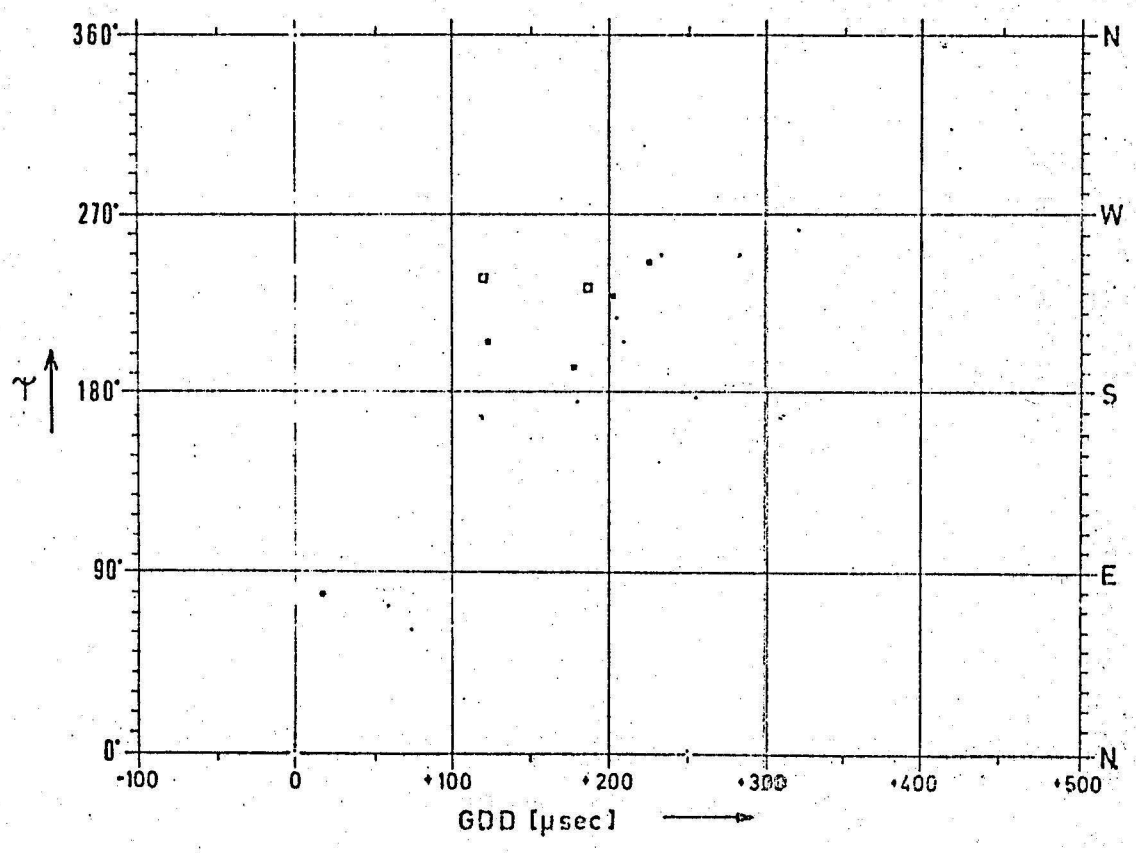

Fig. 23 : GDD - Ψ - plot, Toyokawa , 9.12.70 - 23.12.70, 3^{OO} GMT

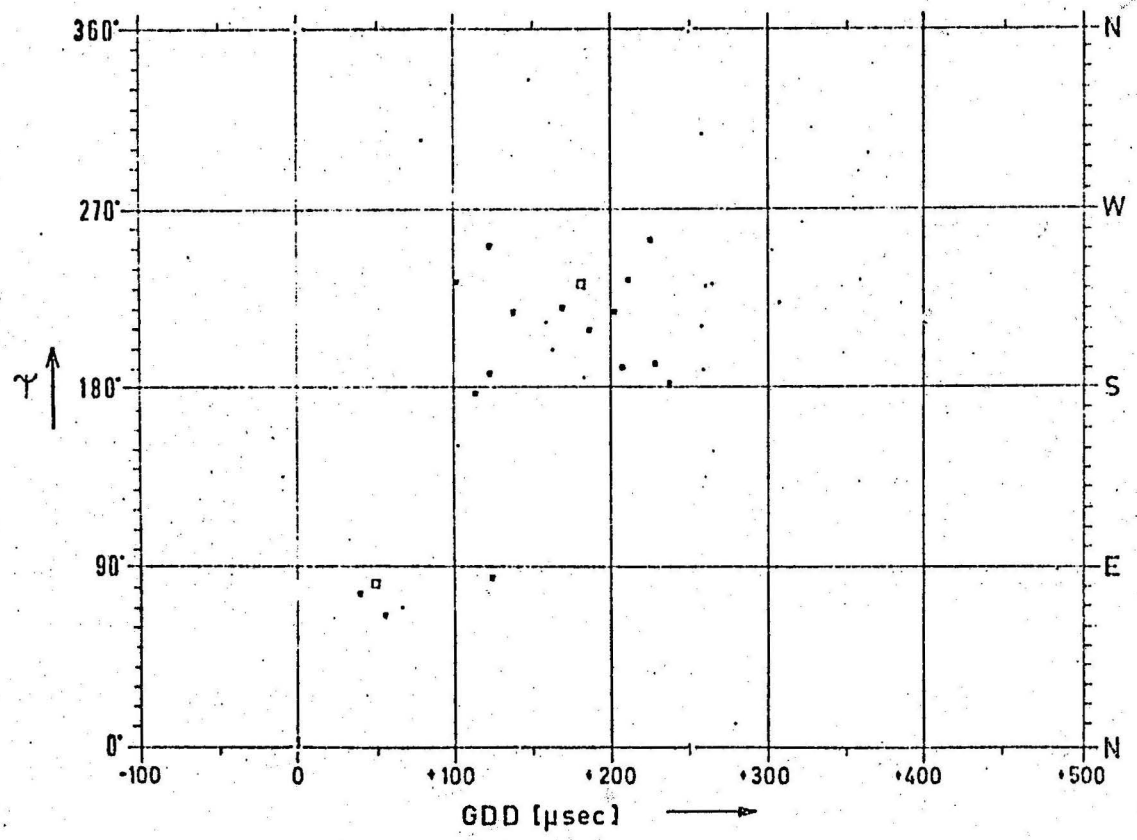

Fig. 24 : GDD - Ψ - plot, Toyokawa, 9.12.70 - 23.12.70, 6^{00} GMT

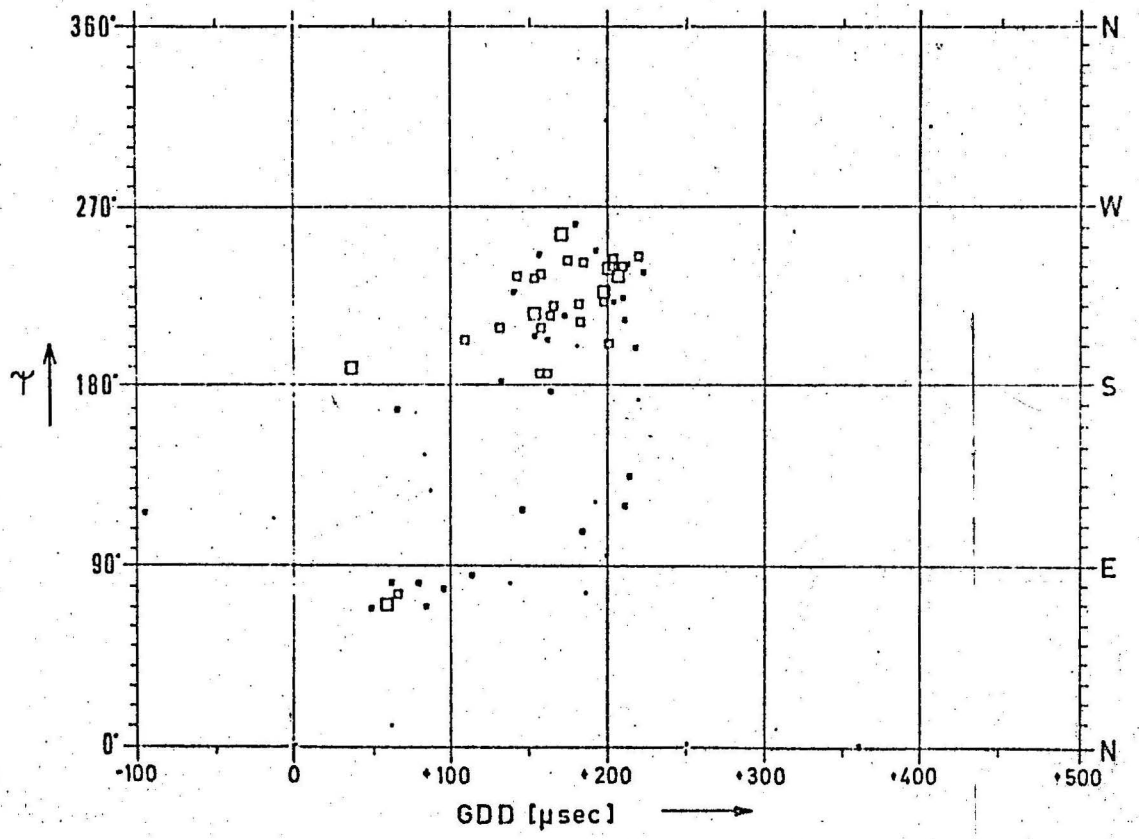

Fig. 25 : GDD - Ψ - plot, Toyokawa , 9.12.70 - 23.12.70, 9^{00} GMT

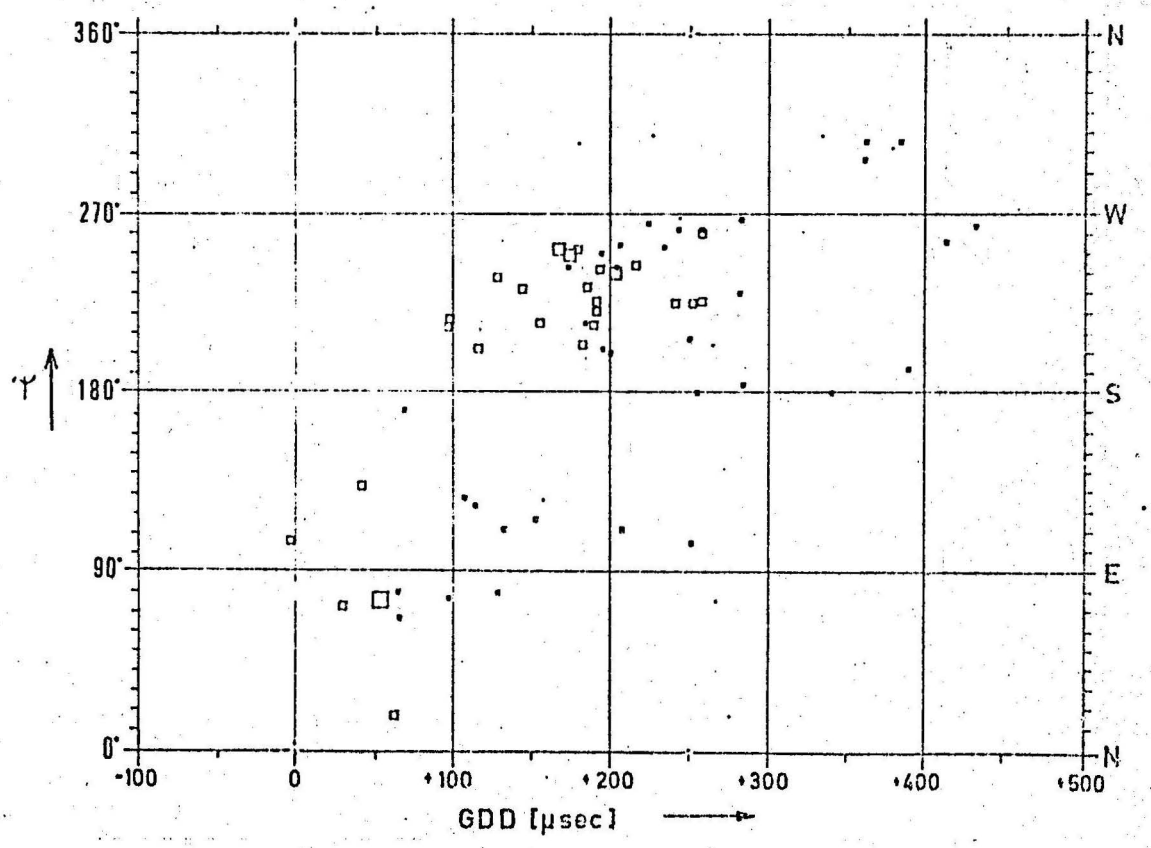

Fig. 26 :. GDD - Ψ - plot, Toyokawa , 9.12.70 - 23.12.70 12^{00} GMT

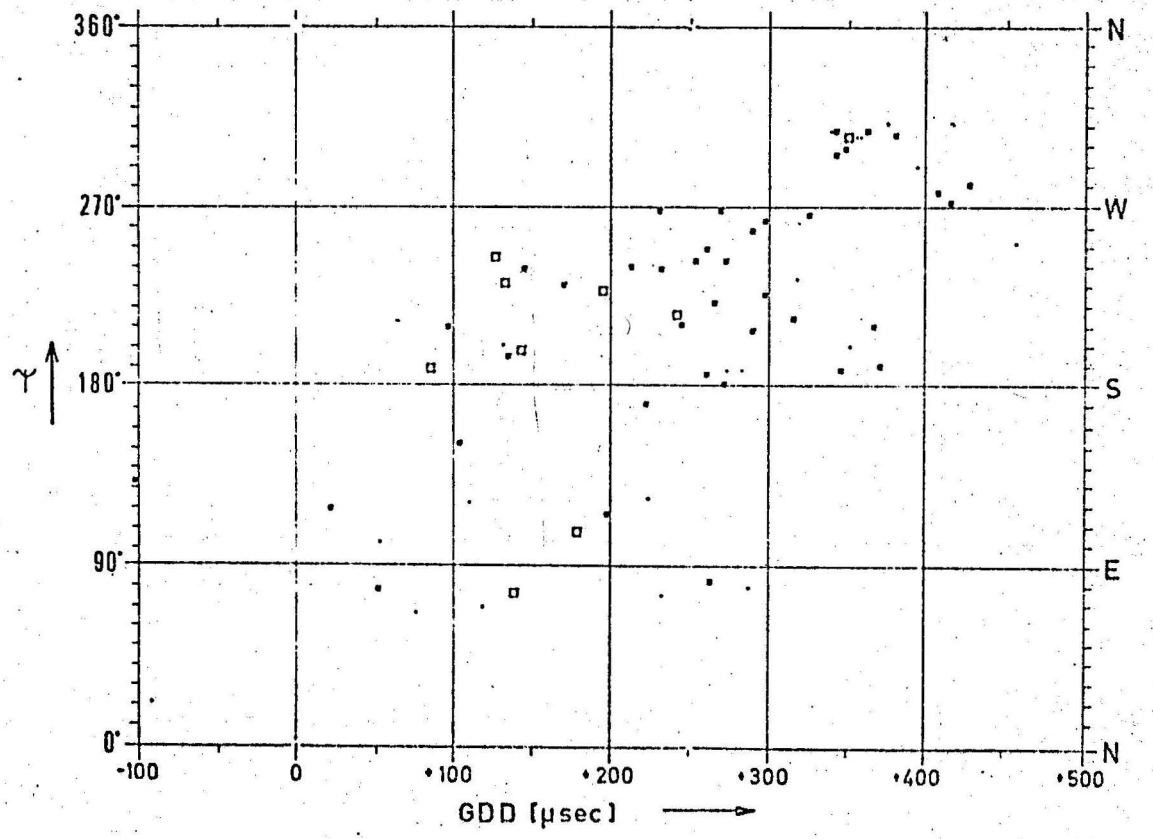

Fig. 27 : GDD - Ψ - plot, Toyokawa , 9.12.70 - 23.12.70, 15^{00} GMT

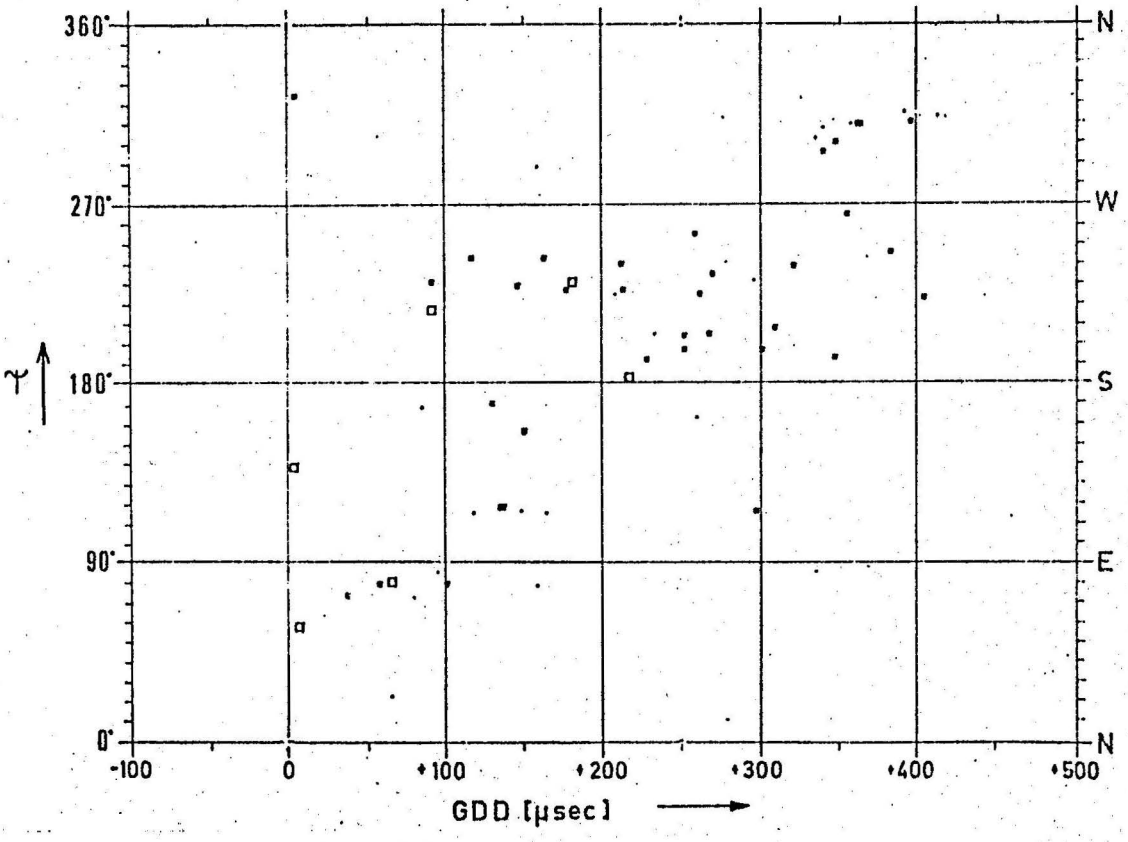

Fig. 28 : GDD - Ψ - plot, Toyokawa , 9.12.70 - 23.12.70, 18^{00} GMT

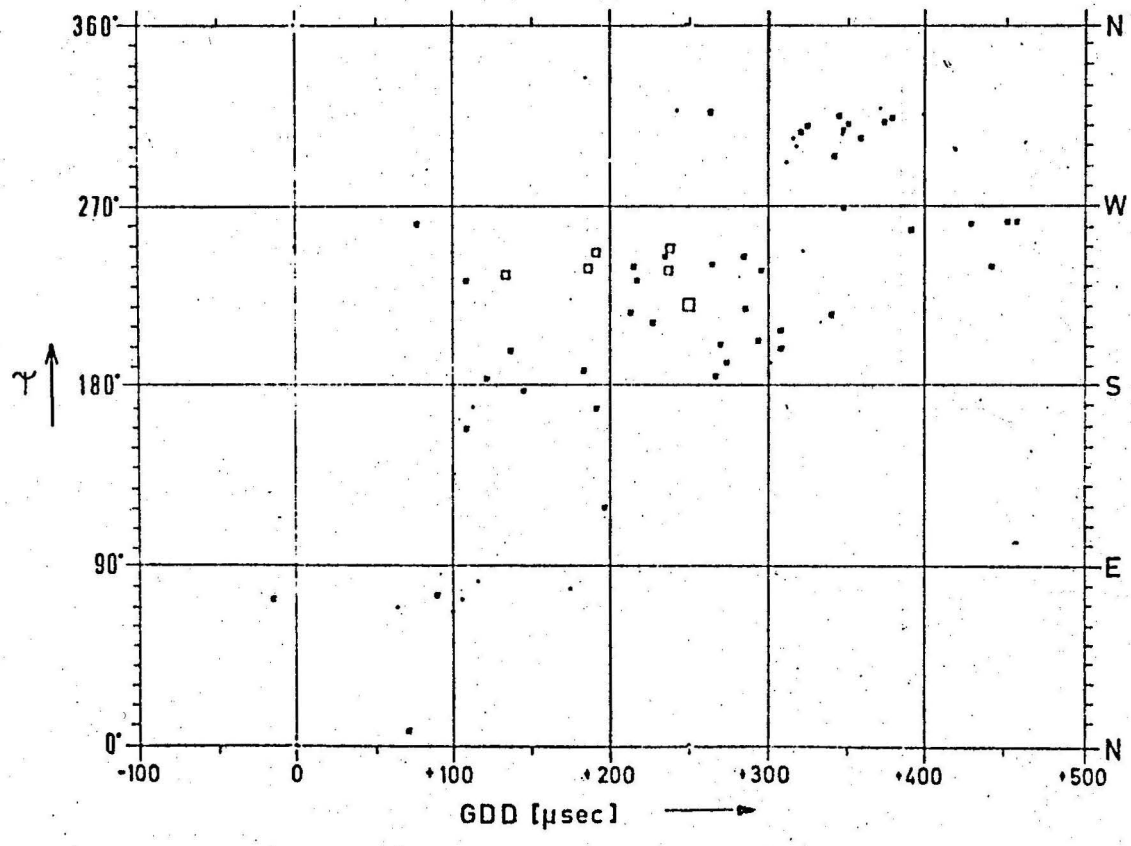

Fig. 29 : GDD - Ψ - plot, Toyokawa, 9.12.70 - 23.12.70, 21^{00} GMT

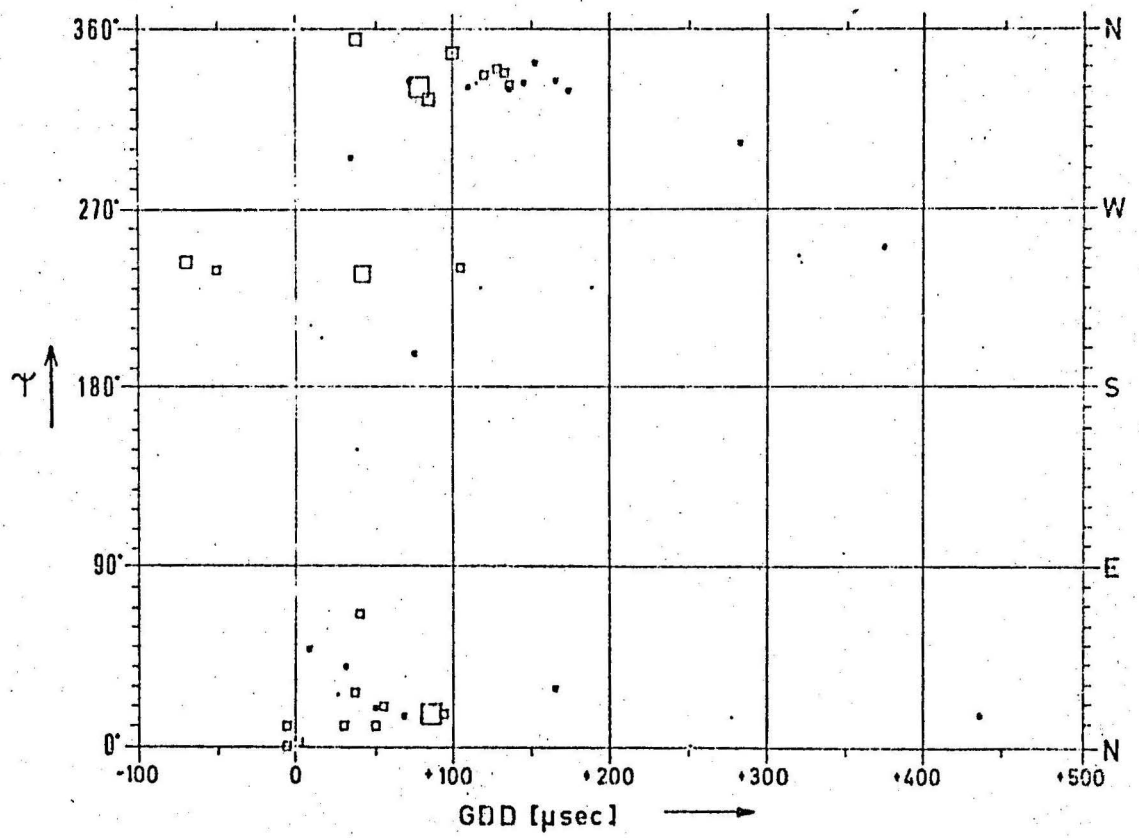

Fig. 30 : GDD - Ψ - plot, San Miguel, 16.11.70 - 30.11.70, 0^{00} GMT

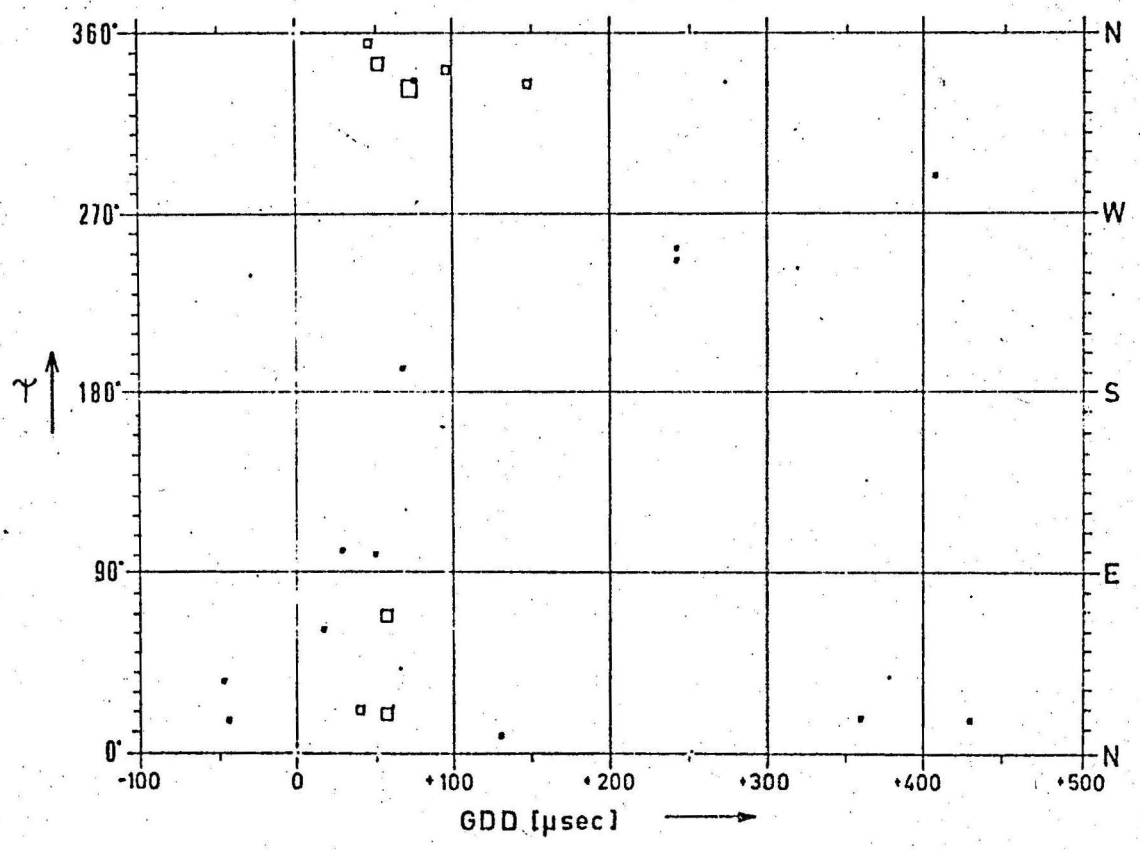

Fig. 31 : GDD - Ψ - plot, San Miguel, 16.11.70 - 30.11.70 3^{00} GMT

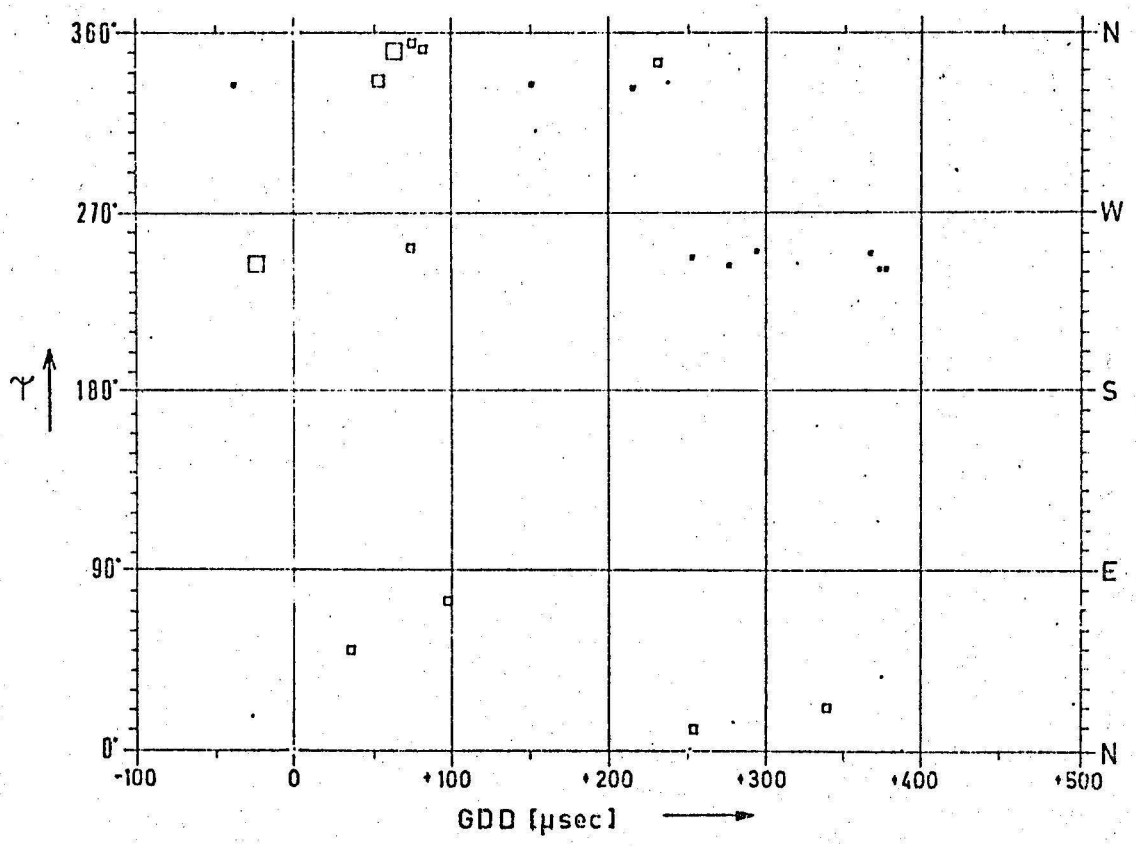

Fig. 32 : GDD - Ψ - plot, San Miguel, 16.11.70 - 30.11.70, 6^{00} GMT

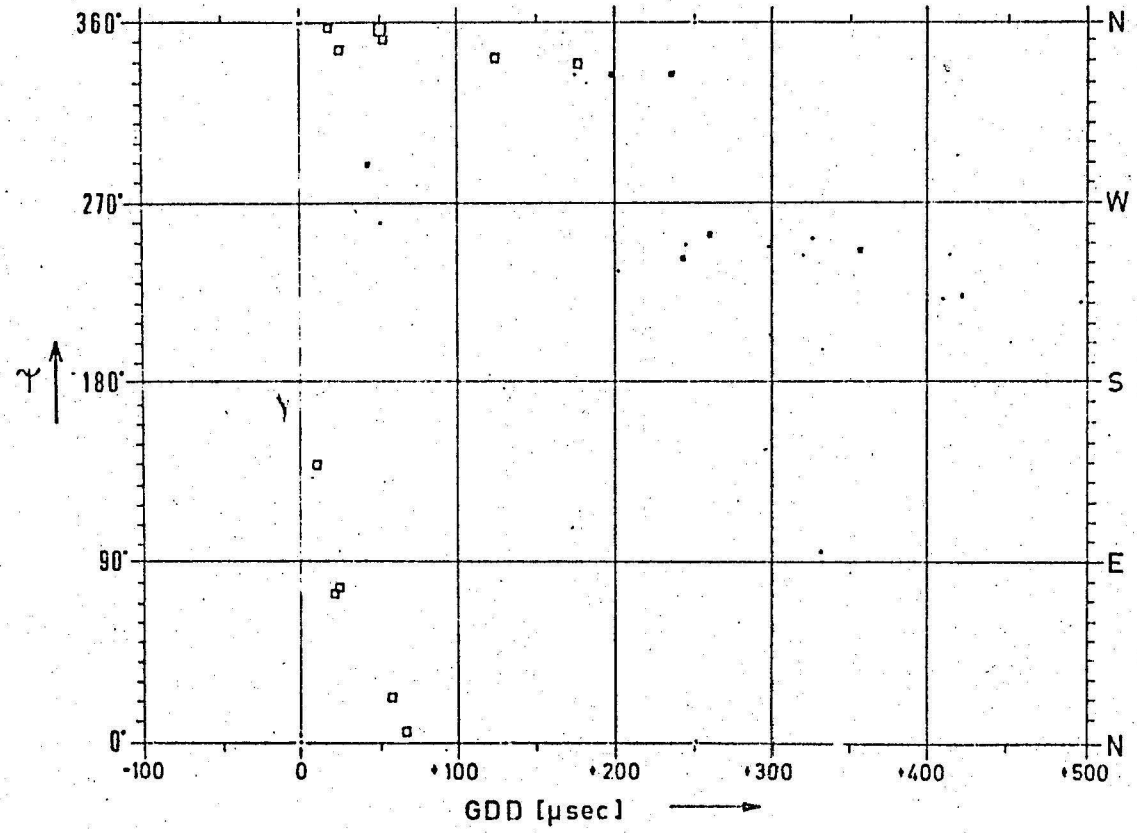

Fig. 33 : GDD - Ψ - plot, San Miguel, 16.11.70 - 30.11.70, 9^{00} GMT

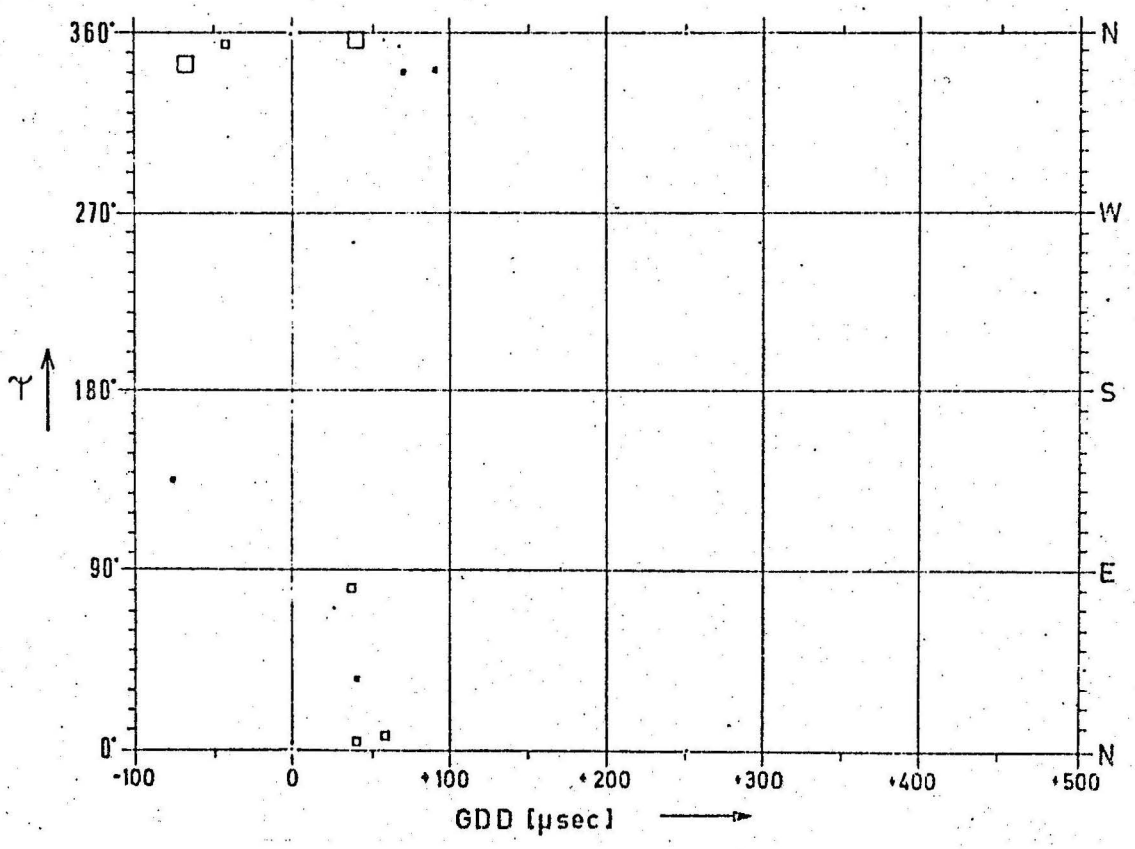

Fig. 34 : GDD - Ψ - plot, San Miguel, 16.11.70 - 30.11.70, 12^{00} GMT

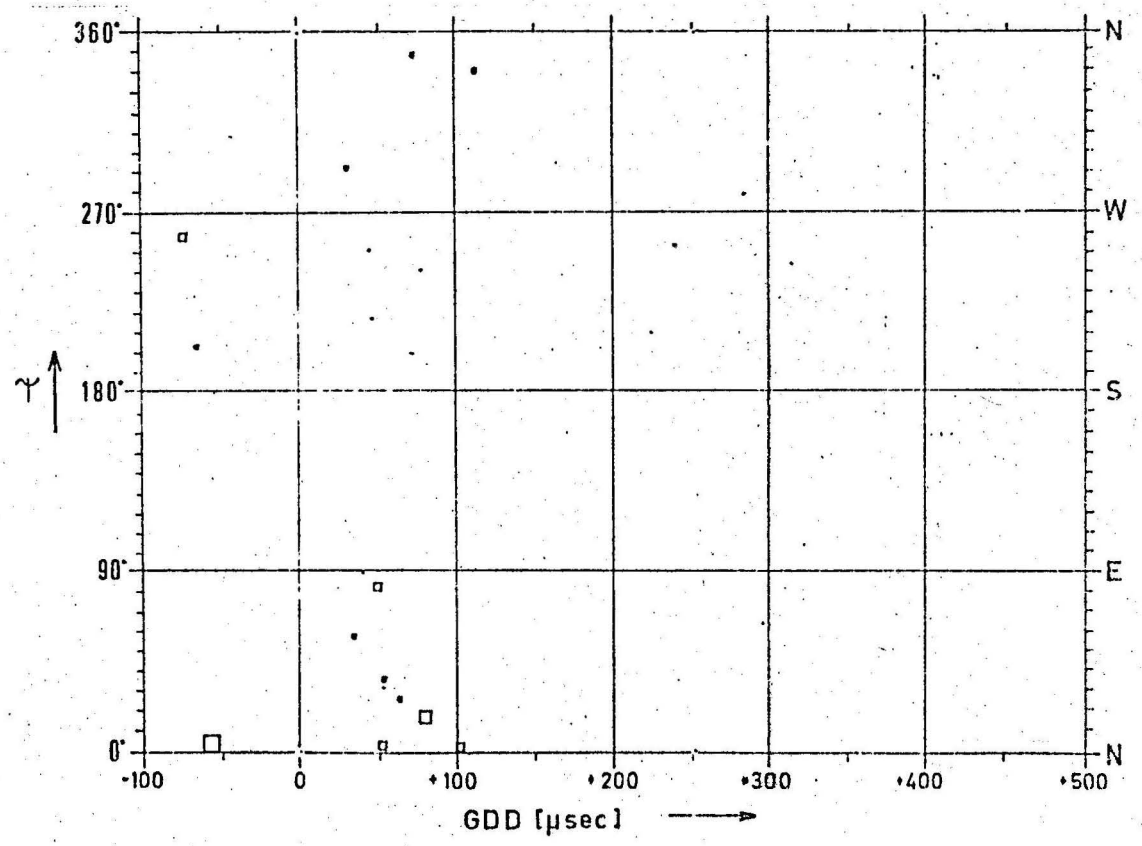

Fig. 35 : GDD - Ψ - plot, San Miguel, 16.11.70 - 30.11.70, 15^{00} GMT

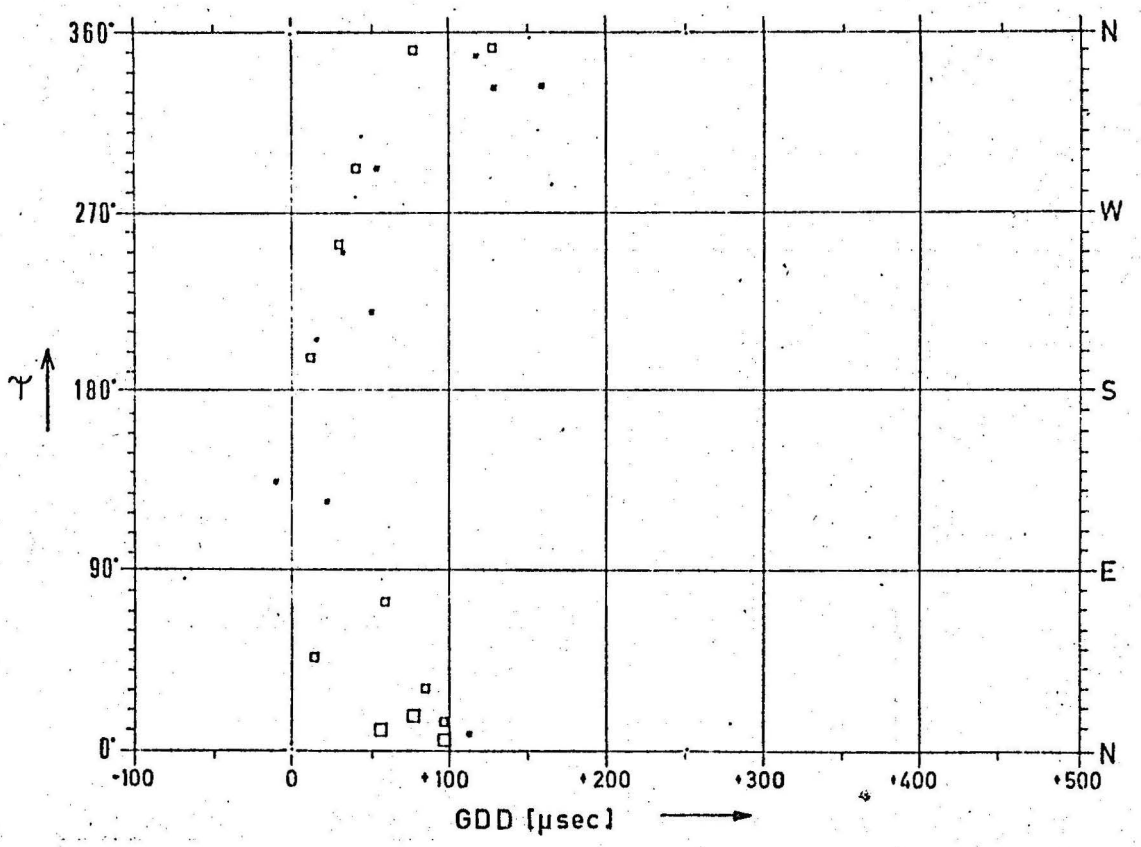

Fig. 36 : GDD - Ψ - plot, San Miguel, 16.11.70 - 30.11.70, 18^{00} GMT

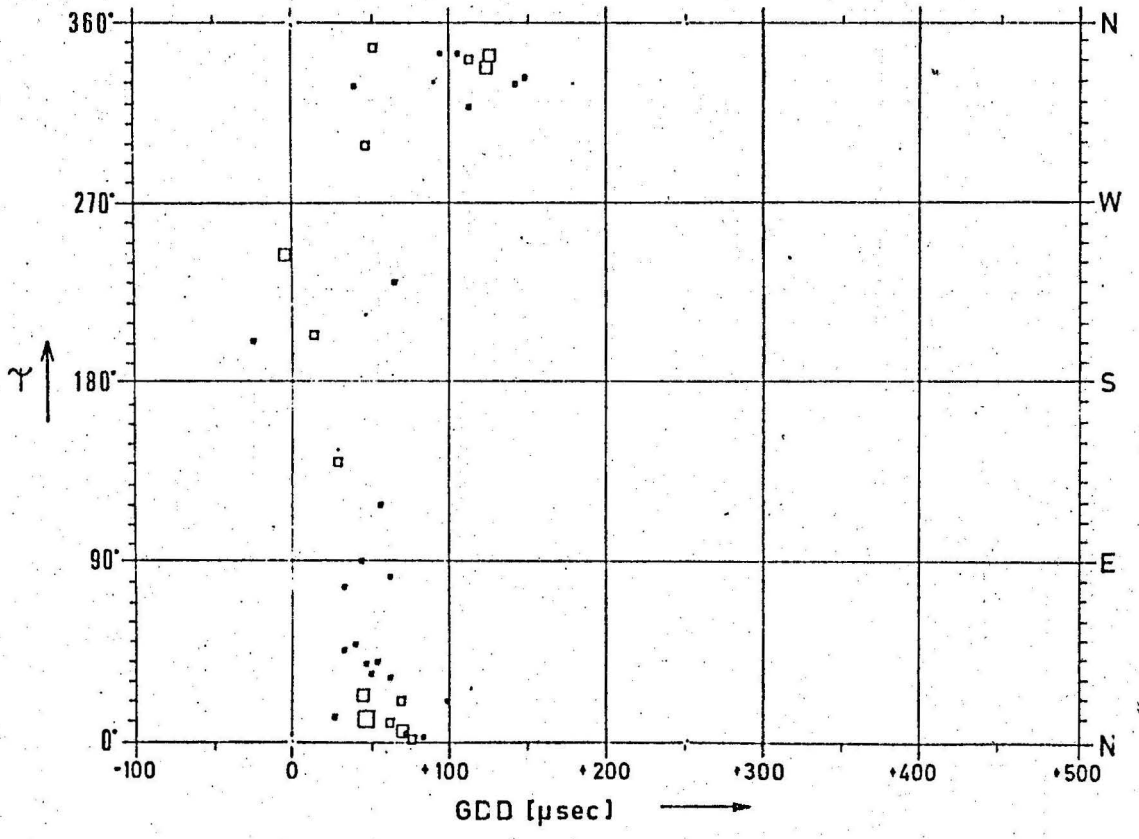

Fig. 37 : GDD - Ψ - plot, San Miguel, 16.11.70 - 30.11.70, 21^{00} GMT

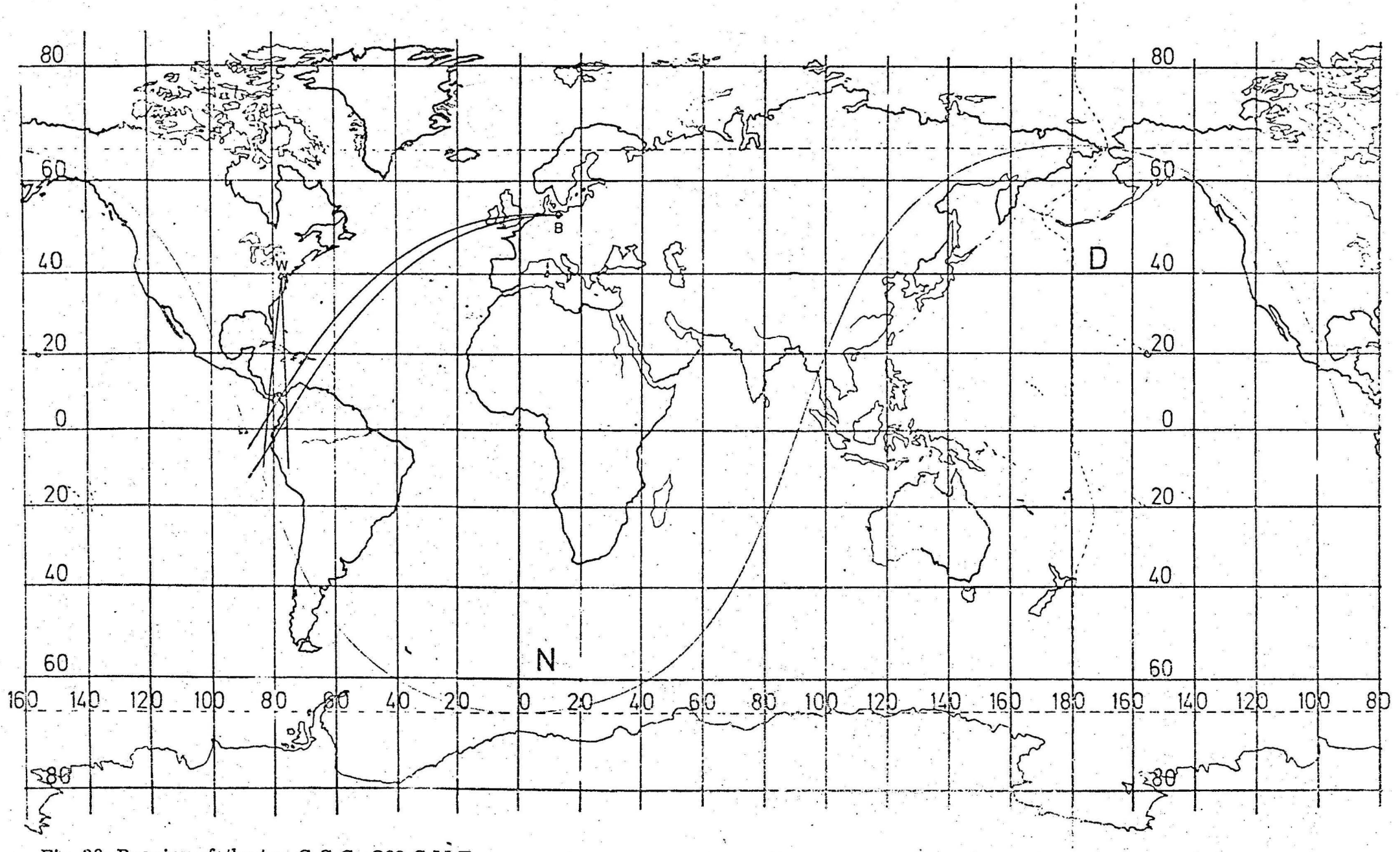

Fig. 38: Bearing of the two C C C, 000 G M T

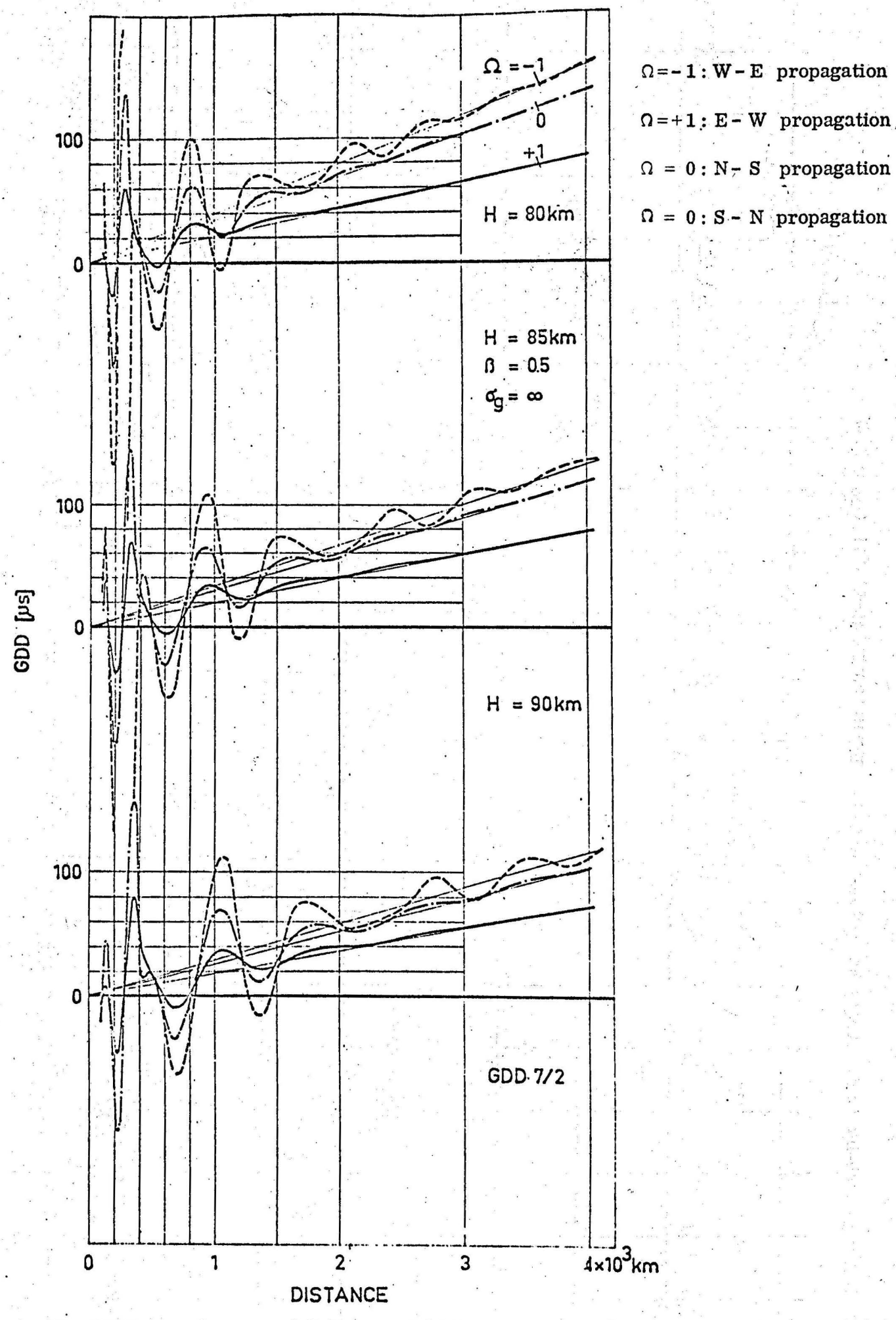

Fig. 39 : GDD as a function of distance, night time model (Harth, 1971)

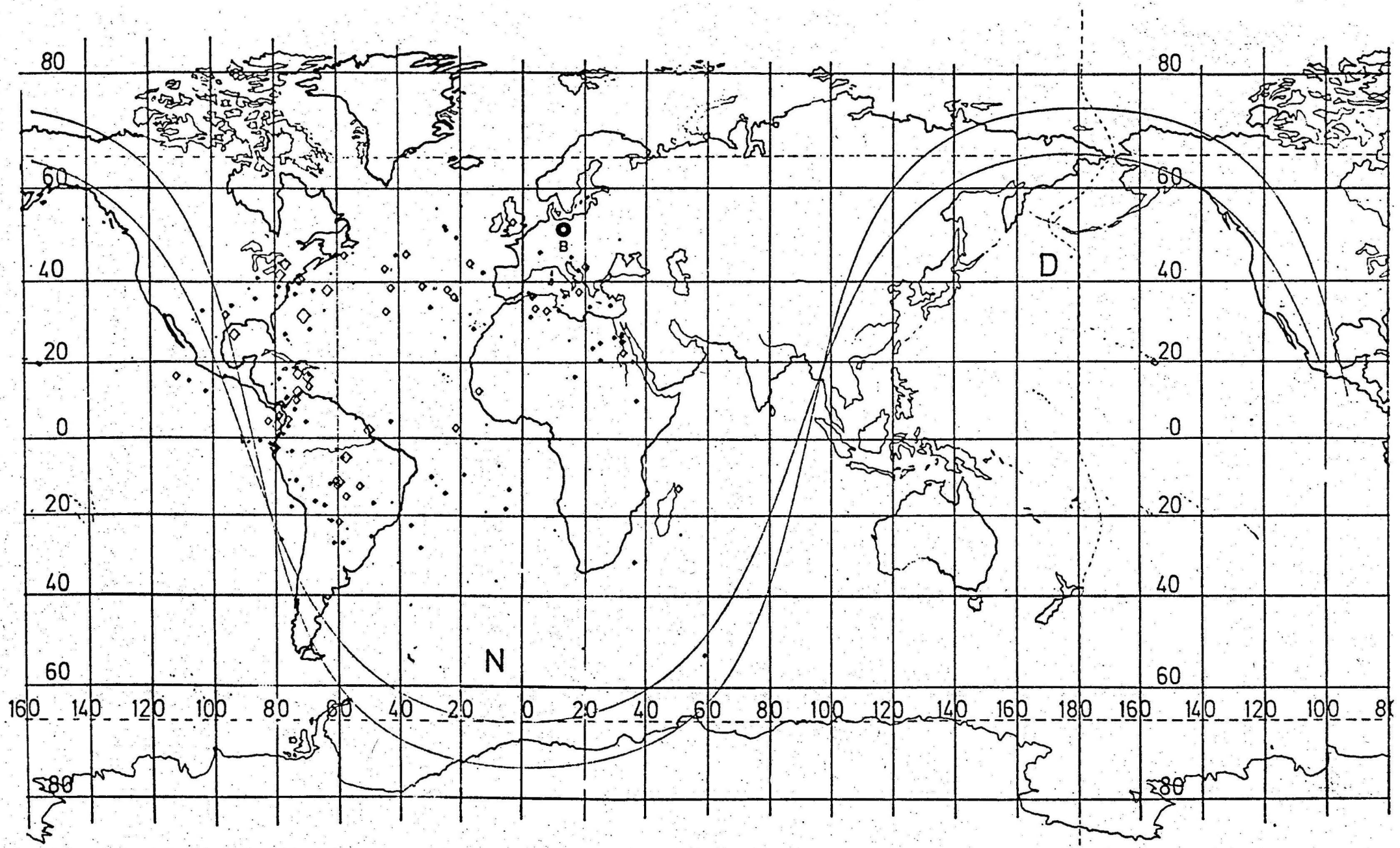

Fig. 40: G D D- Map-plot, night conditions ($\sigma g = \infty$, H=86 km) Berlin, 30. 12. 70–8. 2. 71 0^{00} G M T

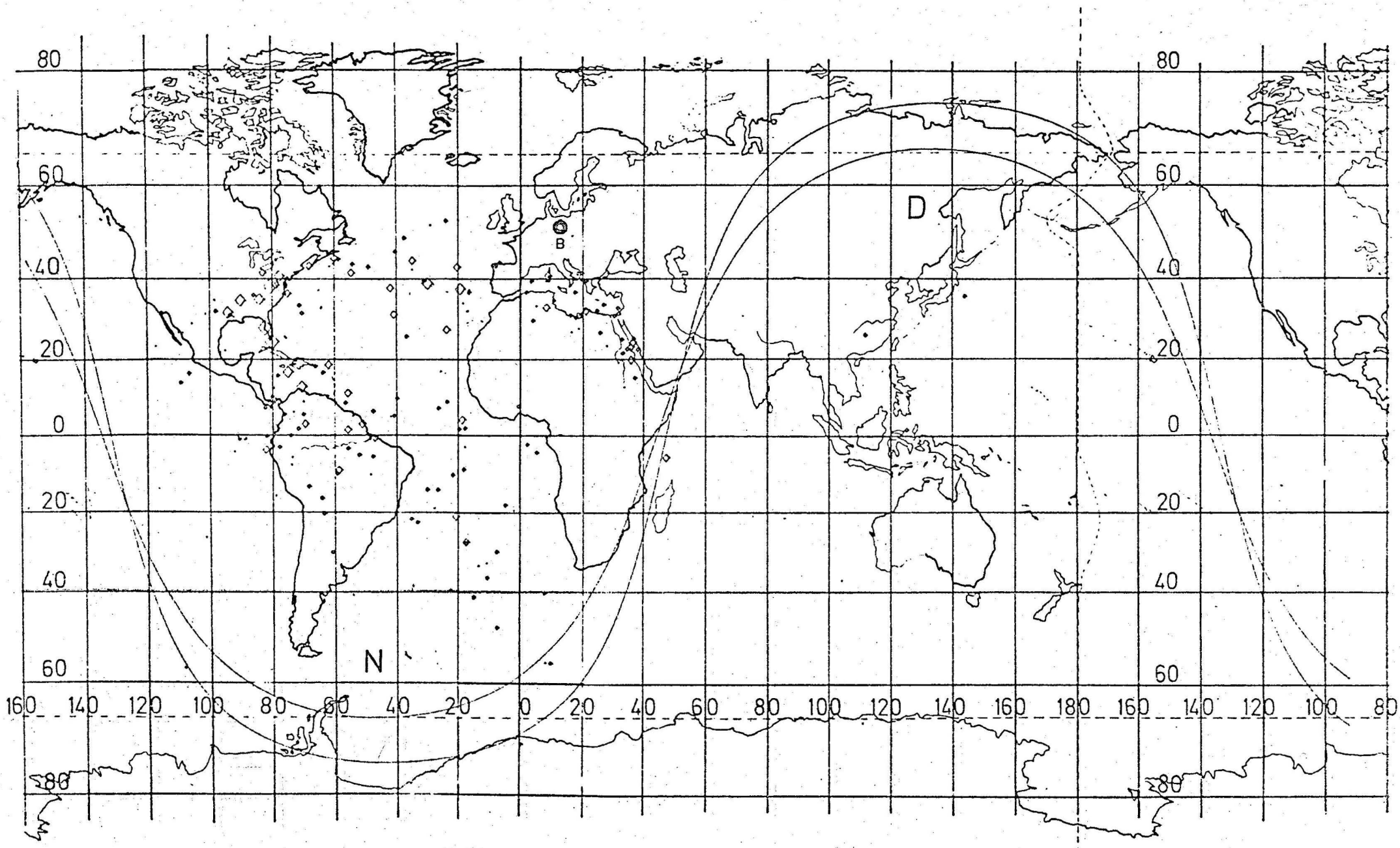

Fig. 41: G D D - Map-plot, night conditions ($\sigma g = \infty$, H=86 km) Berlin, 30. 12. 70-8. 2. 71 3^{00} G M T

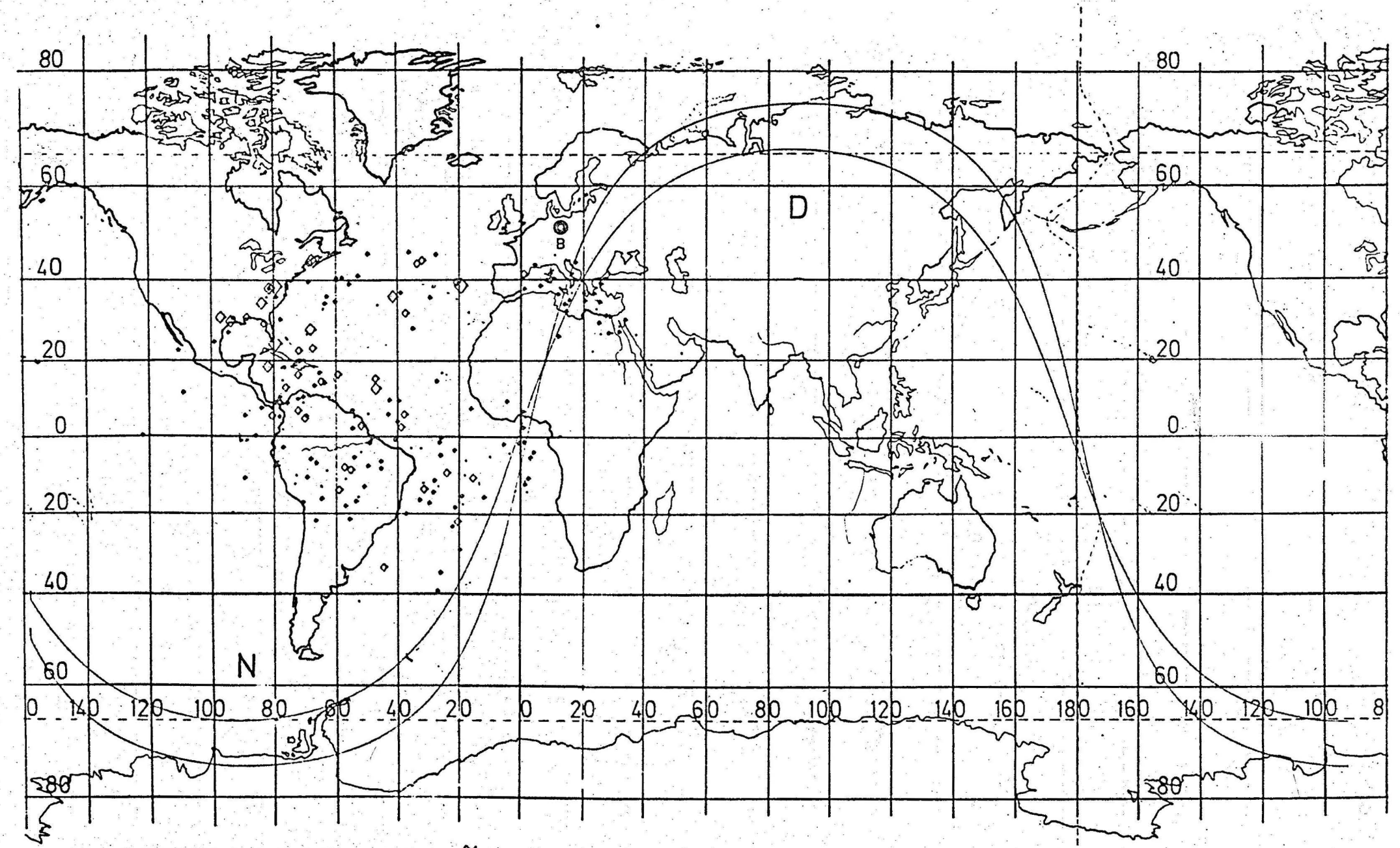

Fig. 42: G D D – Map-plot, night conditions (σ g=∞ , H=86 km) Berlin, 30. 12. 70–8. 2. 71 6^{00} G M T

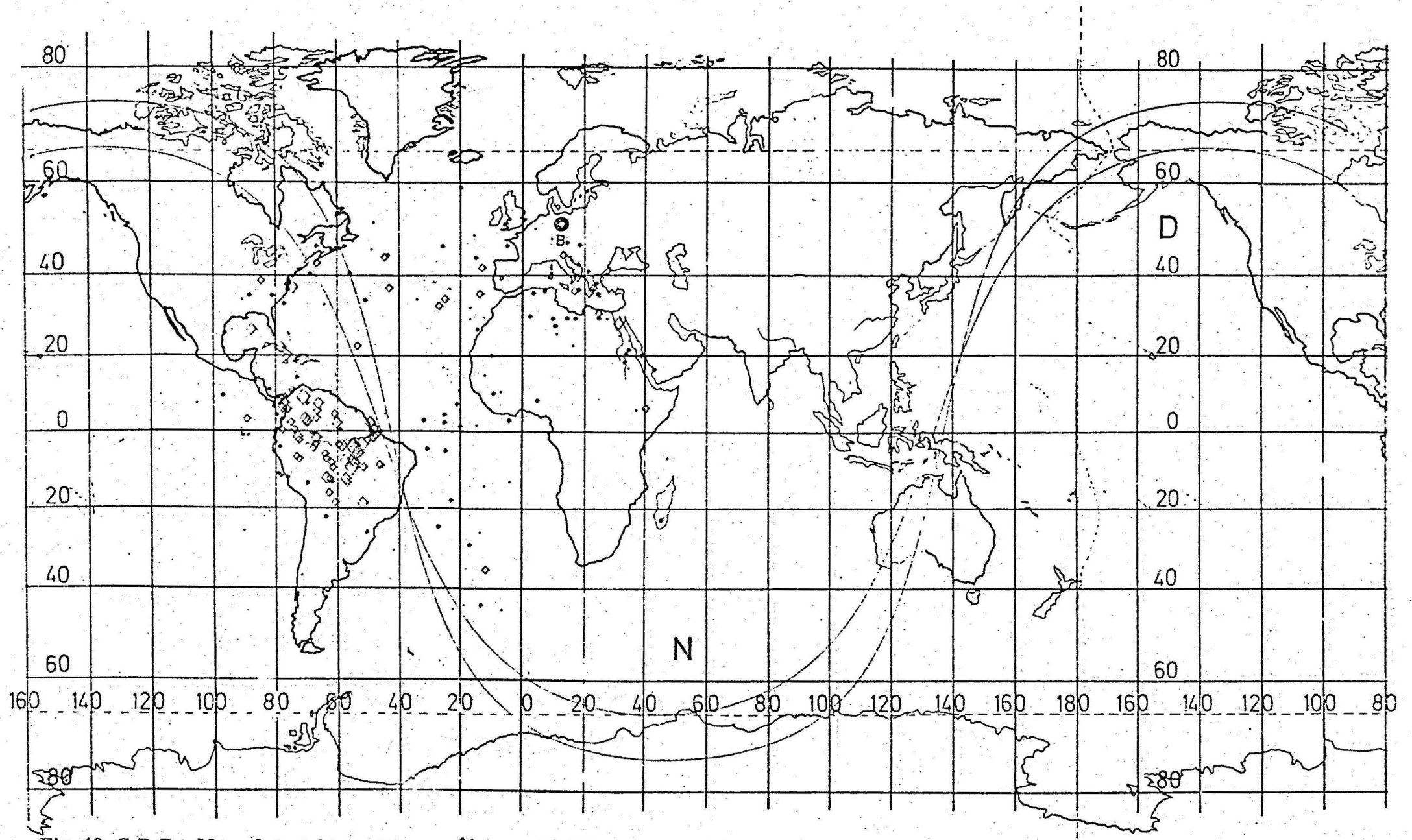

Fig. 43: G D D – Map-plot, night conditions (σ g=∞ , H=86 km) Berlin, 30. 12. 70–8. 2. 71 21^{00} G M T

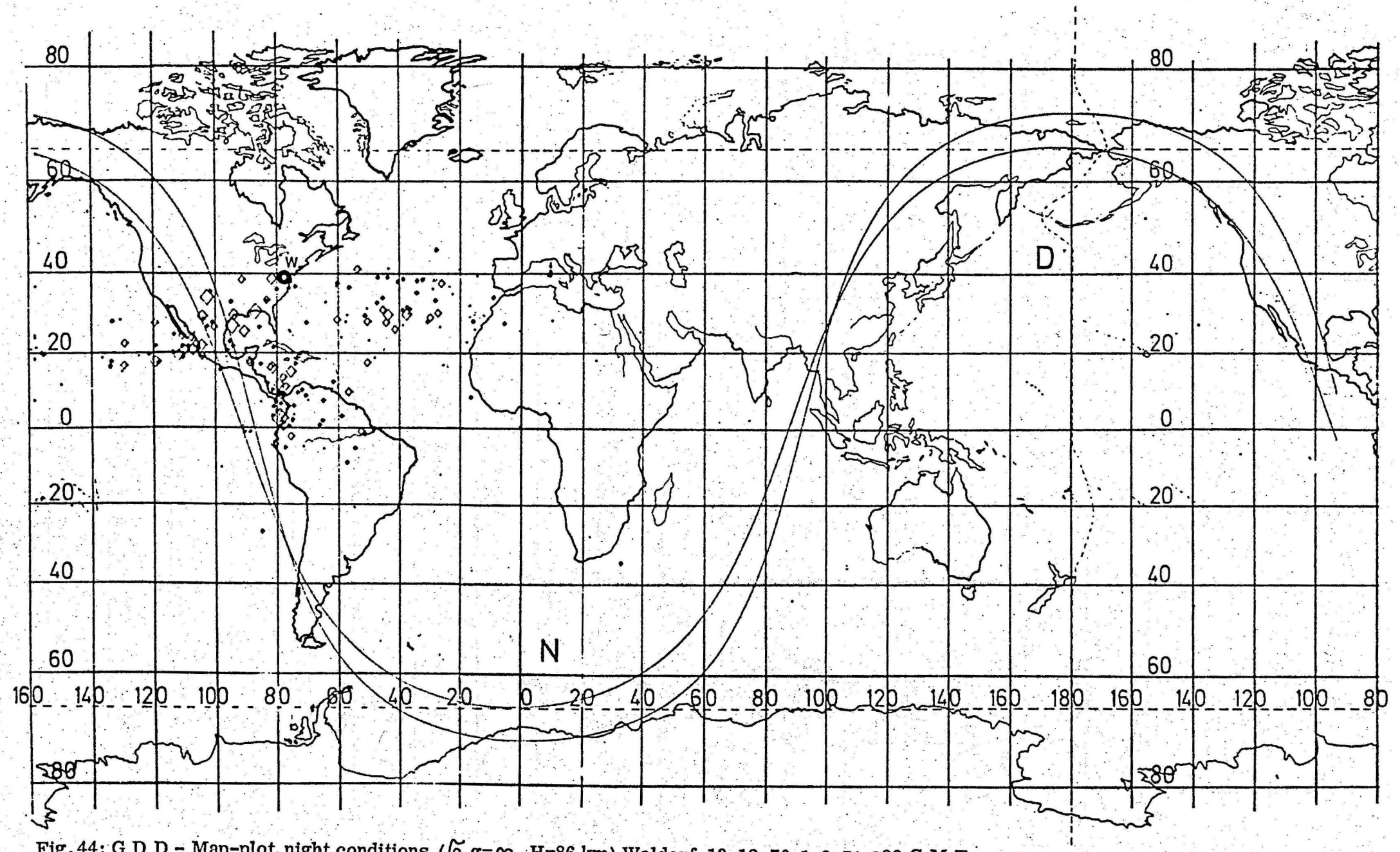

Fig. 44: G D D – Map-plot, night conditions (σ g=∞ , H=86 km) Waldorf, 19. 12. 70–1. 2. 71 0^{00} G M T

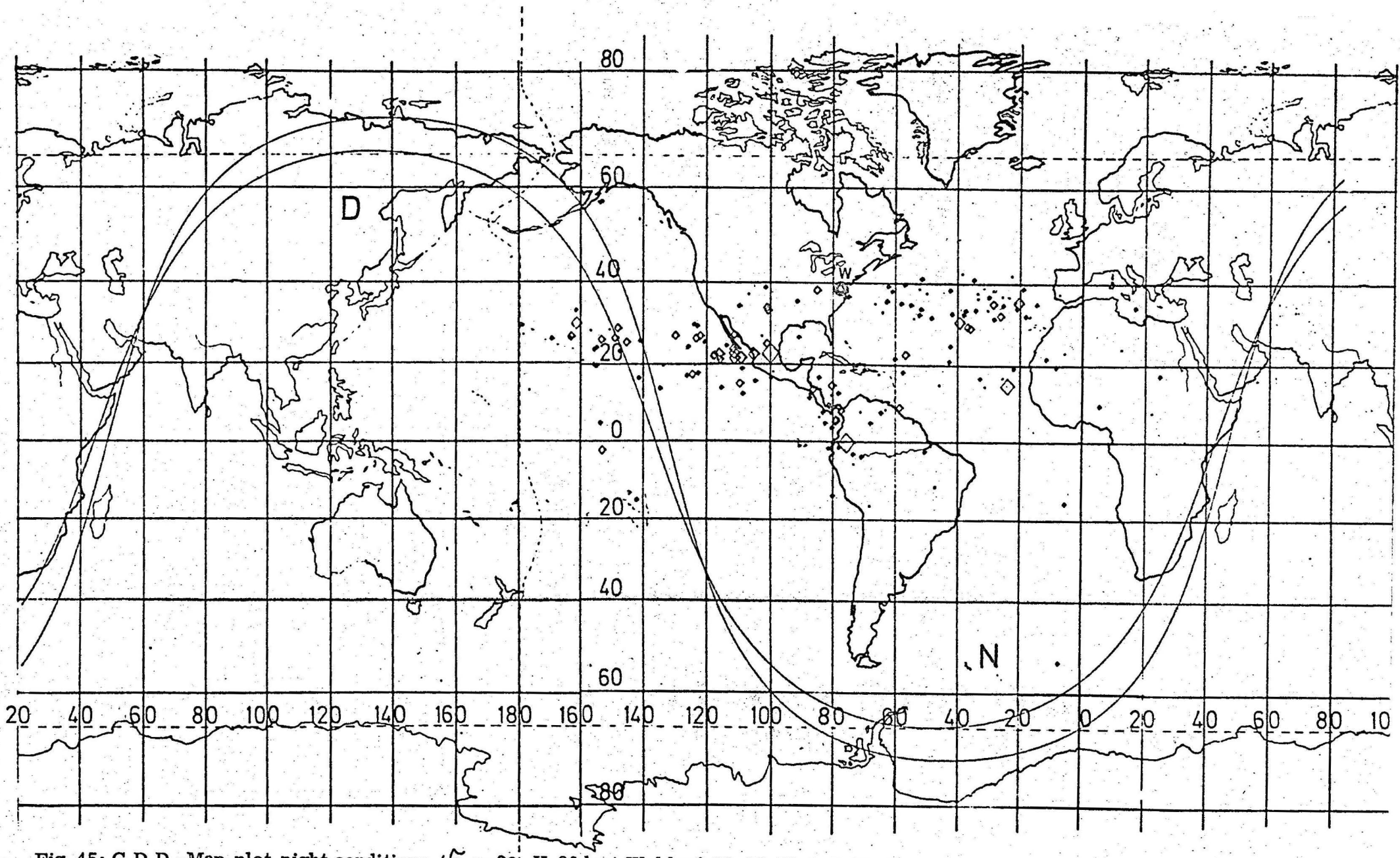

Fig. 45: G D D -Map-plot, night conditions (σ g=∞, H=86 km) Waldorf, 19. 12. 70-1. 2. 71 3^{00} G M T

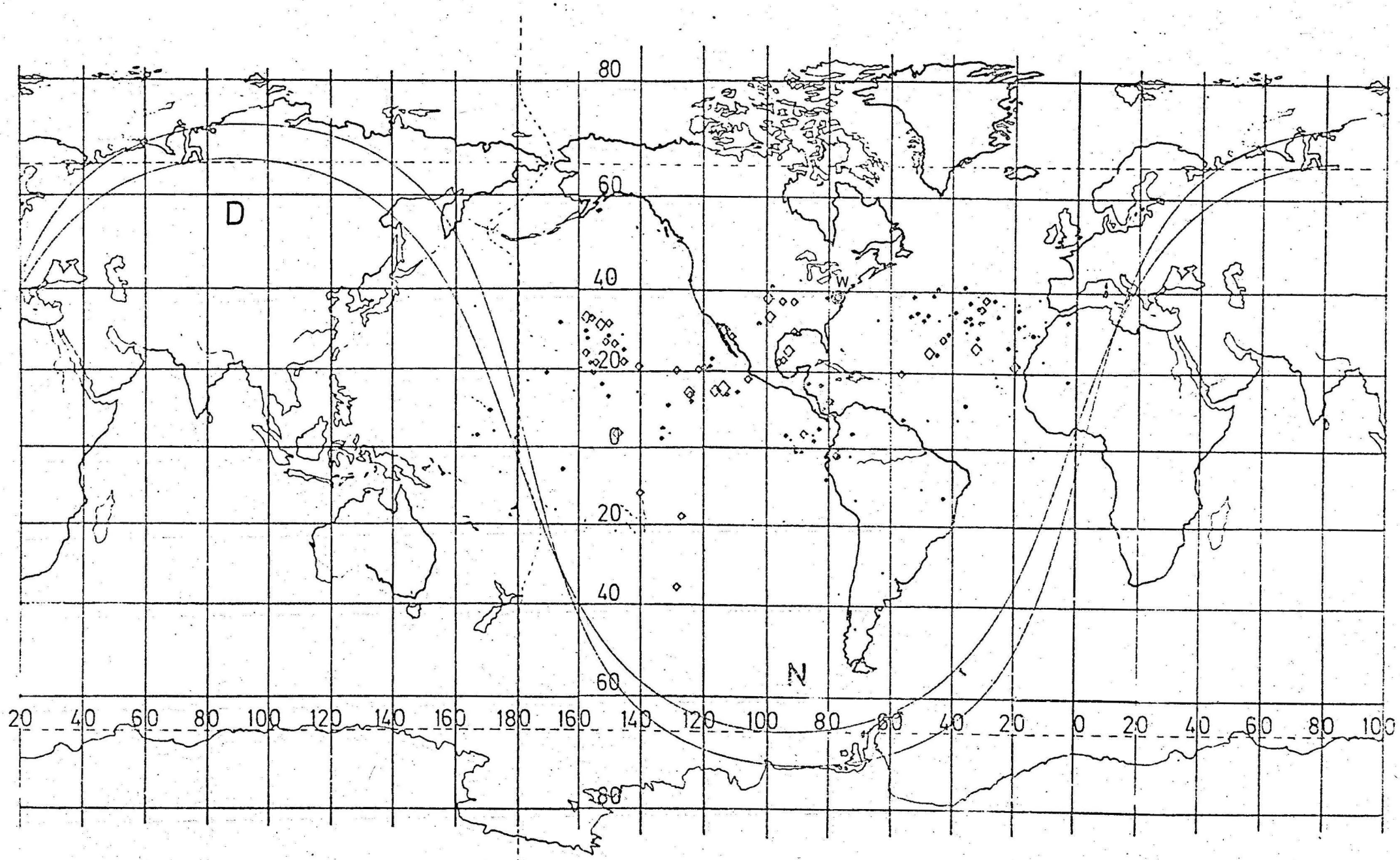

Fig. 46: G D D - Map-plot, night conditions ($\sigma g = \infty$, H=86 km) Waldorf, 19. 12. 70-1. 2. 71 6^{00} G M T

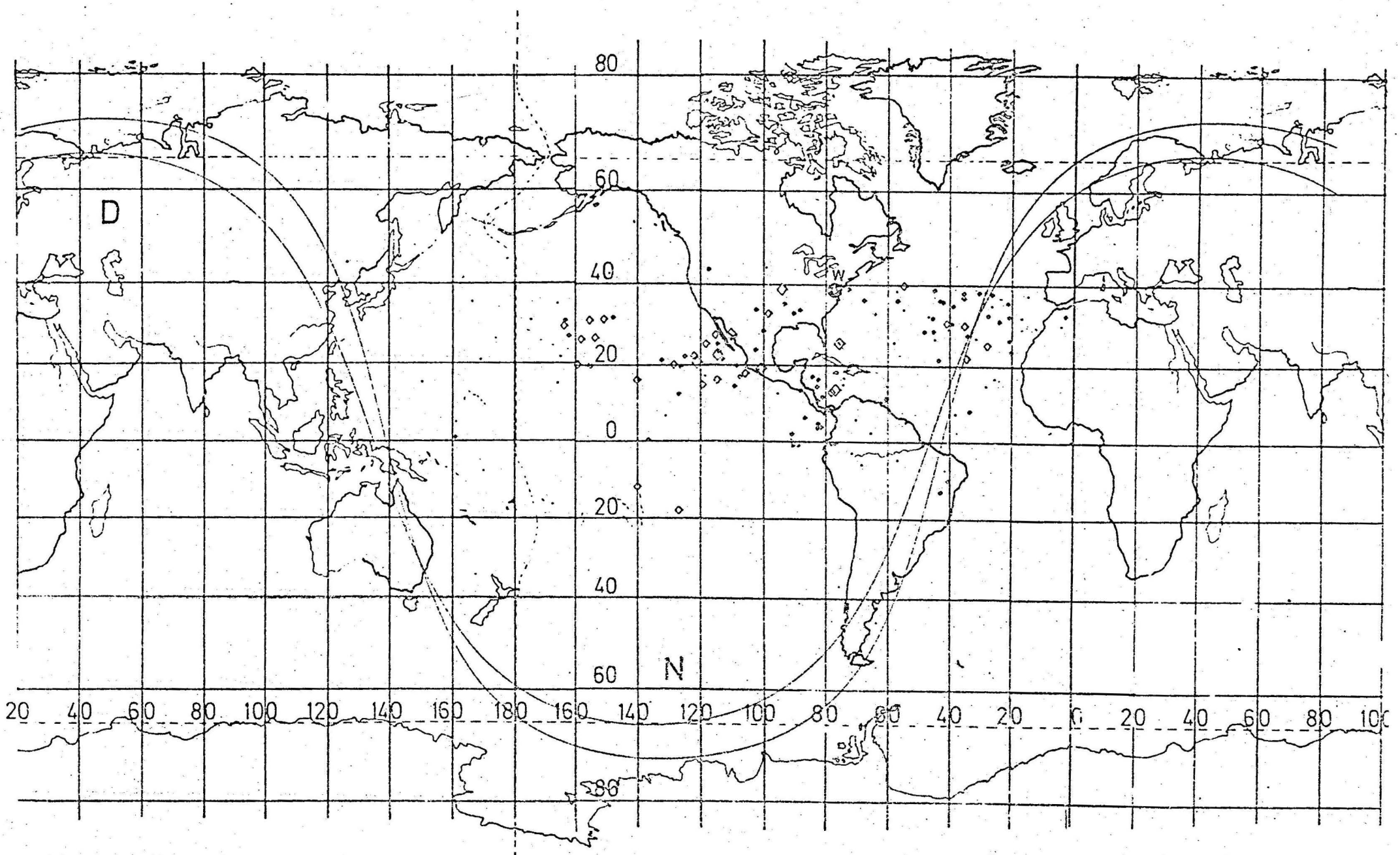

Fig. 47: G D D - Map-plot, night conditions (σ g= ∞ , H=86km) Waldorf, 19. 12. 70-1. 2. 71 9^{00} G M T

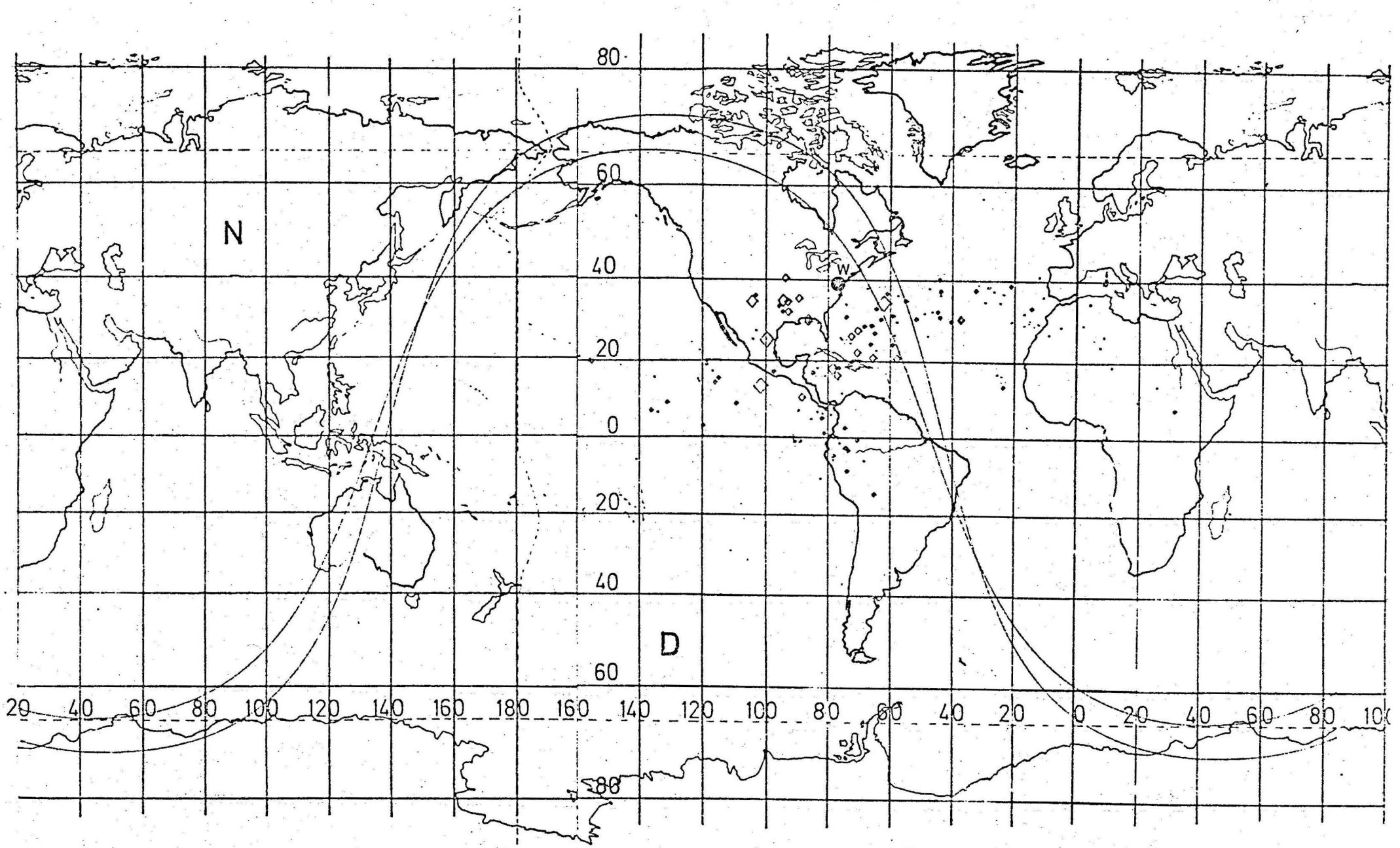

Fig. 48: G D D - Map-plot, night conditions (σ g=∞, H=86km) Waldorf, 19. 12. 70-1. 2. 71 21^{00} G M T

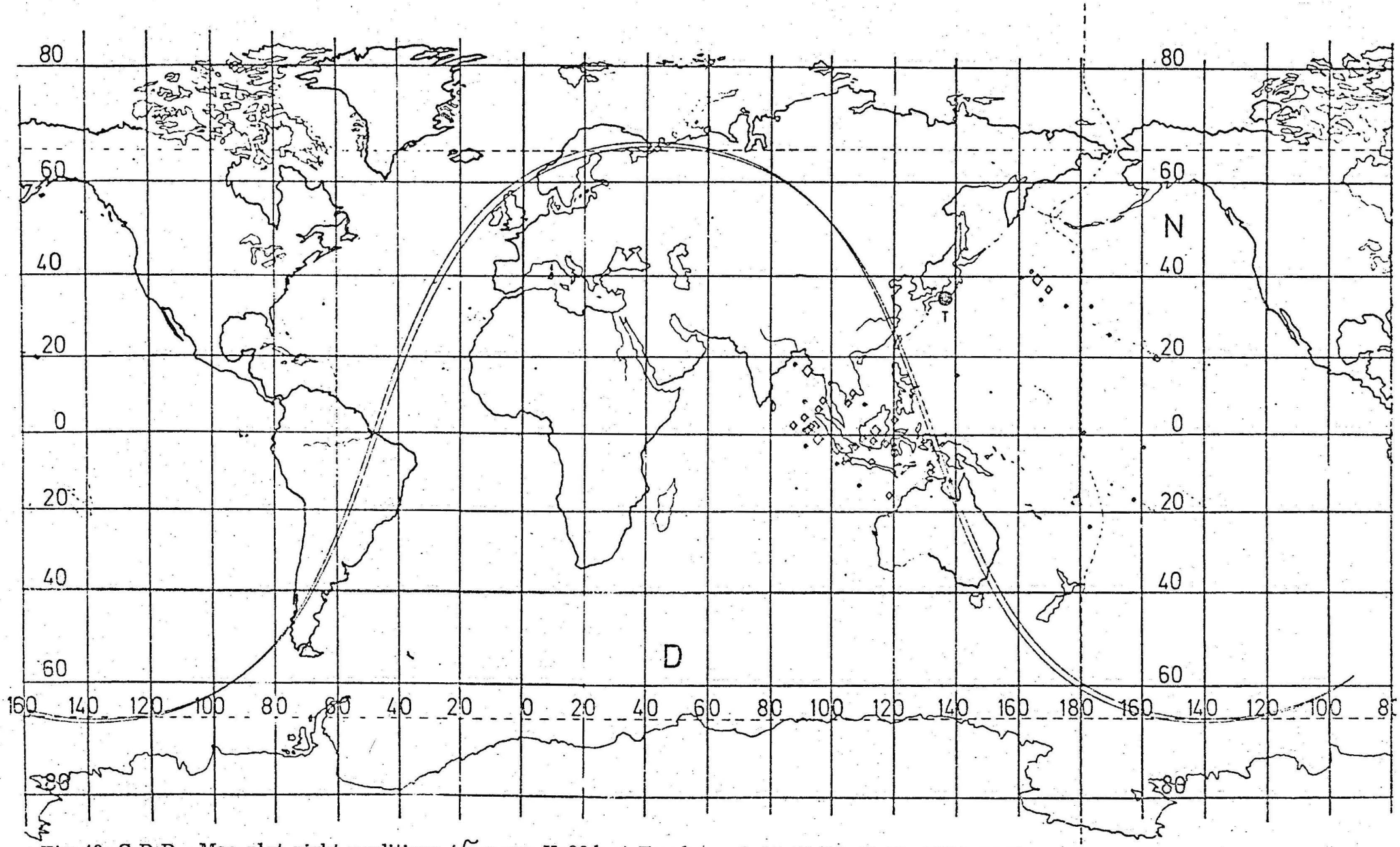

Fig. 49: G D D - Map-plot, night conditions (σ g=∞, H=86 km) Toyokawa, 9.12.70-23.12.70 9^{00} G M T

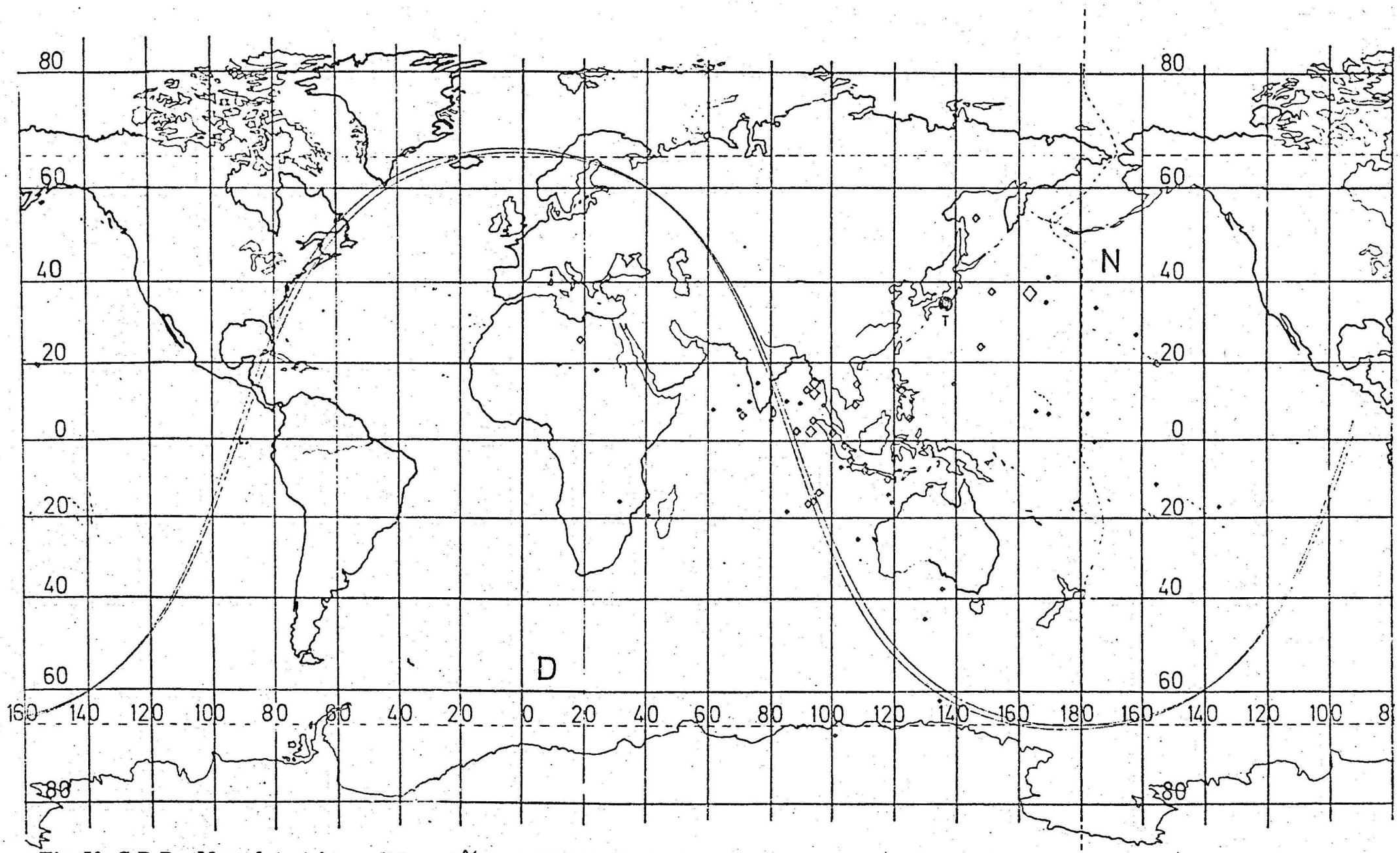

Fig. 50: G D D - Map-plot, night conditions (σ g= ∞ , H=86 km) Toyokawa, 9.12.70-23.12.70 12^{00} G M T

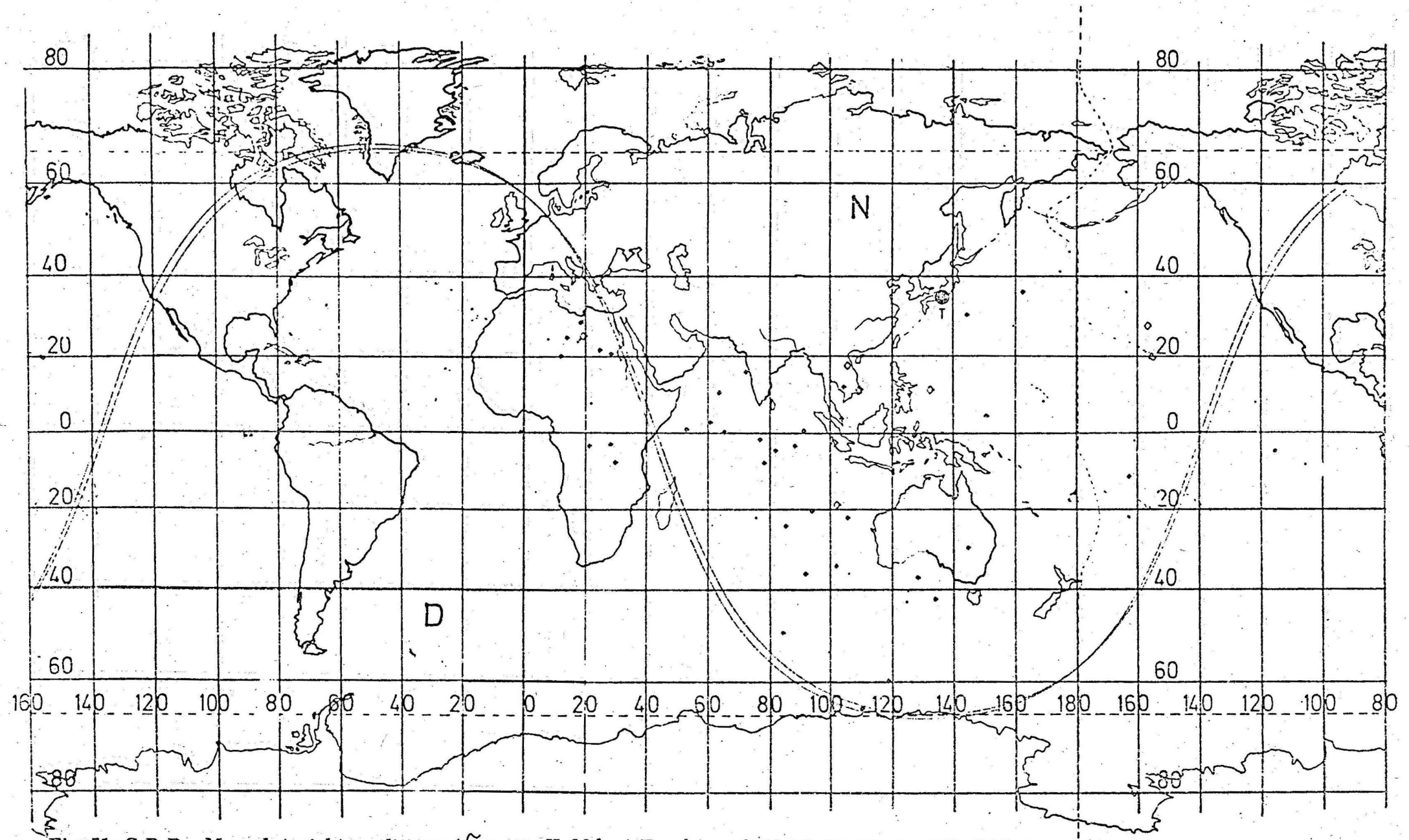

Fig. 51: G D D - Map-plot, night conditions (σ g=∞, H=86 km) Toyokawa, 9.12.70-23.12.70 15^{00} G M T

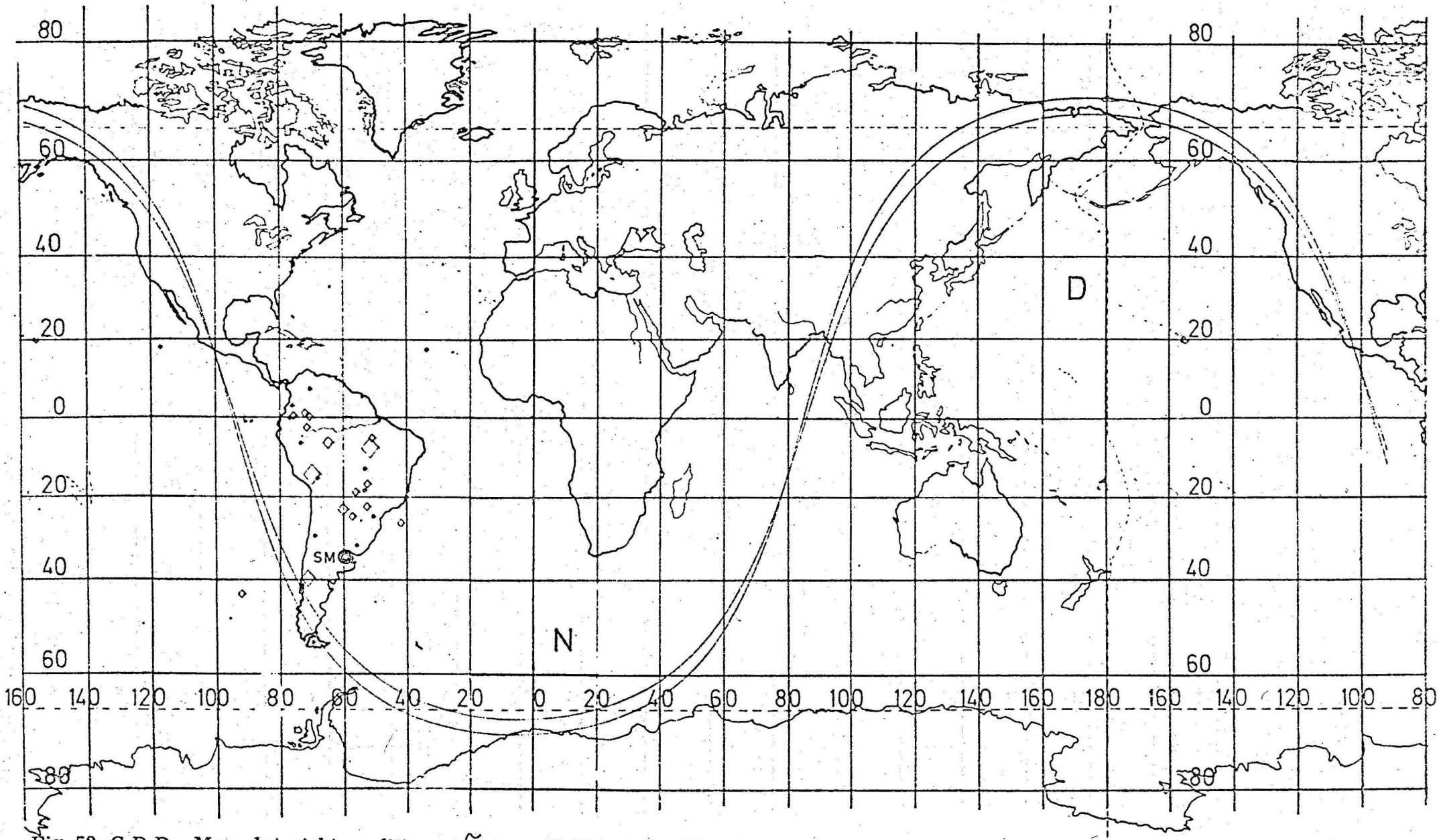

Fig. 52: G D D – Map-plot, night conditions ($\sigma g=\infty$, H=86 km) San Miguel, 16.11.70–30.11.70 0^{00} G M T

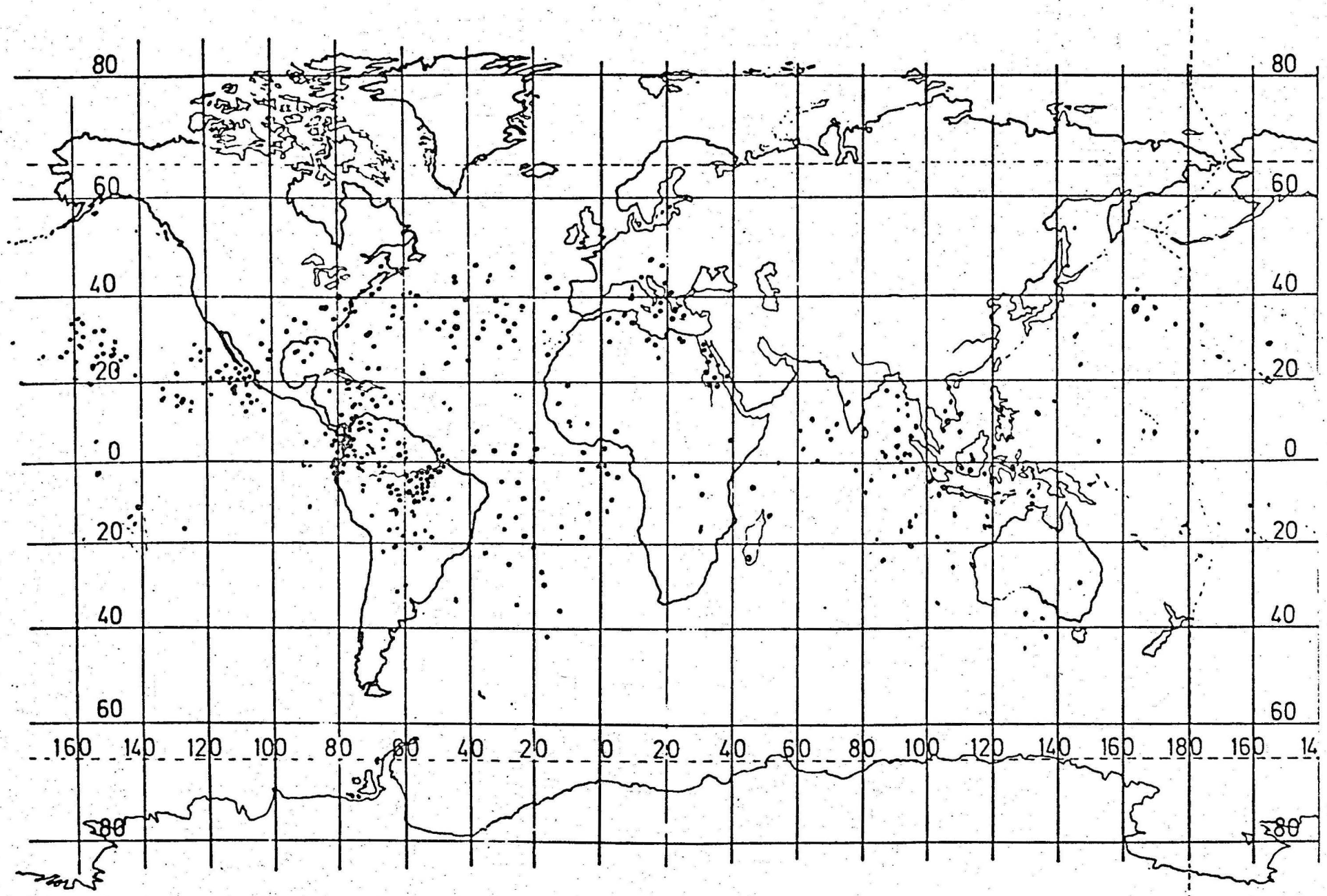

Fig.53: Summary of the Map-plots

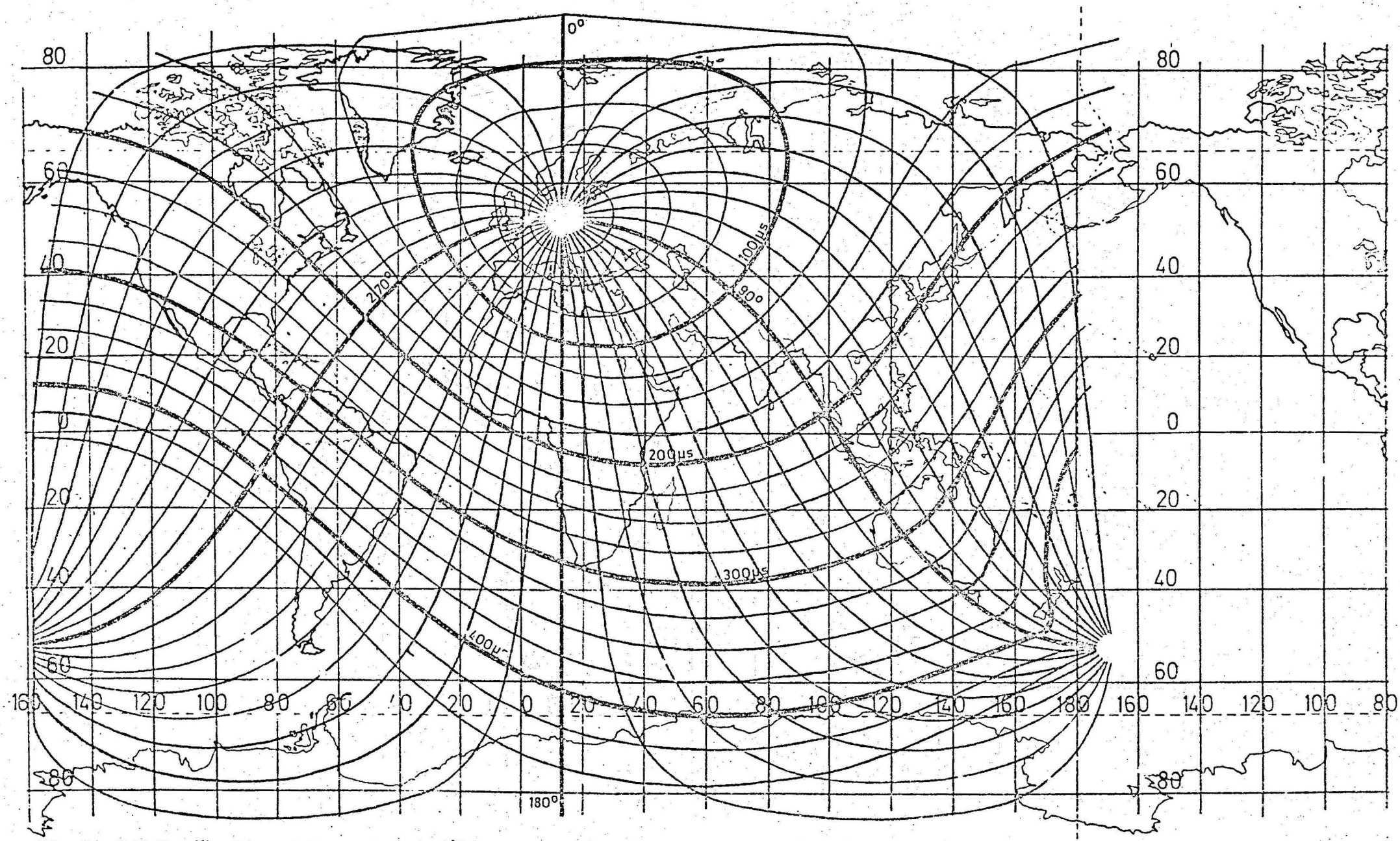

Fig. 54: G D D – Ψ – Map, night conditions (σ g=∞, H=86 km) Berlin

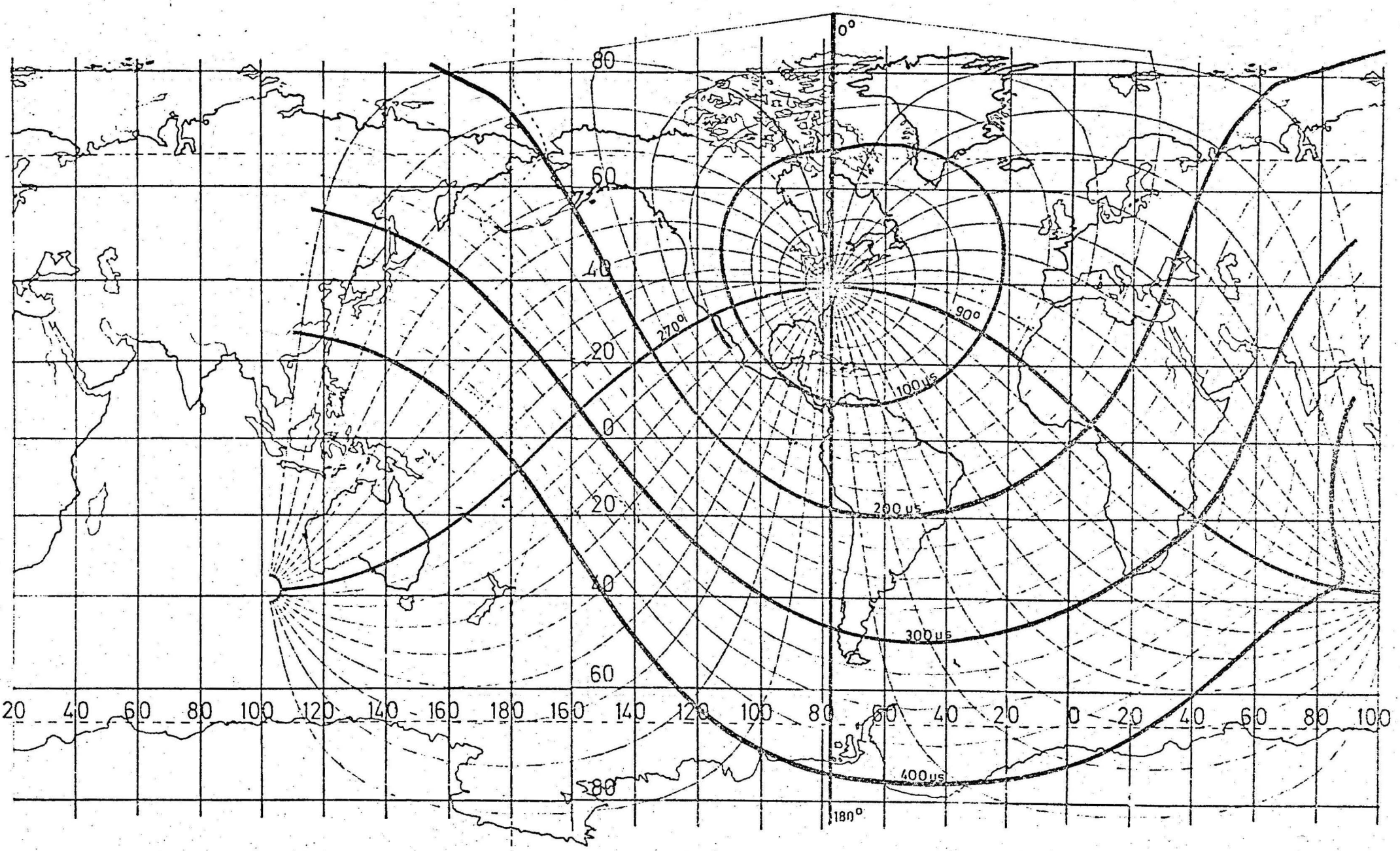

Fig. 55: G D D - Ψ - Map, night conditions (σ g=∞, H=86 km) Waldorf

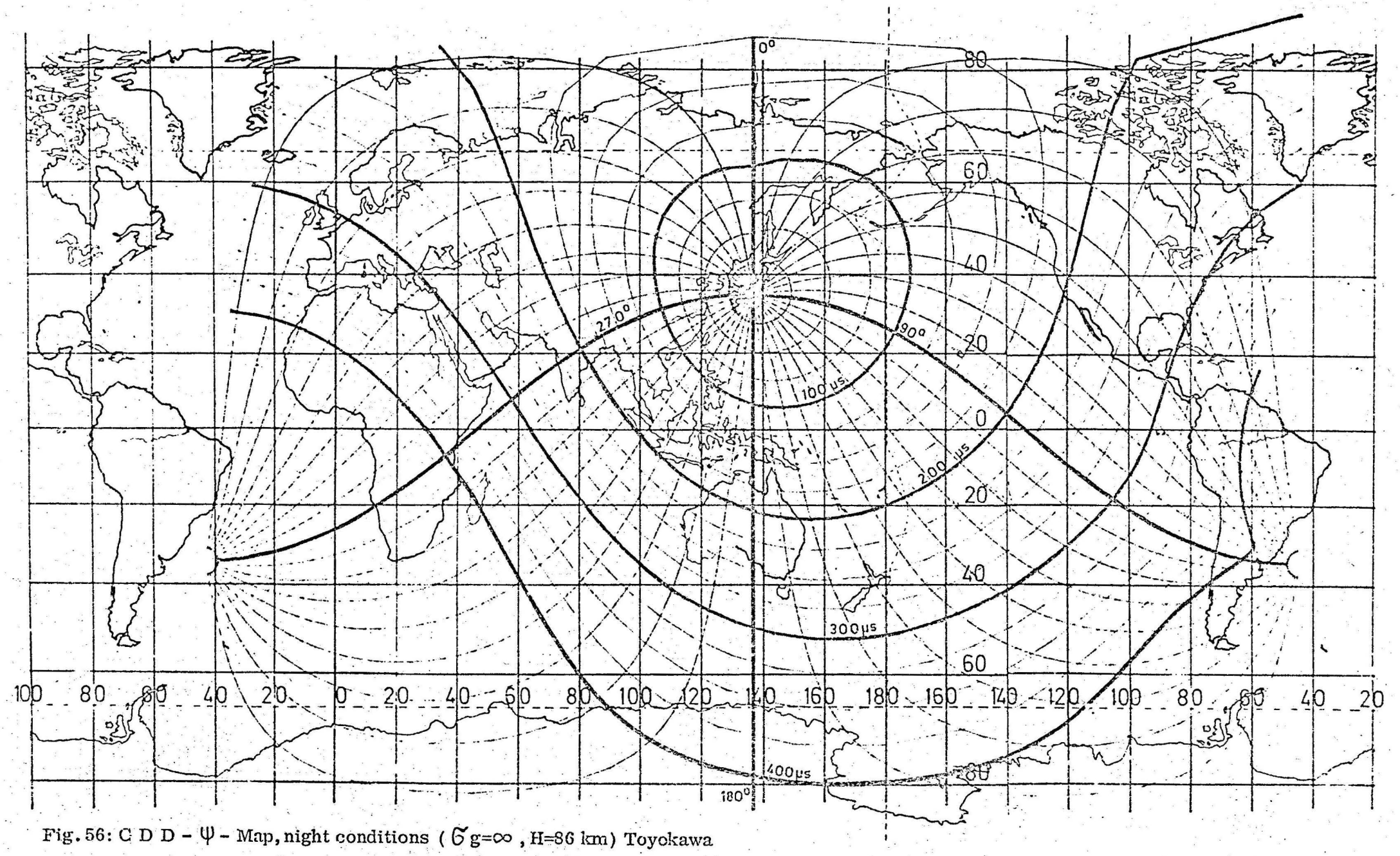

Fig. 56: C D D – Ψ – Map, night conditions ($\sigma g=\infty$, H=86 km) Toyokawa

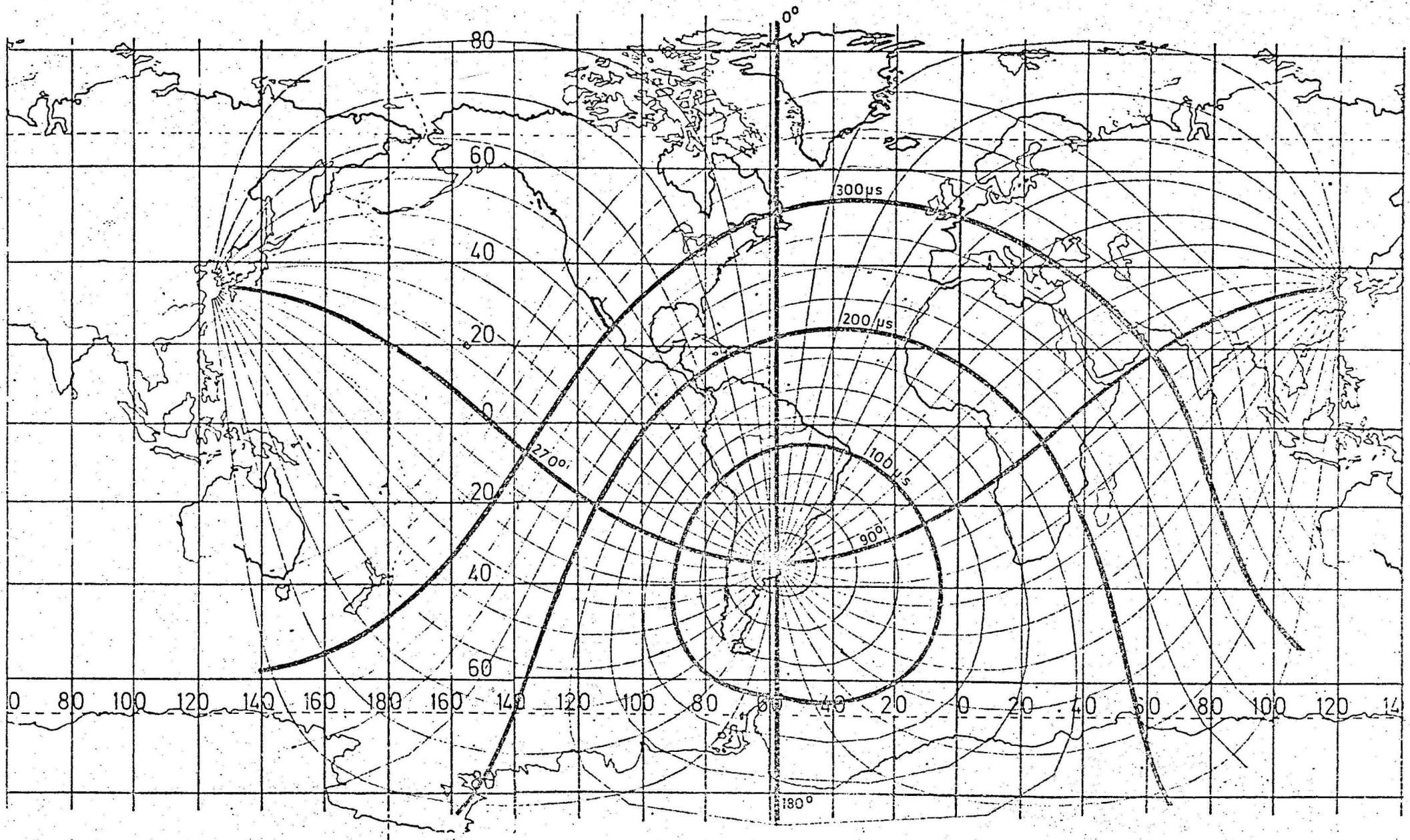

Fig. 57: G D D – Ψ – Map, night conditions (σ g=∞, H=86 km) San Miguel